Exploring impedance spectroscopy as a mean of malaria diagnostic

Simão Nunes Paula

Thesis to obtain the Master of Science Degree in

Biomedical Technologies

Supervisors: Prof. Raul Daniel Lavado Carneiro Martins; Doutora Maria de Fátima Carvalho Nogueira

Examination Committee

Chairperson: Prof. Joaquim Manuel Sampaio Cabral

Supervisor: Doutora Maria de Fátima Carvalho Nogueira

Members of the committee: Prof. Henrique Manuel Condinho da Silveira

November 2014

Acknowledgements

This page is dedicated to all institutions and peoples that contributed for the realization of this thesis. I leave here my acknowledgements:

To *Instituto de Higiene e Medicina Tropical* (IHMT) and *Instituto Superior Técnico* (IST), for allowing the use of the laboratory facilities as well as the equipment which enabled the realization of all practical work.

To the thesis supervisor Professor Raul Carneiro Martins for giving me the opportunity to become part of this project and for his guidance and counselling.

To the thesis co-advisor Professor Patrícia Almeida Carvalho for the access to the Electronic Microscopy Laboratory and its equipment. Also, a big thank you for the encouragement, persistence and help during the realization of the whole project.

To the thesis external advisor Professor Maria de Fátima Nogueira for her support, dedication and availability throughout the theoretical and practical part of this project.

To the Engineer Isabel Nogueira and Pedro Almeida Nolasco for their willingness to help in the operation of the electron microscopes.

To Bruno Gil and Marta Machado for all the collaboration, support and teaching, without them it would not have been possible to finish this project, one big thank you.

To my family, especially to my parents, Jaime Paula and Maria Teresa Paula, firstly for giving me the opportunity to attend and finish the Master's and secondly and more importantly for your concern, motivation, affection and love that you have always shown me. I also want to thank my sister, Filipa Paula, for her positivism and encouragement throughout this project, which always helped me to move on.

Finally, and also important, to all my friends who supported me and helped me overcome more complicated situations during this phase of my life. I want make a very special thank you to a friend, João Madaleno Pereira for his true friendship, help, dedication and concern that contributed to the finalization of this work.

Abstract

Malaria is an infectious disease caused by the parasites from the *Plasmodium spp.* genus and presents problems associated with its treatment and diagnosis. In the present work, it is analyzed the hemozoin crystal's characteristics (morphology, size and electric properties) obtained from different processes – natural source (*P. falciparum* strains 3D7 and Dd2) and synthetic sources and explored the possible use in malaria treatment. Furthermore, impedance spectroscopy was tested as a possible malaria diagnosis technique.

Hemozoin crystals, from natural and synthetic sources, were analyzed using different techniques, such as electronic microscopy (SEM and TEM) and impedance spectroscopy. The analysis of impedance measurements in healthy and infected red blood cells (RBCs) by *P. falciparum* Dd2 and 3D7 strains were made containing different developmental stages (ring, trophozoite, schizont).

Even though the characteristics between synthetic and natural crystals are different, one of the protocols for synthetic hemozoin produced crystals with properties closer to the natural hemozoin. The impedance measurements made in infected–RBCs with different *P. falciparum* stages were indeed different from the impedance measurements in uninfected-RBCs and demonstrated that it is possible to distinguish infected from uninfected blood samples.

These results support the idea that it is possible to approach both crystals formation processes thus simultaneously contributing to the production of antimalarial drugs able to diminish the parasite resistance. We also demonstrate that it is possible to use impedance measurements directly on blood to distinguish non-infected blood from malaria-infected blood which can be used for future development of a label-free diagnostic test.

Keywords: hemozoin characterization, malaria diagnostic, *Plasmodium falciparum,* scanning electron microscopy (SEM), transmission electron microscopy (TEM), impedance spectroscopy (IS)

Resumo

A malária é doença infecciosa causada pelos parasitas do genus *Plasmodium spp*., e que apresenta problemas associados ao seu tratamento e diagnóstico. Neste trabalho, numa primeira parte é demonstrado como a morfologia, tamanho e propriedades eléctricas dos cristais de hemozoina obtidos de diferentes processos formação – fonte natural (*P. falciparum* estirpe 3D7 e Dd2) e fonte sintética (diferentes protocolos) contribuem para a optimização do processo de produção via sintética. Numa segunda parte aplicou-se a técnica de espectroscopia de impedância para medição da impedância dos glóbulos vermelhos não parasitados e parasitados por *P. falciparum* estirpe 3D7 e Dd2, em diferentes estádios (anel, trofozoito e esquizonte), com o objectivo de diferenciar sangue não infectado de infectado por Malária.

Os processos de formação por via sintética podem ser controlados de forma obter cristais com características mais homogéneas. As morfologias, tamanhos e propriedades eléctricas entre cristais sintéticos e naturais demonstraram-se mais semelhantes quando se aplicou um determinado protocolo de formação por via sintética. A impedância dos glóbulos vermelhos parasitados nos diferentes estádios apresentou diferenças em relação à impedância dos glóbulos vermelhos não parasitados. Estes resultados suportam a ideia que é possível aumentar a aproximação entre processos de formação de cristais por via sintética e natural, e simultaneamente contribuir para a produção de medicamentos antimaláricos que diminuam a resistência do parasita. Além disso, demonstram que é possível usar a técnica de espectroscopia de impedância para diferenciação de sangue não infectado e infectado por malária, e aplica-la como técnica de diagnóstico da doença.

Palavras-chave: caracterização de hemozoína, diagnóstico de malária, *Plasmodium falciparum*, microscopia electrónica de varrimento (MEV), microscopia electrónica de transmissão (MET), espectroscopia de impedância (EI)

Table of Contents

List of Figures

List of Tables

Abbreviations

AC	Alternating current
ACC	Automated blood cell counters
BF	Bright field
BSE	Backscattered electrons
CDC	Center for Disease Control and Prevention
CO_2	Carbon Dioxide
CRT	Cathode ray tube
DF	Dark field
DLL	Depolarized laser light
DMSO	Dimethyl Sulfoxide
DNA	Deoxyribonucleic acid
EDS	Energy-dispersive X-ray spectrometry
EDTA	Ethylenediaminetetraacetic acid
EELS	Electron energy-loss spectrometry
EIS	Electrochemical impedance spectroscopy
ELISA	Enzyme-linked immunosorbent assay
EPR	Electron paramagnetic resonance
EXAFS	Extended X-ray absorption fine structure
FCM	Flow cytometry
Hb	Hemoglobin
HEPES	4-(2-hydroxyethyl)-1-piperazineethanesulfonic acid
HIV/AIDS	Human immunodeficiency virus infection / acquired immunodeficiency syndrome
IS	Impedance spectroscopy
LAMP	Loop mediated isothermal amplification
LCD	Liquid-crystal display
LDMS	Laser desorption mass spectrometry
NaOH	Sodium hydroxide
nHz	Native hemozoin
P. falciparum	*Plasmodium falciparum*
PBS	Phosphate buffered saline

PCR	Polymerase Chain Reaction
Pf-iRBCs	*Plasmodium falciparum*-infected red blood cells
PXRD	Powder X-ray diffraction pattern
QBC	Quantitative Buffy Coat
RBCs	Red blood cells
RDTs	Rapid diagnostic tests
RPMI	Culture Medium
RPMI	Roswell Park Memorial Institute medium
SDS	Sodium dodecyl sulphate
SEM	Scanning electron microscopy
SEs	Secondary electrons
sHz	Synthetic hemozoin
TEM	Transmission electron microscopy
TRIS-HCL	Tris-hidrochloride
uRBCs	Uninfected red blood cells
WB	Whole Blood
WHO	World Health Organization
β-hematin	Synthetic hemozoin

1. State of Art and Objectives

1.1. Malaria

Malaria is an infectious disease, which has evolved through the years alongside mankind. Its origin is uncertain but it is believed that the majority of the population with malaria began to develop in eastern and central Africa, more precisely in the Ethiopian region [1-3].

Malaria infection is caused by the protozoan parasites of the genus *Plasmodium spp*. which currently can be identified by 5 species, *Plasmodium falciparum*, *Plasmodium vivax*, *Plasmodium ovale*, *Plasmodium malariae* and *Plasmodium knowlesi*. The specie *Plasmodium falciparum* is transmitted by mosquito *Anopheles gambiae* and is responsible for the most severe infections causing symptoms such as severe malarial anemia, loss of conscience, cerebral malaria, triggering several cases of human mortality [4-6].

The Center for Disease Control and Prevention (CDC) refers that the transmission of malaria depends on the climate and its changes over the years (Fig. 1.1). The disease develops better in tropical and sub-tropical climates, where it is possible for the mosquito *Anopheles* to survive and multiply, thus completing its growth cycle.

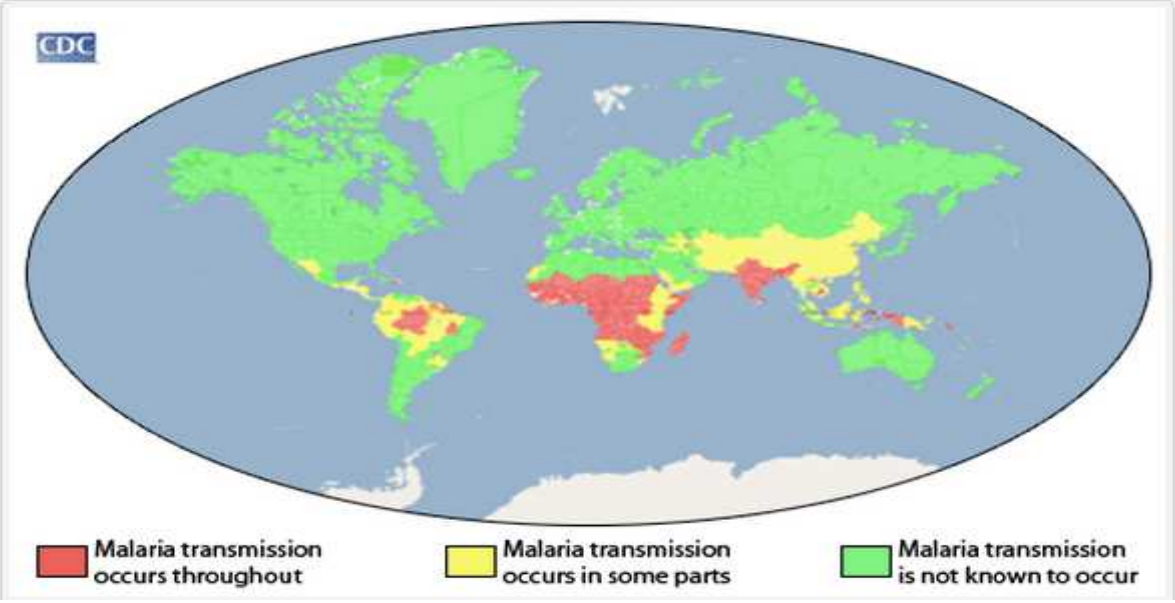

Figure 1.1 - This map shows an approximation of the parts of the world wheres malária transmission occurs [7].

The World Health Organization (WHO) and the World Malaria Report 2013 both refer that there are 97 countries where malaria transmission still occurs and 7 countries that are currently at a prevention status. Factors such as unstable climate, global warming, civil disturbances, travel habits,

HIV and resistance to medicine and insecticides, have contributed negatively towards the fight against malaria and positively towards mortality. Currently there are around 3.4 thousand million people at risk of contracting the disease. On the year 2012 occurred globally 135 to 287 million new cases of malaria and 473 to 789 thousands deaths. The percentage of new cases is of 80 % and happened in Africa, as well as 90% of the deaths, most of which are children (77%) below the age of 5 [8].

Besides contributing to the increase of mortality, malaria has negative effects on the socioeconomic development. The search for new methods of control and elimination of malaria has been fundamental to reduce mortality and to help increase the world welfare. The World Health Organization (WHO) have been developing objectives and strategies for 2016 to 2025, which according to the World Report Malaria 2013 are:

- Prevention through vector (mosquito) control;
    - Nets treated with insecticide;
    - Indoor residual spraying;
    - Management of the sources of larvae;
    - Management insecticide resistance;
- The most important, preventive chemotherapy (preventing the propagation of anti-malaria medicine resistance) [8].

1.1.1. *Plasmodium* life cycle

Plasmodium's life cycle is quite complex since it is constituted by two phases, which occur in two different living beings, the vector mosquito and the vertebrate host [9, 10]. The phase of the sexual reproduction cycle occurs on the vector mosquito, the pre-erythrocytic and erythrocytic phases occur on the human host (Fig. 1.2).

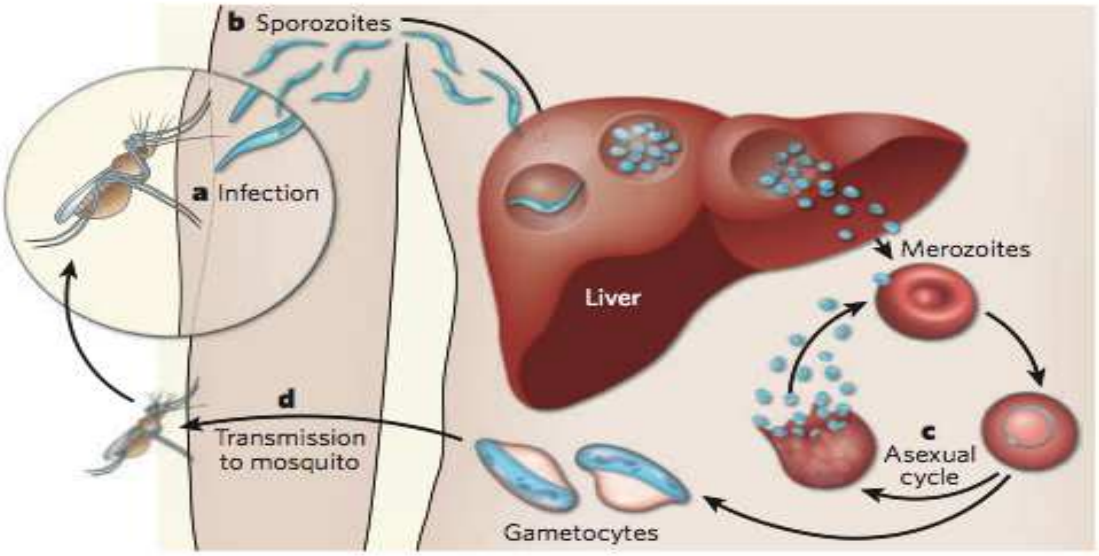

Figure 1.2 - Basic features of the *Plasmodium* life cycle [11].

During the pre-erythrocytic phase, an hepatic infection develops caused by the *Anopheles* mosquito's byte on the subcutaneous tissue during its blood meal (a). At this stage the *Plasmodium* parasite's sporozoites are injected into the blood stream and carried by the body to the liver hepatocytes (b). The liver infection lasts around 6 days and during this time the sporozoites undergo a phase of asexual multiplication, exoerythrocytic schizogony, originating thousands of merozoites uninucleated, which are then carried to the blood stream where they invade the red cells. This invasion gives rise to a new phase of asexual multiplication, intraer……ythrocytic schizogony (c) where the parasite divides and grows, producing merozoites that are going to invade new red cells. The continuous repetition of this intra-erythrocyte phase of the parasite will aggravate the disease. The organ system of the host is affected by the asexual phases of the parasite differently from individual to individual and these are considered pathogenic. With the advancing infection, a small portion of the young merozoites develops into male and female gametocytes, which will later circulate in the peripheral blood. They will return to the mosquito when it feeds of the blood again (d) [4, 6, 10, 12-14].

1.1.2. Hemozoin Formation Process

The intraerythrocytic malaria parasite digests large quantities of host hemoglobin as a major source of amino acids. Simultaneously, heme is released and oxidized to produce hematin (aqua / hydroxyferriprotoporphyrin IX), and this is converted into a compound called malaria pigment or hemozoin [15, 16].

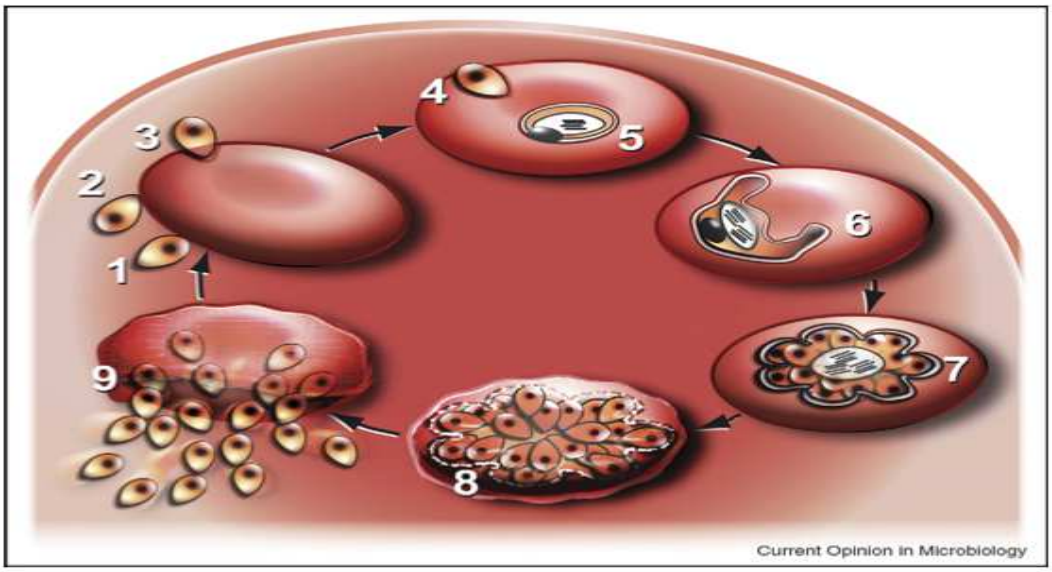

Figure 1.3 - Cycles of asexual parasite replication inside red blood cells [17]. Invasion of merozoites into red blood cells (1-4). Different stages of intraerythrocytic malaria parasite, ring (5), trophozoite (6) and schizont (7 and 8).

The beginning of the process of formation of hemozoin occurs in one of the four stages of the asexual phase of the malaria parasite, intraerythrocyte (Fig. 1.3). The cycle takes around 48 hours to be completed [14, 18]. This phase starts on the merozoites stage (1), it will initially adhere to the red

blood cell (2) and through its apical end will increase the junction with the cell thus enabling the parasite to enter the cell (3, 4). After entering the cell, the parasite starts feeding the surroundings of the cell, originating a new stage with the shape of a small ring (5). On a later stage the parasitic food vacuole is formed, bigger than the previous one and to where the hemoglobin is transported. It is also here that the hemoglobin is degraded in an acidic aqueous environment by proteolytic enzymes in amino acids, which will be used in the protein's biosynthesis and in maintaining osmolality [17, 19-22].

During the degradation occurs an increase on the volume of the cell, which leads to a new trophozoite stage (6). In this stage, around 60% to 80% of the hemoglobin present in the red blood cell is degraded [22-24]. The degradation process triggers the release of a substance toxic to the parasite, heme (ferriprotoporphyrin IX) [15, 16], while at the same time a detoxification process occurs (Fig. 1.4) [25].

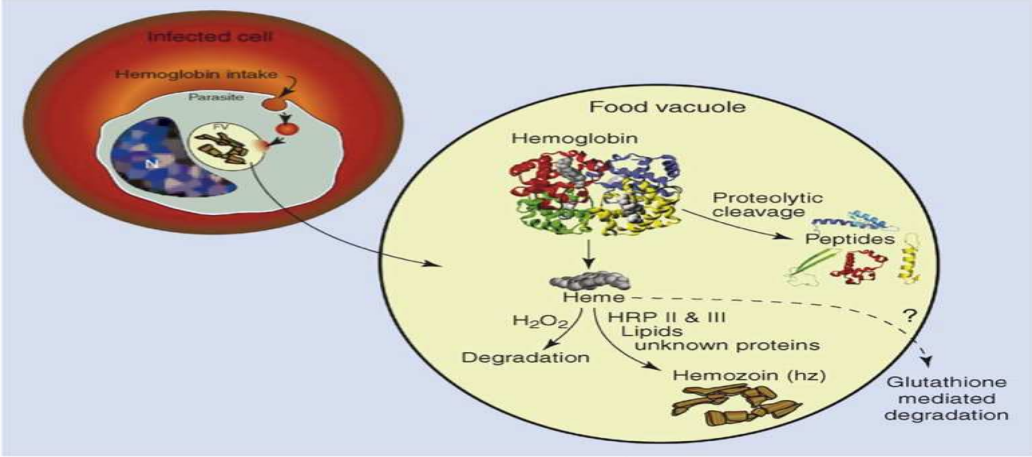

Figure 1.4 - Schematic representation of Hb up take and heme detoxification in malaria parasite [25].

The released heme suffers oxidation in order to produce hematin (aqua / hydroxyferriprotoporphyrin IX), which is then transformed into a crystalline substance, hemozoin. This transformation is given the name of biocrystallization, where the organisms produce crystals with a high molecular weight, organic materials [21, 25-28].

Several hypotheses have been raised about the biological mediators that interfere in the crystallization process, such as enzyme-catalyzed heme polymerases, proteins (specifically histidine-rich protein and heme detoxification protein) and lipid mediation, or a combination of the two. Recent studies revealed that neutral lipids found in the initial stage of trophozoite are sufficient to mediate the process. The observation of lipid nanospheres around the food vacuole in transmission electron microscopy (TEM) micrographs has reinforced the idea of the lipids as mediators [28-31]. About 95% of the hematin used in this process is converted to hemozoin [32], which is not toxic for the parasite [16]. With the consumption of hemoglobin and cytosol until nearly exhausted, the parasite grows and the schizont stage starts (7), resulting from the repetitive nuclear division in several merozoites (8). With at the rupture of the schizont, the hemozoin stored in the food vacuole, merozoites and all cell content are released into the blood flow (9). The hemozoin is then deposited in the internal organs of the host or phagocytosed by neutrophils and monocytes. In the blood, the intraerythrocyte phase is repeated in new red blood cells [19, 25, 33].

1.2. Inhibition of the heme biomineralization process

1.2.1. Antimalarial Drugs

After the 17th century Jesuit missionaries learned, during their travels in Latin America, that by the using the hull of the Cinchona tree it was possible to apply a treatment to the malaria caused fevers. Later on it was identified that quinine was an alkaloid extracted from the Cinchona tree, that, proved to be very effective against malaria [34-36].

With the change over the years on the structure of the quinine, other drugs of the same class were developed, such as, chloroquine (1934), amodiaquine (1951), primaquine (1952), mefloquine (1963), halofantrine (1966), and in the last 30 years piperaquine, lumefantrine and pyronaridine. In general it is accepted that this class of drugs have the same parasite target, which is to interfere with the detoxification of the heme of the parasite [37-39].

Recently it was introduced a new class of drugs, artemisinin, derived from wormwood plant (*Artemisia annua*). This compound has several advantages; it acts well in environments rich in iron, and releases free radicals which can damage the parasite, being at the same time a drug that is well tolerated by the host [40, 41]. The target of artemisinin is inhibition of crystal nucleation of hemozoin, reducing their formation and changing their shape [16, 38].

With the evolution and development of new antimalarial drugs, the parasite evolved as well and due to mutations it adapted to the drugs thus giving origin to strains resistant to these drugs (Fig. 1.5). One process that triggered the increasing of the parasite's resistance was the transfer of its alleles from individual to individual through the mosquito [37, 41-44].

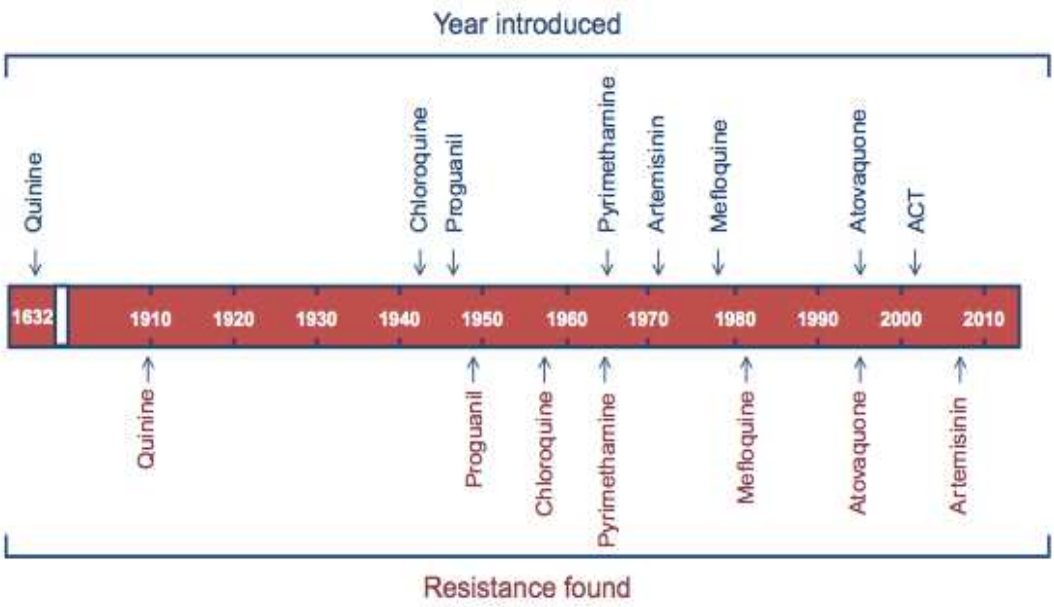

Figure 1.5 - Comparative year of introduction of new antimalarial therapies versus the emergence of clinical resistance [45].

Another problem associated with the treatment and prevention of malaria is the toxicity caused by the drugs used, such as cardiovascular toxicity, ocular toxicity, neurotoxicity, hepatotoxicity and myopathy [39, 44, 46].

The search for new explanations that help understand the resistance mechanism of the parasite to the drugs has been a great challenge over the years. The table 1.1 shows various classes of antimarial drugs and associated problems.

Table 1.1 - The main classes of antimalarials drugs and associated problems [4, 36, 37, 40, 45-48].

Class	Drugs	Associated Problems
Endoperoxides	Artemether	Recrudescence; neurotoxicity; reproductive safety concerns; high cost
	Artesunate	
	Artesiminin	
	Artesimone	
	Dihydroartesiminin	
	OZ439	
	OZ277	
4-aminoquinolines	Amodiaquine	Drug resistance worldwide; bitter taste; nausea; abdominal discomfort; dizziness; retinal pigmentation; blurred vision; electrocardiographic changes; muscular weakness
	Naphthoquine	
	Chloroquine	
	Hydroxchloroquine	
	Piperaquine	
	Pyronaridine	
	AQ-13	
	Tert-butyl isoquine	
8-aminoquinolines	Primaquine	Photochemically unstable; in vitro phototoxic; narrow therapeutic index; development of drug resistance; not used in glucose-6-phosphate dehydrogenase-deficient patients: hemolytic anemia as side effect. Administration of high doses can cause: nausea; headache; disturbance of visual accommodation, pruritus and abdominal cramps.
	Diethylprimaquine	
	Bulaquine	
	Tafenoquine	
	NPC-1161B	
Antifolates	Pyrimethamine	Mouth ulcers; resistance worldwide
	Proguanil	
	Dapsone	
	Cycloguanil	
	P218	
	Chlorpriguanil	

Table 1.1 - The main classes of antimalarials drugs and associated problems (continuation).

Class	Drugs	Associated Problems
Antifolates	Pyrimethamine	Mouth ulcers; resistance worldwide
	Proguanil	
	Dapsone	
	Cycloguanil	
	P218	
	Chlorpriguanil	
Sulfonamides	Sulfadoxine	Allergic reactions to sulfa drugs well know
	Sulfadiazine	
	Sulfamethoxazole	
Antibiotics	Trimethoprim	Limited use; efficacy to be defined; phototoxicity; not used in pregnant women children; gastrointestinal intolerance; skin and nail disorders
	Azithromycin	
	Tetracycline	
	Fosmidomycin	
	Mirincamycin	
	Doxycycline	
	Thiostrepton	
Amino alcohols	Lumefantrine	Severe allergic reactions; resistance worldwide; cardiotoxicity; poor absorption; contraindicated in pregnancy; sporadic resistance; gastrointestinal and neurological disturbances; very expensive
	Halofantrine	
	Mefloquine	
	Quinine	
Others	Riboflavin	Recrudescence; limited experience; rapid development of resistance in monotherapy
	Pentamidin	
	DHEA	
	Cycloheximide	
	Atovaquone	
	Deferoxamine	
	Methylene Blue	
	N-acetyl-D-penicillamine	

1.2.2. Discovery of novel antimalarial drugs

Quinoline class drugs, such as Quinine, Chloroquine and the Mofloquine were the most important at the beginning of malaria control due to their effectiveness, security, low cost and quality. Issues such as resistance and drug toxicity caused an increase in the demand for research of new drugs that acted efficiently against the parasite without causing side effects and at a low cost [49]. The byproducts of parasite ingestion and the host's hemoglobin catabolism have been the subject of research seeking understanding of the how the drugs work and of the resistance of the parasite, hemozoin being a prime example. The biocrystallization of the hemozoin's heme is a mechanism not entirely known. The study and identification of the factors involved in the inhibition of the detoxification process of the parasite will be important for the clinical assays of new drugs. The optimization of the factors will allow for an environment greater efficiency during the assays, and possibly the development of antimalarials less prone to resistance by the parasite [25, 49-51]. The process of hemozoin formation is a valid target for most of the antimalarial drugs and it is considered an appropriate target for developing new antimalarials that hold back the disease or even eliminate it [28, 49].

1.3. Synthetic (β-hematin) and native hemozoin characteristics

1.3.1. Structure of synthetic hemozoin

Various techniques have been used over the years for the characterization of the hemozoin's crystals, resulting from the detoxification process of the malaria parasite [20, 27]. After Fitch and Kanjananggulpan having suggested that hemozoin was composed by iron (III) protoporphyrin IX (Fe III) PPIX, which has a similar structure to an insoluble precipitate Fe (III) PPIX, synthetic β-hematin, researches were conducted in order to characterize and compare them [20, 27, 33, 52]. In 1991, through techniques like X-ray diffraction, infrared spectroscopy, and solubilization studies, it was proved that β-hematin was identical to hemozoin. More in-depth studies were conducted using a technique of extended X-ray absorption fine structure (EXAFS) for the analysis of β-hematin. These studies demonstrated that β-hematin was composed by chains of bonds between the propionate group of one iron porphyrin and the Fe (III) center of its neighbor [20, 33, 50, 53, 54]. With a structure not so well defined, doubts remained as whether β-hematin was identical to hemozoin. In 1997 was utilized synchrotron radiation X-ray powder diffraction for the analysis of lyophilized (freeze-dried) parasitized red blood cells (RBCs), obtaining as a result an identical diffraction pattern of β-hematin removing any doubt regarding the similarities to hemozoin [16, 55]. The structure of β-hematin would only be completely resolved 3 years later with a technique of powder X-ray diffraction pattern (PXRD) by Ritetveld refinement concluding that this corresponded to an hydrogen bonded chain of proponiate linked dimers [26, 27, 33, 56]. Following this structure, recent studies have suggested a new nomenclature for β-hematin, where it is referred as an anhydride hematin [20, 54].

1.3.2. Structure of native hemozoin

Hemozoin was described for the first time as a dark black-brown coloured pigment, found in the internal organs (spleen, brain, liver) of malaria victims [31]. Even though spectroscopy techniques applied to β-hematin up until 2000 confirmed that native hemozoin had an identical structure, the analysis and the showing of the natural structure of the crystal would only occur later [20]. In 2005 was applied a technique of synchrotron radiation X-ray powder diffraction to analyze crystals formed by *Schistosoma Mansoni* and *Rhodnius Prolixus*, subsequently proving that the structures obtained by Rietveld Refinement and their own were a match. These structures were then compared to the structures of β-hematin, also showing similarities. On the same study it was determined the unit cell dimensions, and the Fe (III)-O bond length of the natural crystals and of the β-hematin (synthetic hemozoin) as well. The result of this study was the achievement of very similar values, thus confirming that β-hematin and the natural crystals shared the same unit cell and structure [20, 57]. In 2010 was analyzed and solved the structure of the hemozoin formed by the malaria parasite *P. falciparum* using X- ray power diffraction pattern. Once again it was proved that the parameters of the unit cell and of the Fe (III)-O bond length obtained through these crystals showed similarities with the ones of the β-hematin as well as with the ones formed in 2005 by the organisms *S. Mansoni* and *R. Prolixus*. The only difference found was bigger disarray on the Fe (III)-O bonds of the *P. falciparum's* hemozoin in relation to the β-hematin structure. In the study, hemozoin was characterized as a group of π-π dimers, which are linked by μ-propionate bonds and co-planar [20, 58].

1.3.3. Properties of hemozoin

Native and synthetic hemozoin can be characterized by their physical properties. The usage of different techniques of microscopy and spectroscopy have demonstrated that over the years the crystal size, crystallinity and uniformity of the hemozoin [20]. In studies related to the morphology of hemozoin, two techniques of microscopy are applied, scanning electron microscopy (SEM) and transmission electron microscopy (TEM) [16, 59, 60]. SEM has the aim of an extend micro-structural characterization of the samples, such as thickness, microstructure analysis, identifying defects and impurities [61]. TEM is a technique that allows obtaining the morphology, structure and local chemistry of metals, ceramics, polymers, biological materials and minerals. It also enables the investigation of crystal structures, crystallographic orientations through electron diffraction, as well as second phase, precipitates and contaminants distribution by X-ray and electron energy analysis [62, 63]. Studies have demonstrated that the crystal has well-defined faces [23] with 0.2-1.6 μm in size [16, 59]. Hemozoin is also birefringent, which is the capacity to depolarize light, thus allowing its detection by dark-field and polarization microscopy [30]. Determining the relationship between the external macroscopic morphology of the crystal (crystal habit) and the unit cell structure is important for the molecular understanding of the mechanism of hemozoin formation [59, 64].

The magnetic properties of the crystal are also subject of study. Techniques such as X-band electron paramagnetic resonance (EPR) and magnetic Mössbauer spectroscopy proved that native and synthetic hemozoin exist in a paramagnetic complex, high spin S=5/2 state [20, 30, 31]. Recently

in 2009, the luminescence properties were subject of study, by obtaining uv-visible spectrum of synthetic hemozoin. The crystalline product showed flourescence at 577 nm, either very dry or fully dehydrated [20].

1.4. Malaria diagnostic and detection devices

Nowadays different test and techniques exist that help with malaria diagnosis, however limitations in its applications have emerged (table 1.2). Malaria diagnosis involves identifying malaria parasites (parasitemia) or antigens/products in patient blood. Delays in diagnosis and treatment are leading causes of death in many countries. Several factors can influence the identification and interpretation of malaria parasitemia in a diagnostic test, as different stages of erythrocytic schizogony, the endemicity of different species, the interrelation between levels of transmission, population movement, parasitemia, immunity, drug resistance, persisting viable or non-viable parasitemia, sequestration of the parasites in the deeper tissues, and the use of chemoprophylaxis [65]. Other issues associated with a bad diagnosis is the poor maintenance of testing equipment and lack of experience or knowledge from the technicians interpreting the results, for example when observing the various stages of the parasite on the microscope [5]. Severe infectious diseases, such as tuberculosis or HIV/AIDS can complicate more patient evaluation [65].

Table 1.2 - Tests, Techniques and Limitations in Malaria Diagnostic [4, 5, 30, 37, 65, 66].

Diagnosis of Malaria	Tests and Techniques	Principle of the Method and Devices	Limitations
Clinical	Examination of patients	Based on the patients signs and symptoms, and on physical findings at examination	Non-specific nature of the signs and symptoms (overlapping of malaria with other diseases)
Laboratory	Peripheral blood smears	Visualization of morphological distinguishable stages of parasites under right microscope by thick and thin blood smear and staining	Require considerable expertise and trained healthcare workers; Examination is its relatively low sensitivity, particularly at low parasite levels
	Quantitative Buffy Coat (QBC) technique	Blood staining with acridine orange and detection by epifluorescent microscope	Requires expertise in reading; expensive; species identification may be difficult

Table 1.2 – Tests, Techniques and Limitations in Malaria Diagnostic (continuation).

Diagnosis of Malaria	Tests and Techniques	Principle of the Method and Devices	Limitations
Laboratory	Pigment Detection	Detection of hemozoin (malaria pigment) by Dark-field microscopy	Not as sensitive as thick blood films
	Rapid diagnostic tests (RDTs)	Detection of parasite antigens or enzyme	Show wide variations in sensitivity of remote malaria-endemic areas; have to be used in conjunction with other methods to confirm the results
	Serological tests	Detection of antibodies against parasites	Time-consuming; cannot be automated, which limits the number of sera that can be studied daily; requires fluorescence microscopy and trained technicians
Molecular	PCR technique	Specific amplification of malaria DNA	Lengthy procedure; high cost, and the need for specially trained technicians
	LAMP technique	Detection of turbidity by a turbidity meter after amplifying DNA sequences	Reagents require cold storage; clinical assays are needed to validate the feasibility and clinical utility
	Microarrays	Hybridization of DNA isolate and quantified by fluorescence-base detection	Low sensitivity; cumbersome procedures
	Flow cytometry (FCM) assay	Detection of hemozoin by flow cytometer	Labor intensiveness; need for trained technicians; costly diagnostic equipment, and that false positives may occur with other bacterial or viral infections
	Automated blood cell counters (ACC)	Use of depolarized laser light (DLL) to detection of malarial pigment in activated monocyte	More obvious if parasitemia > 0.5%
	Mass spectrophotometry	Identification of heme by direct ultraviolet laser desorption mass spectrometry (LDMS)	Expensive; still in early stages of development for diagnosis of malaria

The search for new diagnostic techniques which can reduce the interpretation error and that can identify the disease efficiently is of the utmost importance in non-endemic continents where its infected population is often asymptomatic [65]. In addition, it is also important in regions where malaria is endemic, and where often infections involve two or more species of *Plasmodium*; these mixed infections often go unrecognized or underestimated in diagnosis [67]. One of the biggest reasons for the need of innovation in testing equipment and diagnosis is the detection is severe malaria caused by the parasite *P. falciparum*, particularly cerebral malaria [68]. The infected red blood cells by *P. falciparum* have the ability of connecting themselves with the vascular endothelium through a process called cythoadherence. As a consequence sequestration phase of red blood cells occurs containing mature forms of the parasite in organs (heart, lung, brain, liver, kidney, subcutaneous tissues and placenta), early trophozoite stage (Fig. 1.6 B) to schizont stage (Fig. 1.6 C) rupture, where infected red blood cells (iRBCs) are no longer detectable in peripheral blood smears, complicating the diagnosis. Only infected red blood cells at the ring stage (Fig. 1.6 A) will circulate on the peripheral blood and might be detected [6, 10, 40, 69]. Early diagnosis allows effective case management and strategically helps to reduce malaria morbidity and mortality, to reduce the risk of parasite resistance to medicines and increases malaria surveillance [40].

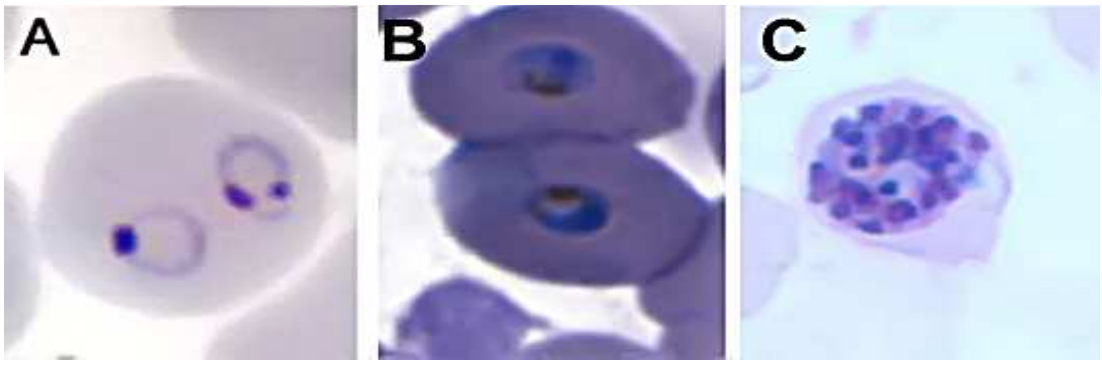

Figure 1.6 – Stages of malaria parasite on thin blood smear. This thin film Giemsa-stained micrographs reveals ring-stage (A) trophozoite-stage (B) and schizont-stage (C) of *Plasmodium falciparum* [70].

One of the possible techniques that can be used as an innovative method for malaria diagnosis is impedance spectroscopy (IS). This analytical technique can be applied to characterize the electric properties of materials, as solids and liquids electrolytes, electrical and structural ceramics, magnetic ferrites, polymers and protective paint films, batteries and fuel cells and also living tissue. When an electrical field is applied to an interface, crystallographic, mechanical, compositional, and electrical properties polarize in a unique way, modifying the charge distribution of the system under study [71]. Currently is utilized in the development of various biosensors. This method offers a complementary technique for in vivo detection of a variety of cancers including malignancy in the liver, bladder, skin and breast. Due to the invasion of the red blood cells by the malaria parasite morphological changes occur in the cytoplasm and cell membrane, causing biochemical changes. These modifications are associated to biophysical modifications of electrical, optical, mechanical, and magnetic properties. The variation in electrical properties of infected red blood cells can be detected by spectroscopy impedance and thus work as a diagnosis method [68, 72, 73].

1.5. Objectives of the work

The present work had two aims, first was the production of β-hematin (synthetic hemozoin) crystals under acidic conditions from hemin, using well-established protocols, and direct comparison of their microstructural features and passive electrical properties with the ones of native hemozoin crystals extracted of infected erythrocytes by *P. falciparum* Dd2 and 3D7 strains. Scanning electron microscopy (SEM), transmission electron microscopy (TEM) and impedance spectroscopy (IS) have been used as characterization techniques.

The second aim was to test a new technique of malaria diagnosis through impedance measurements in healthy RBC´s and infected RBC´s by *P. falciparum* Dd2 and 3D7 strains in synchronized and unsynchronized culture. The technique applied was impedance spectroscopy with two types of devices with the same principle measurement (circuit), but with variation in the frequency range measures (low and high frequencies), for determination of discrimination degree between impedances.

2. Material and Methods

2.1. Culture media and solutions

In the following section, from 2.1.1 to 2.1.6, are presented the constitutions and processes for the preparation of the culture medium as well as the solutions for the different protocols applied during the experimental work.

2.1.1. Culture medium (RPMI) complete for *Plasmodium falciparum*

Constituted by 1.04 % RPMI 1640 (Sigma), 25 mM HEPES (Sigma), 6.8 M Hypoxanthine (Sigma), 0.2% Sodium Bicarbonate (Merck), 0.5% AlbuMaxII (Invitrogen™).

2.1.2. Sodium Hydroxide solution

Prepared by 1:10 dilution of 1 M NaOH solution in ultrapure water (Milli-Q).

2.1.3. Hemin solution Protocol 1

Prepared by dissolving 21.2 mg of hemin (Sigma) in 4.5 ml of 0.1 M NaOH .

2.1.4. Hemin solution Protocol 2

Prepared by dissolving 13 mg of hemin in 5 ml of 0.1 M NaOH.

2.1.5. Sodium Bicarbonate solution

Prepared one solution of 100 mM Sodium Bicarbonate at pH 9.1 by dissolving 252.03 mg of $NaHCO_3$ (Merck) in 30 ml of ultrapure water (Milli-Q).

2.1.6. Solution A

Prepared by dissolving 50 mg of 0.5% SDS (Sigma) and 20 mg of proteinase K (2 mg/ml) (Sigma) in 10 ml of 10 mM TRIS-HCL (pH=8) solution (Sigma).

2.2. Production of synthetic hemozoin (β-Hematin)

2.2.1. Protocol 1

Prepared using a modified protocol of Slater *et al.* as follows [53]. After prepared 4.5 ml of hemin solution, was transferred 1 ml of solution to each four different tubes properly marked (Fig. 2.1). The hemozoin polymerizations were initiated by addition to each tube of 350 µl of glacial acetic acid (Sigma) and by heating at 80ºC overnight (approximately 12 hours) in heating block. The following day, tubes with pellet, synthetic hemozoin (sHz), were washed four times in ultra pure water (Milli-Q) centrifuged at 3300 xg for 15 min. and washed again two times for 3 hours in sodium bicarbonate solution with pH 9.1 and centrifuged at 3300 xg for 15 min. Finally tubes with pellet were washed four

additional times in ultrapure water (Milli-Q) centrifuged at 3300 xg for 15min., resuspended in 1 ml of PBS solution. The heme-equivalent of crystals has been determined from interpolation using standard hemin solution absorbances determined with a TRIAD Series LT Multimode Detector (Dynex Tecnologies), using a calibration curve (appendix A). Synthetic hemozoin was stored at 4ºC.

2.2.2. Protocol 2

After preparing 5 ml of hemin solution, 1 ml of solution was transferred to each five different tubes properly marked (Fig. 2.1). The hemozoin polymerizations were initiated by addition to each tube of 150 µl of ultrapure water and 150 µl of glacial acetic acid (Sigma) and incubation at 37º C overnight (approximately 24 hours). The following day, tubes with pellet, synthetic hemozoin (sHz), were centrifuged at 3300 xg for 15 min. and the supernatant discarded. Afterwards, the pellet was resuspended in 1 ml of DMSO (Sigma) and centrifuged at 3300 xg for 15 min. The previous process was repeated five and six times until supernatant becomes translucent. Finally, pellet was washed two times in ultrapure water (Milli-Q) by centrifuging at 3300 xg for 15 min and resuspended in 1 ml of PBS solution. The heme-equivalent of crystals has been determined from interpolation using standard hemin solution absorbances determined with a TRIAD Series LT Multimode Detector (Dynex Tecnologies), using a calibration curve (appendix A). Synthetic hemozoin was stored at 4ºC.

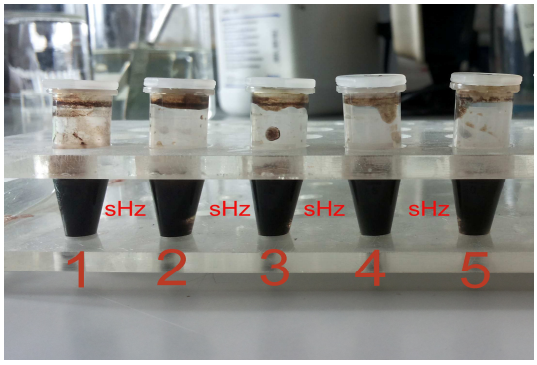

Figure 2.1 – Exemple of synthetic hemozoin production

2.3. Production of native hemozoin

2.3.1. Preparation of non-parasitized red blood cells

From healthy human donors was harvested 10 to 20 ml of venous blood (plus EDTA) - free of any kind of medication. Each sample is divided in 5 ml aliquots and centrifuged at 950 xg for 5 minutes in order to remove the leukocytes blood fraction. In order to wash the erythrocytes, the 10 ml of incomplete RPMI medium (without AlbuMaxII) were added to each sample followed by mixing through inversion. The mixture was centrifuged at 950 xg for 5 min. The supernatant was removed and this washing step was repeated two to three times.

To the final erythrocytes pellet was added 10 ml of (completed) RPMI medium. The erythrocytes cell suspension (50%) was preserved at 4℃ during, a max imum, of 15 days.

2.3.2. *In vitro* culture of *Plasmodium falciparum*

In vitro culture growing of *P. falciparum* clones, was performed according to Trager & Jensen (1976) [74], Thaithong *et al.,* (1994) [75] and Cranmer *et al.,* (1997) [76] with some modifications. In order to grow this type of *Plasmodium*, erythrocytes were maintained in RPMI culture medium at 37℃ with a 5% of CO_2. The hematocrit was considered to be 5%. The parasite development was assessed through the observation of blood smears stained with 20% Giemsa (Merck) using an optical microscope. When parasitemia reached 5 to 8% of infected erythrocytes, new dilutions and new cultures were made.

2.3.3. Extraction of native hemozoin from parasite cultures

P. falciparum (strain 3D7 and Dd2) hemozoin (or native hemozoin, nHz) was extracted of frozen culture with high parasitemia of trophozoites and schizonts (Fig. 2.2). First, frozen cultures were washed one time in ultra pure water (Milli-Q) centrifuged at 1900 xg for 10 min. and the supernatant aspirated. The pellet obtained was added to 10 ml of saponin solution (Sigma) and incubated at 37ºC until lysis was complete. After centrifuging at 1900 xg for 10min., the pellet was washed four times in ultra pure water centrifuged at 6600 xg for 5min., sonicated in 2% SDS (≈ 2min), washed four times with 2% SDS by centrifuged at 6600 xg for 5 min and then incubated overnight at 37ºC with solution A. After being washed two times with 2% SDS and undergoing centrifugation (6600 xg for 5min), the pellet was incubated in 6 M urea solution at room temp in an agitator for 6 hours and then washed two times with 2% SDS and two times with ultrapure water (Milli-Q) centrifuged at 6600 xg for 5min. Purified nHz was resuspended in 500 µl of ultrapure water. The heme-equivalents were determined by interpolation of standard hemin solution absorbances (read in TRIAD Series LT Multimode Detector (Dynex Tecnologies), using a calibration curve. Purified nHz was stored at 4ºC.

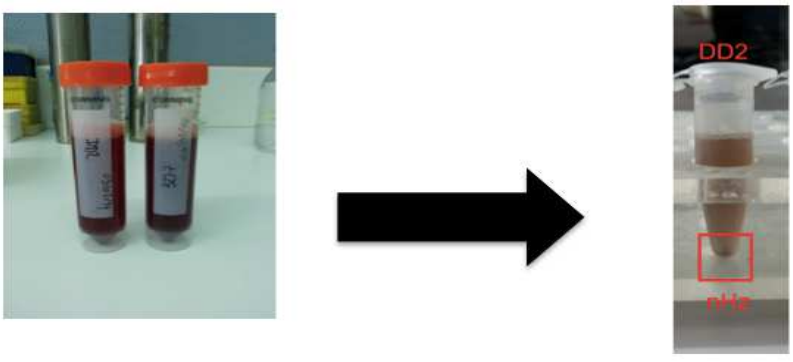

Figure 2.2 – Exemple of native hemozoin production

2.4. Hemozoin crystals quantitation (heme equivalents)

The amount of hemozoin in the ultrapure water and PBS buffer suspensions was quantified as heme-equivalents by interpolation in a standard calibration curve of hemin solution. First, it was prepared in an ELISA plate (Fig. 2.3) three equal wells with 4 mM of hemin solution + 0.1 M NaOH and three identical wells with hemozoin suspension + 0.1 M NaOH (depolymerization). Successive dilutions (1:2) were made from the 4 mM hemin solution plus NaOH. The same dilutions were applied in the hemozoin suspensions when necessary. After approximately 35 minutes, the plate was inserted in TRIAD Series LT Multimode Detector (Dynex Tecnologies) and the absorbance read at 405 nm. The standard concentrations of hemin were calculated using the following expression:

$$\boldsymbol{C}standard\ hemin = \frac{\boldsymbol{C}initial\ hemin\ solution\ x\ \boldsymbol{V}hemin\ solution\ well}{\boldsymbol{V}\ total\ well}$$

The calibration curve was made using the standard concentrations of hemin as *x* and the respective absorbances as *y* (appendix A). The concentration of hemozoin crystals was interpolated from the calibration curve.

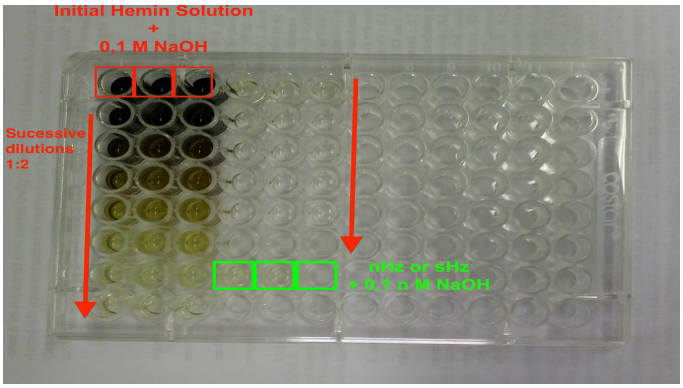

Figure 2.3 – Plate of ELISA with intial hemin solution (successive dilutions 1:2) and suspensions of hemozoin native or synthetic.

2.5. Scanning Electron Microscopy

2.5.1. Working principle

The **scanning electron microscope (SEM)** (Fig. 2.4) permits the observation and characterization of heterogeneous organic and inorganic materials on a nanometer (nm) to micrometer (µm) scale. The popularity of the SEM stems from its capability of obtaining three-dimensional-like images of the surfaces of a very wide range of materials. Although the major use of the SEM is to obtain topographic images in the magnification range 10-10.000 x, the SEM is much more versatile, as we shall now see. The fields of application of this technique range from the micro-structural characterization of the samples to applications in Geology, Medicine and Biology, powder characterization, as well as many others [61].

The two major components of an SEM are the electron column and the control console. The electron column consists of an electron gun and two or more electron lases, which influence the paths of electrons traveling down an evacuated tube. The base of the column is usually taken up with vacuum pumps that produce a vacuum of about 10^{-4} Pa. The control console consists of a cathode ray tube (CRT) viewing screen and the knobs and computer keyboard that control the electron beam. The electron gun generates electrons and accelerates them to energy in the range 0.1-30 keV (100-30.000 electron volts). The base of the column is usually taken up with vacuum pumps that produce a vacuum to remove air molecules that would impede the passage of the high-energy electrons down the column. The control console consists of an LCD viewing screen that digitally displays the detectors signal, knobs and a computer keyboard that controls the electron beam [61, 77].

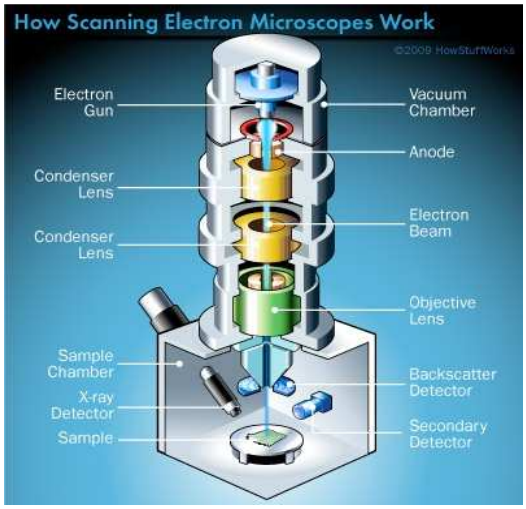

Figure 2.4 – Scanning Electron Microscope.

The SEM's principle of operation is based on an electron beam focused on the sample that originates on a cathode, usually made of tungsten heated by an electric current. The contrast in an image of SEM arises when the signal collected from the beam-specimen interaction varies from one location to another. When the electron beam (primary electrons) impinges on the specimen, many types of signal are generated and any of these can be displayed as an image. The electronics of the detector system converts the signals to point-by-point intensity changes on the viewing screen and produces an image. The two signals most often used to produce SEM images are secondary electrons (SEs) and backscattered electrons (BSE). The number of secondary electrons varies with geometry and other properties of specimen. Secondary electrons are collected when a positive voltage is applied to the collector screen in front of the detector. Then, electrons captured by the scintillator/photomultiplier are amplified for display on the viewing cathode ray tube (CRT) [61].

2.5.2. Preparation and analysis of specimens

SEM was used to observe of the morphology of sHz and nHz crystals in order to characterize their shape, size and structure. On top of metallic sample holder were placed 10 µl of nHz and sHz resuspended in ultrapure water (Milli-Q) and allowed to dry 3 to 4 hours in room temp (Fig. 2.5), using artificial light for acceleration of the drying process. Then, the specimens were coated two times with a

carbon layer in a Q150R Rotary-Pumped Sputter Coater/Carbon Coater and they were examined in a JEOL 7001F field emission scanning electron microscope, at *Instituto Superior Técnico*, using an accelerating voltage of 15.0 kV. Secondary electron images were acquired while operating the microscope in a low vacuum mode by digital photo documentation system.

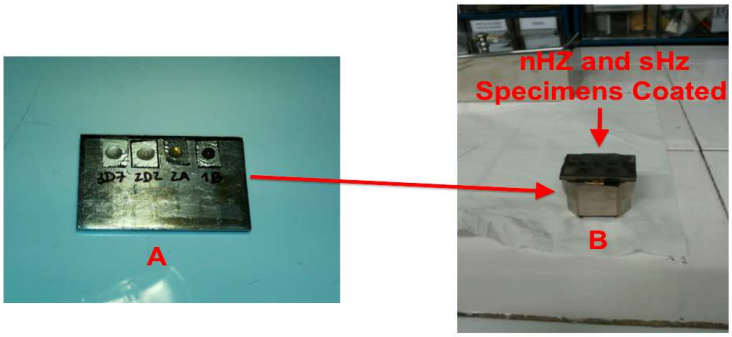

Figure 2.5 - Preparation of specimens (nHz and sHz suspensions) for SEM in room temp on top of metallic (A) sample holder (B).

2.6. Transmission Electron Microscopy

2.6.1. Working principle

The **transmission electron microscope (TEM)** (Fig. 2.6) has become the premier tool for the microstructural characterization of materials, since it allows detailed investigation of the morphology, structure, and local chemistry of metals, ceramics, polymers, biological materials and minerals [62, 63].

Magnifications of up to 500.000 times and resolutions below 100 pm are routinely achieved. Diffraction can be performed in regions smaller than 50 nm and quantitative and qualitative elemental analysis can be attained from features smaller than 10 nm. The instrument includes an electron gun, which emits electrons and accelerates them between a cathode and an anode. The most common types of transmission electron microscopes have thermionic guns capable of accelerating the electrons through a selected potential difference in the range 120 to 200 keV. The condenser lens system of the microscope controls the specimen illumination, which ranges from uniform illumination of a large area at low magnification, through a stronger focusing for high magnification observation. TEM specimen stage designs include airlocks to allow for the insertion of the specimen holder into the vacuum with a minimal increase in pressure in other areas of the microscope. The specimen holders are adapted to hold a standard size of grid upon which the sample is placed. The standard TEM grid size is a 3.05 mm diameter ring, with a thickness and mesh size raging from a few to 100 μm. The grid is typically made of copper, except when analytical methods are employed and in this case it can be made of molybdenum, gold or platinum, and is placed into the sample holder [63, 77].

By focusing the electron beam, diffraction patterns can be measured from microscopic regions, and it is often possible to select a single microcrystal for a diffraction measurement. The

optics of electron microscopes can be used to make images of the electron intensity emerging from the sample. For example, variations in the intensity of electron diffraction across a thin specimen, called “diffraction contrast,” is useful for making images of defects such as dislocations, interfaces, and second phase particles. This technique of “phase-contrast imaging” is used to form images of columns of atoms. Besides diffraction and spatial imaging, the high-energy electrons in TEM cause electronic excitations of the atoms in the specimen. “Analytical TEM” uses two types of spectrometries to obtain chemical information from electronic excitations, energy-dispersive x-ray spectrometry (EDS) and electron energy-loss spectrometry (EELS) [62].

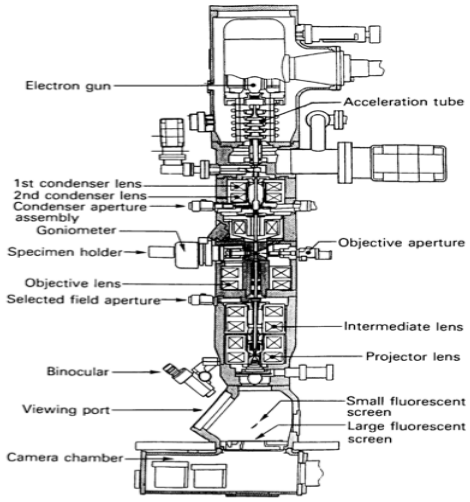

Figure 2.6 - Transmission electron microscope [62].

By positioning an “objective aperture” at a specific location in the back focal plane, an image is made with only those electrons that have been diffracted by a specific angle. This defines two imaging modes, **Bright- field and a Dark-field** (Fig. 2.7) [62].

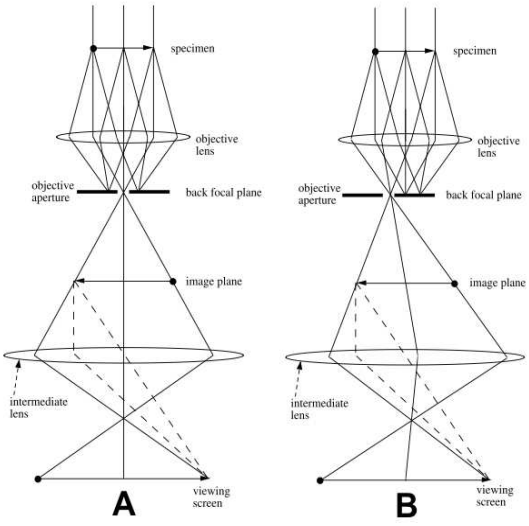

Figure 2.7 - Bright- field (A) and Dark-field (B) TEM imaging modes [62].

• When the aperture is positioned to pass only the transmitted (un-diffracted) electrons, a *bright-field* (BF) image is formed [62].

• When the aperture is positioned to pass only some diffracted electrons, a *dark-field* (DF) image is formed [62].

2.6.2. Preparation and analysis of specimens

TEM was used for the analysis of the microstructure of the sHz and nHz crystals in order to characterize their shape, size and structure. On top of mounting grid with absorbent paper underneath were dropped 10 µl of nHz and sHz resuspended in ultrapure water (Milli-Q) dispersing the crystals of hemozoin. The hemozoin was allowed to dry at room temperature. Since the solvent does not react with the sample material only the hemozoin crystals were left in the grid. Then, the grid was inserted in Gatan TEM sample holders (Fig. 2.8) and examined in Hitachi H8100 transmission electron microscope, at *Instituto Superior Técnico*, using an accelerating voltage of 200 kV. Bright-field images were acquired by digital photo documentation system.

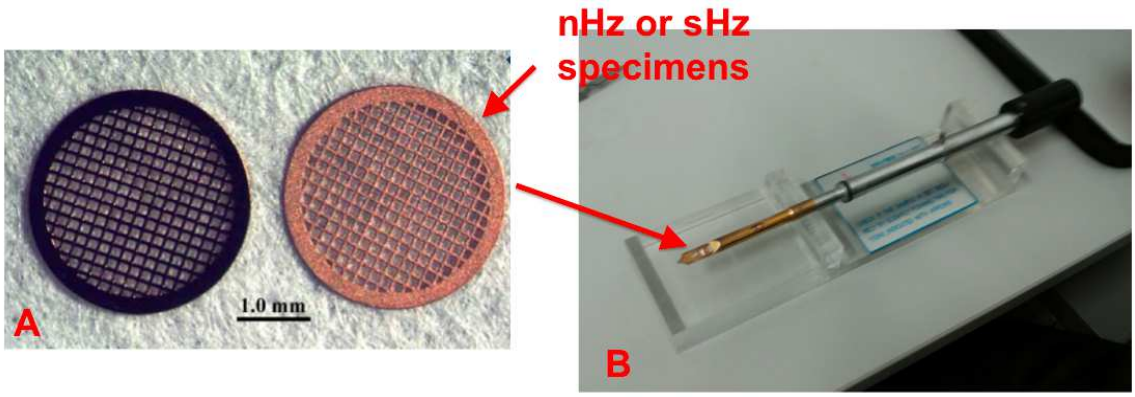

Figure 2.8 - Preparation of specimen (nHz and sHz suspensions) for TEM in grid (A) and inserted in Gatan sample holders (B).

2.7. Impedance Spectroscopy

2.7.1. Method principle

Electrical impedance is the measure of the opposition that a circuit presents to a current when a voltage is applied. Ohm's Law states that the current (I) passing through two points of a metallic wire is directly proportional to the potential difference (V) between those points. The proportionality constant is the resistance (R), given by Eq. 1.

$$R = \frac{V}{I} \qquad \text{Eq. 1}$$

For an AC circuit, it is necessary to consider the concept of Impedance (Z), since in this type of circuit is necessary to account the effect of the inductance and capacitance of the conductors.

The impedance is represented by the complex ratio described in Eq. 2:

$$Z = |Z|e^{j\theta} \quad \text{Eq. 2}$$

Where |Z| corresponds to the ratio of the voltage amplitude to the current amplitude, and θ corresponds to the phase-shift between the applied signal (excitation signal) and the response (output) signal. This phase-shift is known by relaxation time and corresponds to the time required for a perturbed system, previously in equilibrium, to find a new equilibrium state. The characteristics of amplitude and phase obtained represent the polar form of the impedance.

The impedance can be also converted and represented in Cartesian form described in Eq. 3:

$$Z = R + jX \quad \text{Eq. 3}$$

Where R corresponds to the real part, equivalent to electrical resistance and X to the imaginary part, which represent the reactance.

In conclusion, electrical impedance is the total resistance of an AC circuit, i.e. when a certain component creates resistance and wastes energy as heat. If the component doesn't waste energy as heat then it is called reactance. Both resistance and reactance are components of what it is called impedance [71, 78, 79].

Impedance spectroscopy is an analytical technique that allows the study of dielectric materials, i.e. solids and liquids that are polarized when an electrical field is applied but do not conduct electricity in the same manner as an electrical wire. The technique can be divided in two branches: electrochemical impedance spectroscopy (EIS), which deals with aqueous electrochemistry and impedance spectroscopy (IS) that describes all the other measurements dealing with solid electrolytes [71].

When a low conductivity material is perturbed by an external electrical field, a number of processes will take place throughout the cell, including the transport of electrons through electronic conductors, transfer of electrons at electrode–electrolyte interfaces to or from charged or uncharged atomic species which originate from the cell materials and its atmospheric environment (oxidation or reduction reactions). The responses of the different processes can spread out through 12 orders of magnitude in the frequency range. Interfacial processes can require a sweep down to frequencies as low as 10 µHz for adequate resolution. On the other hand, bulk response can be observed up to 50 MHz. Impedance spectroscopy offers the possibility to separate the kinetics of the different processes involved in a single experiment, simply by sweeping the frequency of the applied AC excitation signal. Similarly to other spectroscopy techniques (visible, FTIR and others), certain phenomenon will

typically respond at specific frequencies and that information allows the sample under study to be characterized [71, 80].

2.7.2. Measurement Principle

In this present work, two different impedance spectroscopy devices were used. The first one has the ability of reading low frequencies, $I_{freq} \in$ [10 kHz – 82.5 kHz], and the second one was the ability of reading high frequencies such as $I_{freq} \in$ [250 kHz – 5 MHz]. The principle underlying the operation of both devices is the same being the read frequencies the only distinction. Its operation is presented in Fig. 2.9.

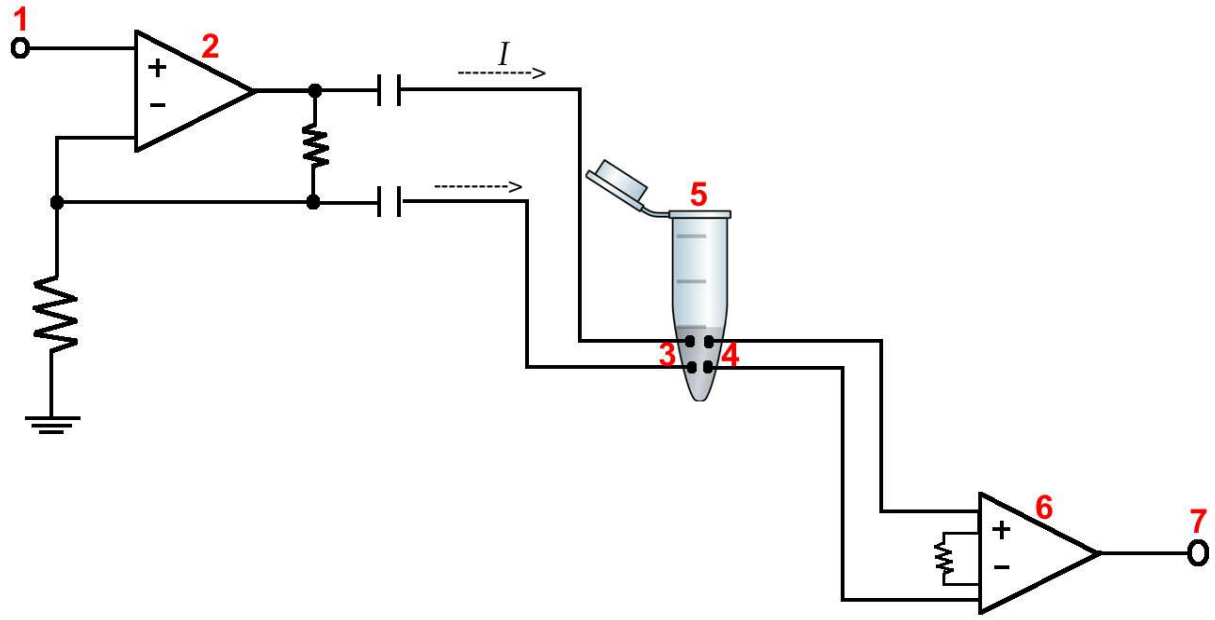

Figure 2.9 – Measurement principle of impedance spectroscopy for low and high frequencies devices.

The input signal of the circuit (Fig. 2.9) is a voltage (V_i) (1) which is converted to an output current (I_o) (2) due to the transcondutance amplifier. With the increasing of the signal's frequency, the current (I_o) is applied to the sample being analyzed (5) by two electrodes (3). At the same time, a voltage (V) is measured in the same sample (4). The resulting impedance is measure by a potential difference and will correspond to the electrical resistance (R), according to Ohm's Law (equation 1). Since the signal obtained has low amplitude, its value (real data) is amplified using an instrumentation amplifier (6) and then is quantized into binary data, $V_{impedance}$ (7).

With the high frequencies circuit a Crest Factor of 1.405 for excitation signal was used in order to normalize the amplitude of the signal to the peak-to-peak values of the sine wave, thus allowing for a better discretization of the signal.

2.7.3. Experimental protocol

2.7.3.1. Synchronization of in vitro cultures of *Plasmodium falciparum*

Since all *P. falciparum* development stages (rings, trophozoites, schizonts and occasionally gametocytes) were observed during in vitro culture of erythrocytes it is important to achieve synchronization of the cultures before the execution of impedance spectroscopy assays.

The osmotic fragility of malaria-infected erythrocytes is known to increase during the development of the parasite [81, 82]. Based in this observation, synchronization was achieved by applying an osmotic shock to erythrocytes using sorbitol (5%) for that purpose [83]. Cultures presenting a 10% level of parasitemia, with predominance of young parasites, were centrifuged (676 xg during 5 minutes). The supernatant was discard and to the pellet were added 10 volumes of 5% D-Sorbitol (Merck) previously sterilized by filtration (0.2 µm filters, Millipore). After 10 minutes of incubation at 37℃, the mixture was centrifuged and washed twice with RPMI (without plasma). The erythrocytes pellet, recovered after the last centrifugation, was resuspended in the already stated culture conditions. If required, this protocol can be repeated 6 to 8 hours later.

2.7.3.2. Parasitemia determination

During the manipulation of *in vitro* cultures of *P. falciparum*, the parasitemia was determined from blood smears by counting 4000 erythrocytes per sample and is given as number of parasites per 100 erythrocytes – (erythrocytes infected/ total erythrocytes counted) x 100.

2.7.3.3. Non-parasitized and parasitized red blood cells assays

Having in mind the culture parasitemia calculated in 2.7.3.2 can proceed to the non-parasitized and parasitized red blood cells assays. For that purpose, two different tubes were prepared: A – RBCs parasitized with *P. falciparum* (strain 3D7 or Dd2) and B – healthy RBCs thus being non-parasitized (control).

Each tube with RBCs parasitized was submitted to four different conditions: the first one was an assay in culture medium (RPMI) with all parasite stages present (1A); the second one was an assay performed in culture medium (RPMI) but just with ring stage (2A); the third one was an assay performed in Whole Blood (WB) from the donor in which were present all parasite stages (3A); a four assay performed in Whole Blood (WB) from the donor synchronized for the ring stage (4A); the last assay was performed again in WB but this time it was synchronized for the schizont stage (5A). The procedure can be summarized in table 2.1.

Each mixture was then consecutively diluted (1:2) six to eight times with RPMI + uninfected RBCs (1A and 2A) or WB (3A, 4A and 5A). Finally, using the previously built impedance spectroscopy devices (Fig. 2.10), the non-parasitized and parasitized red blood cells assays were analyzed in two

different electrodes configuration (parallel and cross) by reading their phase (θ) and amplitude (Ohm). Through the data obtained we proceeded to the construction of Nyquist plots.

Table 2.1 - Preparation of non-parasitized and parasitized red blood cells assays.

Tubes	Assays in Culture Medium (RPMI) / Unsynchronized Culture (all stages) (1)	Assays in Culture Medium (RPMI) / Synchronized Culture (ring stage) (2)	Assays in Whole Blood (WB) from the donor / Unsynchronized Culture (all stages) (3)	Assays in Whole Blood (WB) from the donor / Synchronized Culture (ring stage) (4)	Assays in Whole Blood (WB) from the donor / Synchronized Culture (schizont stage) (5)
A	1.12% Infected RBCs (parasitemia) that were in culture medium + Culture Medium (≈ 5% hematocrit)	2% Infected RBCs (parasitemia) that were in culture medium + Culture Medium (≈ 5% hematocrit)	1.12% Infected RBCs (parasitemia) that were in culture medium + Whole Blood (RBCs, WBCs and Plasma) from the donor (≈ 45% hematocrit)	2% Infected RBCs (parasitemia) that were in culture medium + Whole Blood (RBCs, WBCs and Plasma) from the donor (≈ 45% hematocrit)	2% Infected RBCs (parasitemia) that were in culture medium + Whole Blood (RBCs, WBCs and Plasma) from the donor (≈ 45% hematocrit)
B (control)	Uninfected RBCs + Culture Medium (≈ 5% hematocrit)	Uninfected RBCs + Culture Medium (≈ 5% hematocrit)	Whole Blood (RBCs, WBCs and Plasma) from the donor (≈ 45% hematocrit)	Whole Blood (RBCs, WBCs and Plasma) from the donor (≈ 45% hematocrit)	Whole Blood (RBCs, WBCs and Plasma) from the donor (≈ 45% hematocrit)

2.7.4.4. Hemozoin crystals assays

From the previous assays it is known that sHz samples obtained using protocol 1 had a concentration of 10.79 mM and those obtained using protocol 2 had a concentration of 1.48 mM. On the other hand the nHz sample extracted and purified from *P.falciparum* strain Dd2 culture had a concentration 1.35 mM.

In order to analyze both samples, two distinct tubes were prepared, in PBS buffer, containing sHz (protocol 1 and protocol 2) with an equal concentration, in terms of heme equivalents, as the nHz. Successive dilutions (1:4) were made from each tube using PBS buffer as solvent. Finally, using the previously built impedance spectroscopy devices (Fig. 2.10), the nHz and sHz assays were analyzed in two different electrodes configuration (parallel and cross) by reading their phase (θ) and amplitude (Ohm). Through the data obtained we proceeded to the construction of Nyquist plots.

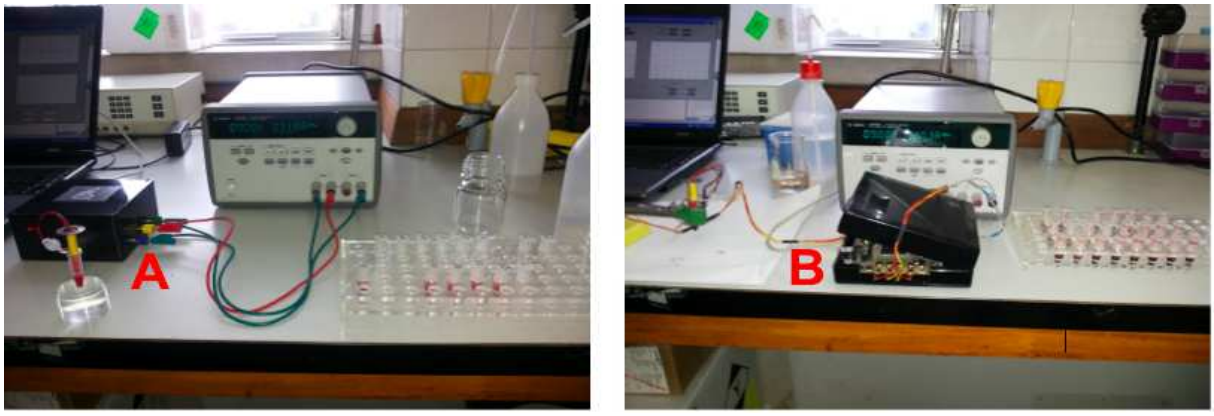

Figure 2.10 – Impedance spectroscopy assays with high frequencies device (A) and low frequencies device (B).

3. Results

3.1. Characterization and properties of different hemozoin crystals

3.1.1. Scanning Electron Microscopy

In **Figures 3.1 and 3.2** it is possible to observe images obtained through SEM with different magnifications, where A (1, 2 and 3) corresponds to micrographs of the nHz from *P. falciparum* strain 3D7's; B (1, 2 and 3) corresponds to micrographs of the nHz from *P. falciparum* strain Dd2's; C (1, 2 and 3) corresponds to micrographs of β-hematin chemically synthesized (sHz) using protocol 1; D (1, 2 and 3) corresponds to micrographs of β-hematin chemically synthesized (sHz) using protocol 2.

On micrographs A1, A2 and B2 it can be observed the heterogeneity of the crystals size, showing a very regular form. Its morphology exhibits very well defined faces, with flat and smooth shapes. Moreover, some crystals present large shapes and some small ones as well, with lengths ranging from 0.2 µm to 1.4 µm, and width ranging from 100nm to 500 nm. During the observation of these crystals on SEM it was possible to verify that they easily aggregate to each other, as it can be seen in micrographs A1, A2 and B2. In the right side of micrograph B2 it can be found a structure of crystals with brick-like shapes. Notably, in micrograph A3 and B3 it can be observed two crystals with a uniform shape on its sides, similar to parallelepiped, with length 1.6 µm and width 300 nm (A3), and length 1.4 µm and width 200 nm (B3). Some crystals contain membranes and proteins aggregated which weren't completely removed during the process of extraction and purification to the nHz (A1 and B2).

On the micrographs of protocols 1 and 2 it can be observed the heterogeneity of the different sizes of the crystals. Micrographs D corresponding to protocol 2 show less heterogeneity in crystals. The micrographs C show the presence of some thinner crystals and micrographs D show larger crystals. All micrographs crystals show lengths ranging from 0.2 µm to 1.5 µm, and width ranging from 80 nm to 250 nm. Notably, the shape of some crystals is more extended in different directions, like a needle, as it can be observed in micrographs C and D. Moreover, these crystals showed similarities with parallelepiped but with some irregularities in its shape.

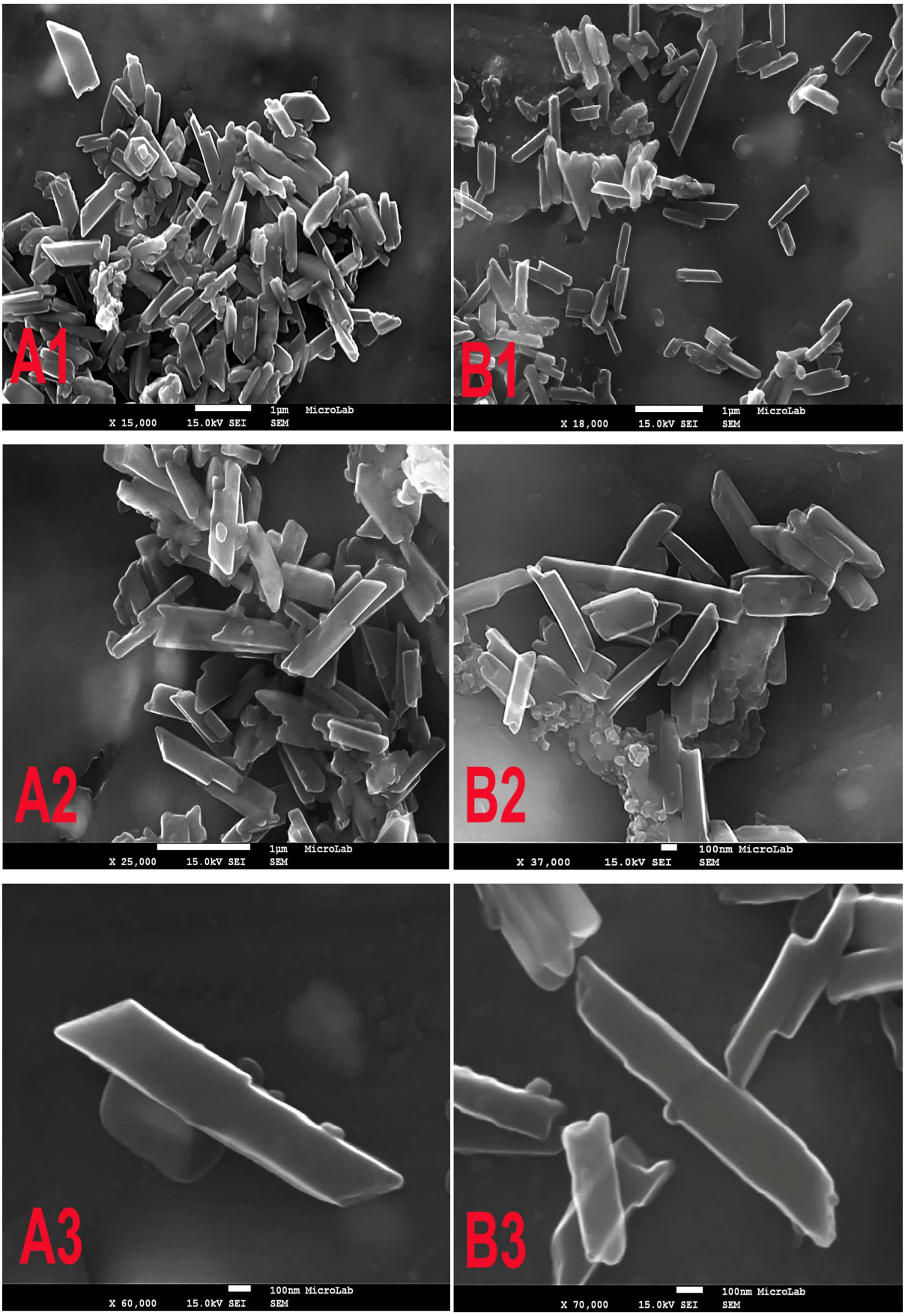

Figure 3.1 – Electron micrographs showing heterogeneity of shape and size for crystals of native hemozoin. FEG-SEM images (SEs) of hemozoin from *P. falciparum* strain 3D7 (A1, A2 and A3) and Dd2 (B1, B2 and B3) for different magnifications.

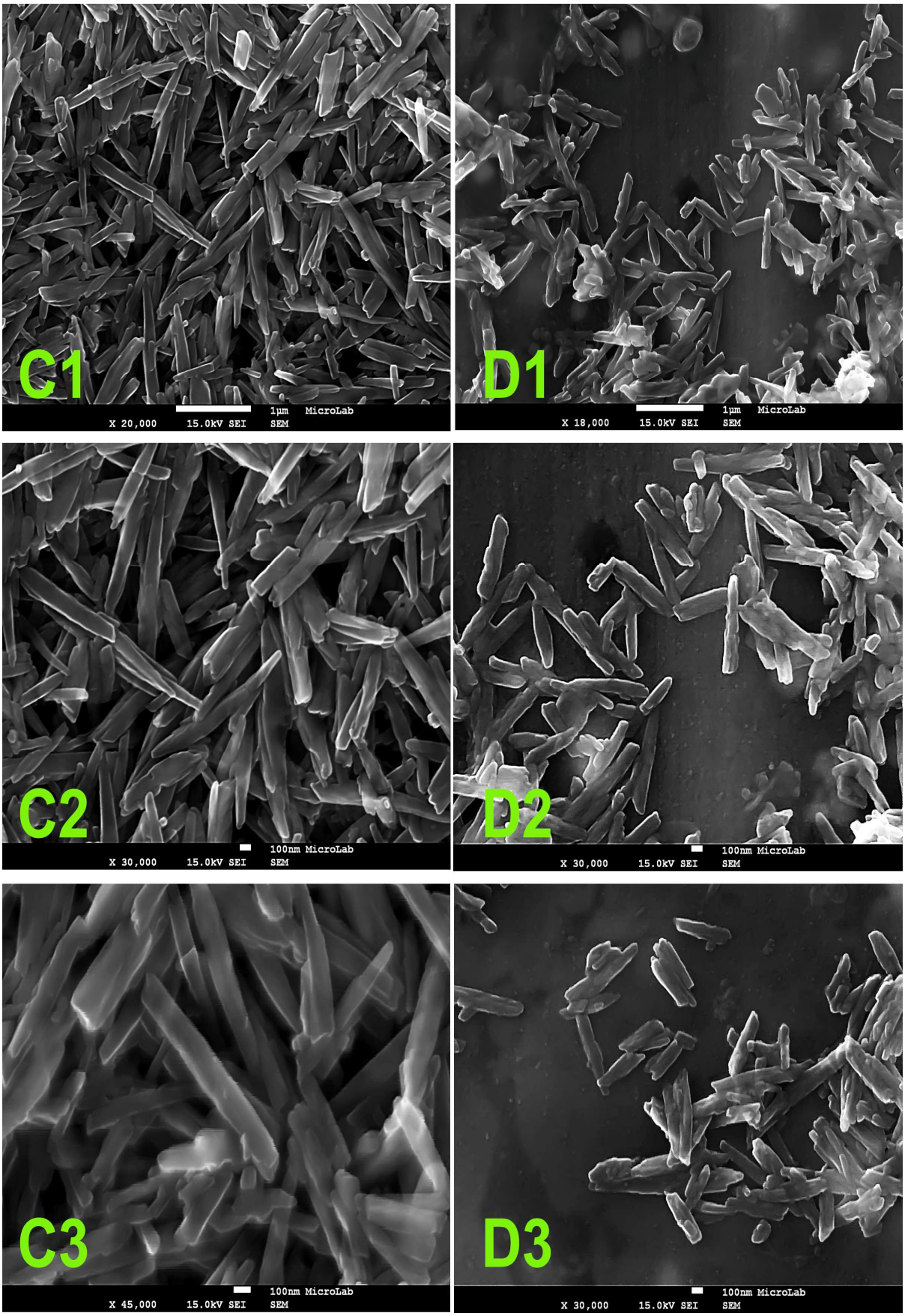

Figure 3.2 - Electron micrographs showing heterogeneity of shape and size for crystals of β-hematin (synthetic hemozoin). FEG-SEM images (SEs) of synthetic hemozoin produced from Protocol 1 (C1, C2 and C3) and Protocol 2 (D1, D2 and D3) for different magnifications.

3.1.2. Transmission Electron Microscopy

In **Figures 3.3, 3.4 and 3.5** it is possible to observe images obtain through TEM with different magnifications, where E (1, 2, 3 and 4) corresponds to micrographs of the nHz from P. falciparum strain 3D7's; F (1, 2, 3 and 4) corresponds to micrographs of the nHz from P. falciparum strain Dd2's; G (1, 2 and 3) corresponds to micrographs of β-hematin chemically synthesized (sHz) using protocol 1; H (1, 2 and 3) corresponds to micrographs of β-hematin chemically synthesized (sHz) using protocol 2.

On micrographs E1 and F1 a great heterogeneity of crystals' size can be observed, with length ranging from 0.3 µm to 1.4 µm, and width ranging from 100 nm to 400 nm. Like in SEM, in every micrograph the crystals present a well-defined morphology with regular plane faces similar to those of a parallelepiped. In micrograph F1 it can be observed that the crystals' microstructure shows up worn at the edges of its faces thus originating shapes more rectangular than parallelepiped, as well as crystals with brick-like shapes with different dimensions and located on the right side of the micrograph. In micrographs E2 and F2 the increased magnification allowed for a better observation of the microstructures, taking the morphology of a parallelepiped. Adopting this morphology, the dimensions for crystals in E2 are 900 nm x 200 nm x 100 nm, and for the ones in F2 the dimensions are 700 nm x140 nm x 50 nm (1) and 790 nm x 150 nm x 50 nm (2). The two micrographs, E4 and F4, which correspond to the magnification of the faces' edges of the crystals shown in micrographs E2, E3 and F3, which allow for their microstructure to be observed in great detail. In this area it is possible to see that the crystal is organized in several layers (indicated by the yellow arrow) evenly distributed along a diagonal line.

For the different synthetic hemozoin crystals shown in micrographs G1 and H1, it can be observed the heterogeneity in their shape and size, this being greater for G1. Long and thin shapes, similar to a blade or a needle, are observed on the crystals in micrographs G, with length ranging from 0.14 µm to 1.8 µm, and width ranging from 40 nm to 150 nm. On the same micrographs there are some crystals that show plane faces and with more uniform surfaces on the sides. In micrographs H frequently observed crystals with more regular shapes and plane faces, similar to a parallelepiped or a rectangle. There are also in these micrographs crystals shaped like needles, although they are less frequent. The crystals in micrographs H have lengths ranging from 0.18 µm to 1.25 µm, and width ranging from 50 nm to 150 nm. By observing the microstructure of the crystals at higher resolutions, like in micrographs G2, G3, H2 and H3, it is verified that their organization has no layers and that there is some irregularities in their shaping.

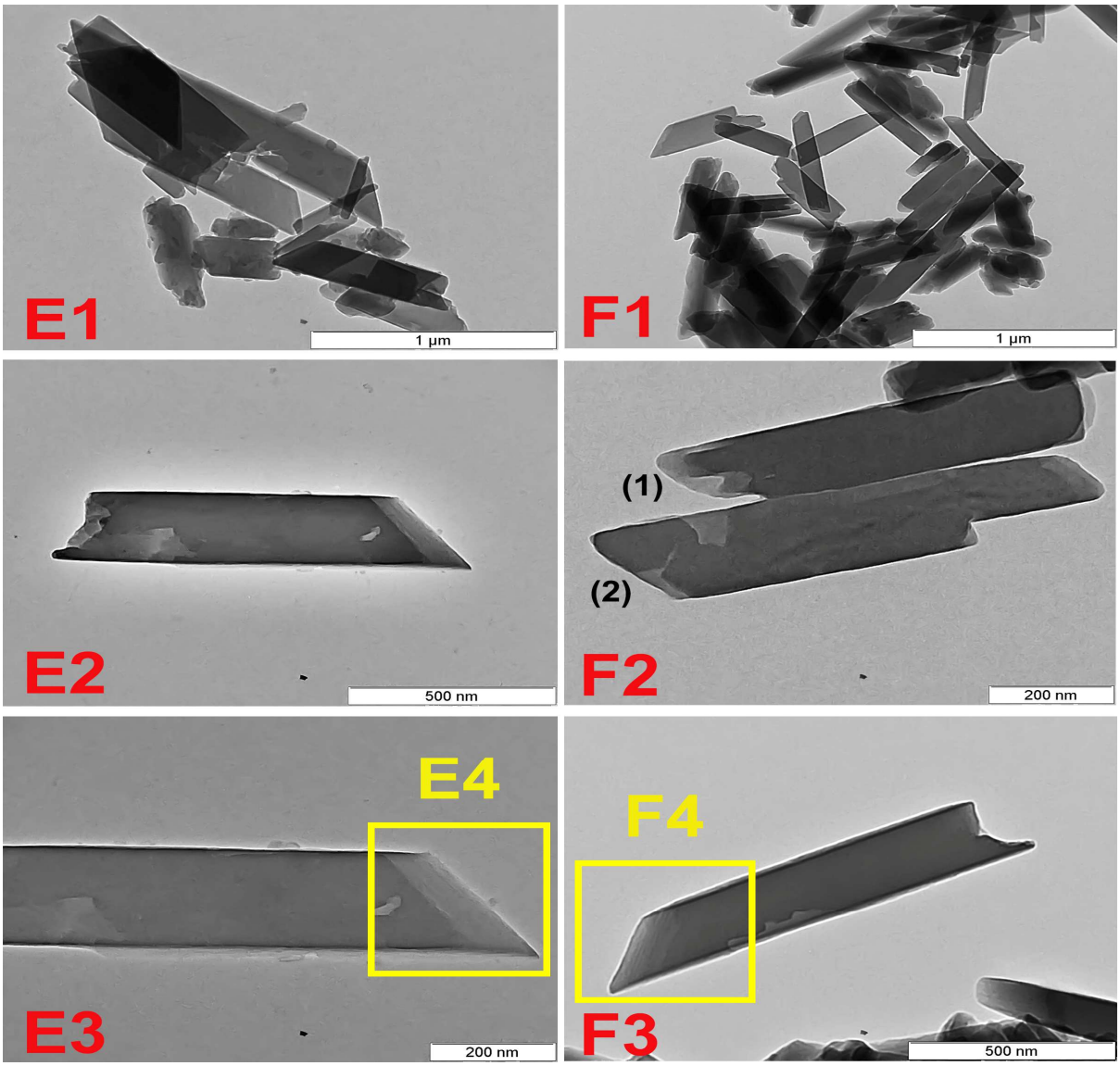

Figure 3.3 - Electron micrographs showing heterogeneity of shape and size for crystals of native hemozoin. TEM bright-field images of hemozoin from *P. falciparum* strain 3D7 (E1, E2 and E3) and Dd2 (F1, F2 and F3).

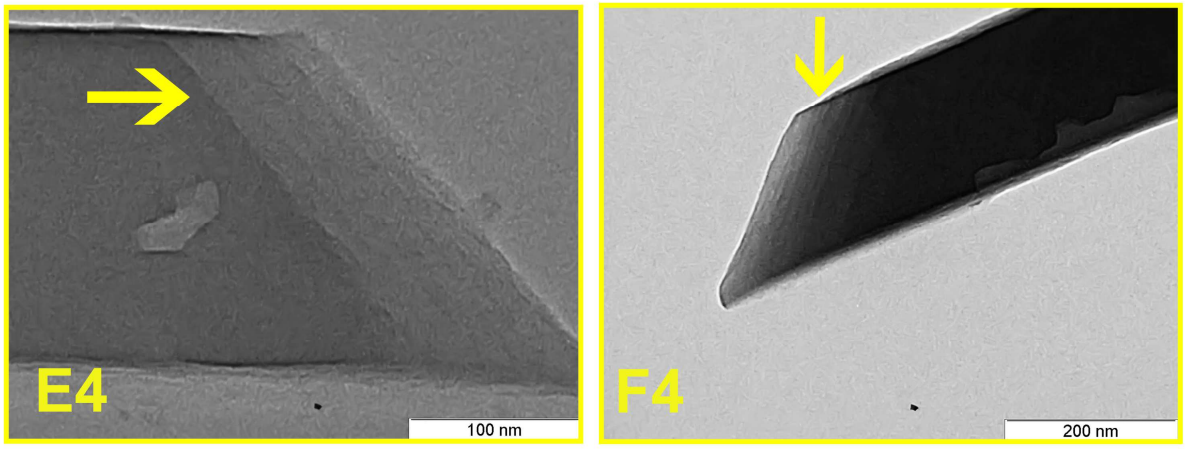

Figure 3.4 - Electron micrographs showing the various layers (indicated by yellow arrow) which form the face of native hemozoin crystals. TEM bright-field images of hemozoin from *P. falciparum* strain 3D7 (E4) and Dd2 (F4).

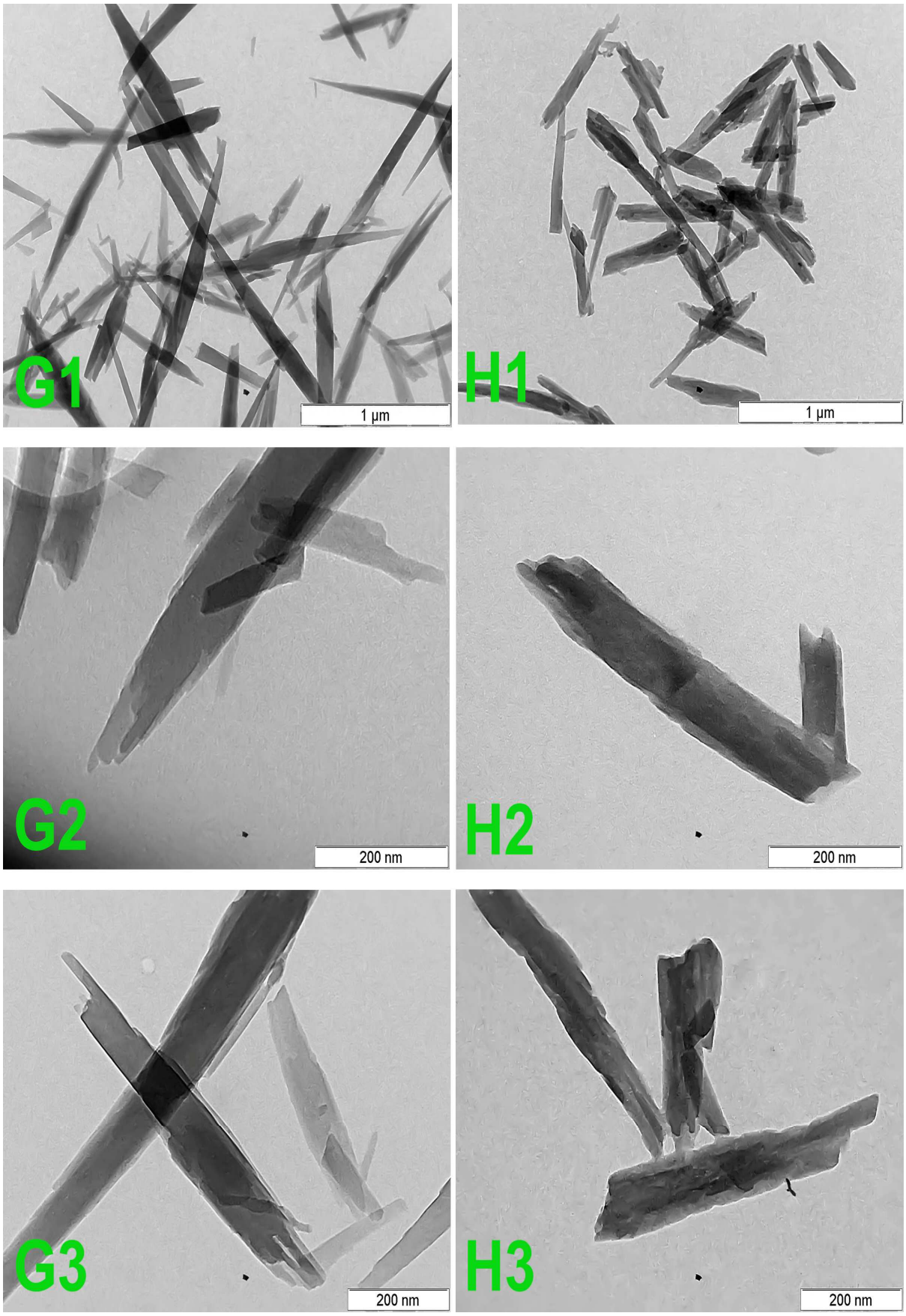

Figure 3.5 - Electron micrographs showing heterogeneity of shape and size for crystals of β-hematin. TEM bright-field images of synthetic hemozoin produced from Protocol 1 (G1, G2 and G3) and Protocol 2 (H1, H2 and H3).

Table 3.1 - Summary of the characteristics (morphological and size) of the native (*P. falciparum* strains 3D7 and Dd2) and synthetic (Protocols 1 e 2) crystals obtained by SEM and TEM.

	Microscopia Electrónica de Varrimento (MEV)			
	nHz 3D7	**nHz Dd2**	**sHz Protocol 1**	**sHz Protocol 2**
Micrographs	**A**	**B**	**C**	**D**
Morphology	Shapes: - Parallelepiped - Heterogeneous Well defined faces: - Planes - Regulars	Shapes: - Parallelepiped - Heterogeneous - Rectangular (brick-like) Well defined faces: - Planes - Regulars	Shapes: - Thins - More heterogeneous	Shapes: - Large - Heterogeneous
Length (µm)	0.2-1.6	0.2-1.4	0.2-1.5	0.2-1.5
Width (nm)	100 -500	100- 500	80-250	80-250
	Microscopia Electrónica de Transimssão (MET)			
Micrographs	**E**	**F**	**G**	**H**
Morphology	Shapes: - Parallelepiped - Heterogeneous Well defined faces: - Planes - Regulars - Organized in several layers	Shapes: - Parallelepiped - Heterogeneous - Rectangular (brick-like) Well defined faces: - Planes - Regulars - Organized in several layers	Shapes: - Long - Thins - Blade - Needle - More heterogeneous Well defined faces: - Without several layers	Shapes: - Parallelepiped - Rectangular - Needle - Heterogeneous - Some irregularities Well defined faces: - Regulars - Planes - Without several layers
Length (µm)	0.3-1.4	0.3-1.4	0.14-1.8	0.18-1.25
Width (nm)	100 - 400	100- 400	40-150	50-150
Depth (nm)	100	50	-	-

3.1.3. Impedance Spectroscopy

The following are overlapped Nyquist graphs related to impedance measurements carried out in suspensions of native hemozoin (strain Dd2) and synthetic hemozoin (Protocol 1 and Protocol 2), with equal initial concentrations of 1.35 mM successively diluted with PBS on 1:4 (Fig. 3.6 to 3.9). The graphs are ordered from 1 (highest concentration) to 5 (lowest concentration), in order to analyze the evolution of the impedance with the decreasing of the concentration of the crystals in a PBS environment, and at the same time compare and characterize the passive electric properties of the different hemozoin crystals both naturally (extracted from *Plasmodium falciparum in vitro* cultures) and chemically obtained. The suspensions were analyzed using two identical devices but with different ranges for the frequency of the excitation signal - one with a high frequency range, the other with a low frequency range - and likely to operate in the traditional tetrapolar configuration for impedance measurement with variable arrangement of electrodes, crossed and parallel.

The qualitative analysis of the Nyquist graphs for **low frequencies** in a crossed configuration (Fig. 3.6) shows that the evolution of the impedance curves exhibits a large discrepancy in electrical resistance and reactance with the decreasing concentration (1 to 5), without any coherence. In the parallel configuration (Fig. 3.7) the evolution of the impedance curves of the crystals remained unchanged with decreasing concentration, with the exception of graphs 1 and 3, where nHz and sHz P1 suffer incoherent changes in the impedance curve, showing quite high reactance.

The qualitative analysis of the Nyquist graphs for **high frequencies** shows that the evolution of the impedance curves exhibits a greater coherence. For the crossed configuration (Fig. 3.8), nHz and sHz P2 show impedance curves in which the electrical resistance and reactance decrease with the decreasing concentrations over the graphs (1 to 5). However, sHz P1 impedance curves show that there is an increase (5) in electrical resistance while at the same time a decrease in reactance (1 to 5) with the decreasing concentrations over the graphs (1 to 5). With the evolution of the graphs (1 to 5) is it possible to observe the approach of the impedance curves of nHz, and sHz P1 and P2, to the impedance curve of the PBS (white) (5). The impedance curves of nHz and sHz P2 almost overlap and they also present an identical evolution in terms of reactance and electrical resistance (1 to 5), which makes this the most noticeable result on the graph showing a concentration of 0.337 mM (2). Although some impedance curves of sHz P1 also overlapping the curves of nHz and sHz P2 (1 to 5), these however show some inequality in its evolution.

By changing the configuration of the electrodes for the parallel configuration (Fig. 3.9), it can be verified that the evolution of the graphs of nHz and sHz P1 and P2 are similar to those of the crossed configuration, but with impedance curves that exhibit higher reactance and electrical resistance, that are very slowly approaching the impedance curve of the PBS (white) (1 to 5). In the impedance curves nHz and sHz P2 reactance does not vary much, however the electrical resistance shows a slight decrease with the decreasing concentration over the graphs (1 to 5). Again, it is possible to observe strong similarities and greater overlapping in the impedance curves of nHz and sHz P2 (1 and 2) than what is observed in the crossed configuration curves. As in the crossed configuration, impedance curves of sHz P1 show decreasing reactance (1 to 5) and an increase in

electrical resistance (1 and 5) as the concentration decreases over the various graphs (1 to 5), presenting a great inequality and without much overlap in relation to the impedance curves of nHz and sHz P2.

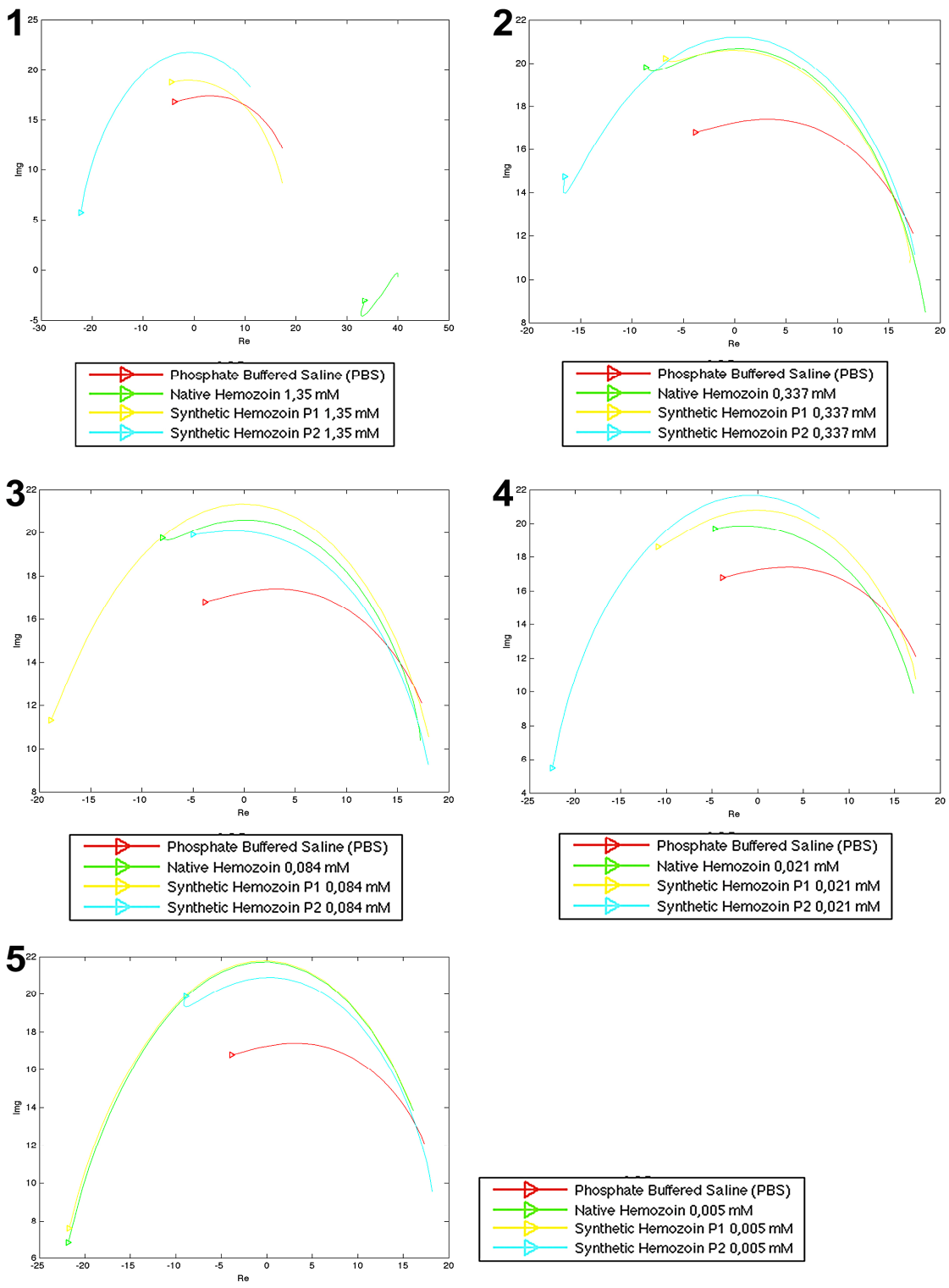

Figure 3.6 – Nyquist plots of impedance spectroscopy for native (*P. falciparum* strain Dd2) and synthetic (Protocol 1 and 2) hemozoin crystals assays with low frequencies device, $I_{freq} \in$ [10 kHz – 82.5 kHz], using electrodes in parallel configuration. The nyquist plots overlaid on the image shows the variation of impedance in function of a frequency response for hemozoin (nHz and sHz) suspensions concentrations in PBS (white). Concentrations 0.337 mM (2), 0.084 mM (3), 0.021 mM (4) and 0.005 mM (5) were obtained from successive dilutions 1:4 an initial concentration of 1.35 mM (1). The initial value of the impedance and of the lower frequency (10 kHz) is represented by the symbol **Δ** in each plot**.** The Nyquist plot has a Real part (x axis), equivalent to electrical resistance in Ohms, and an Imaginary part (y axis), given by reactance in Ohms, which together constitute the impedance.

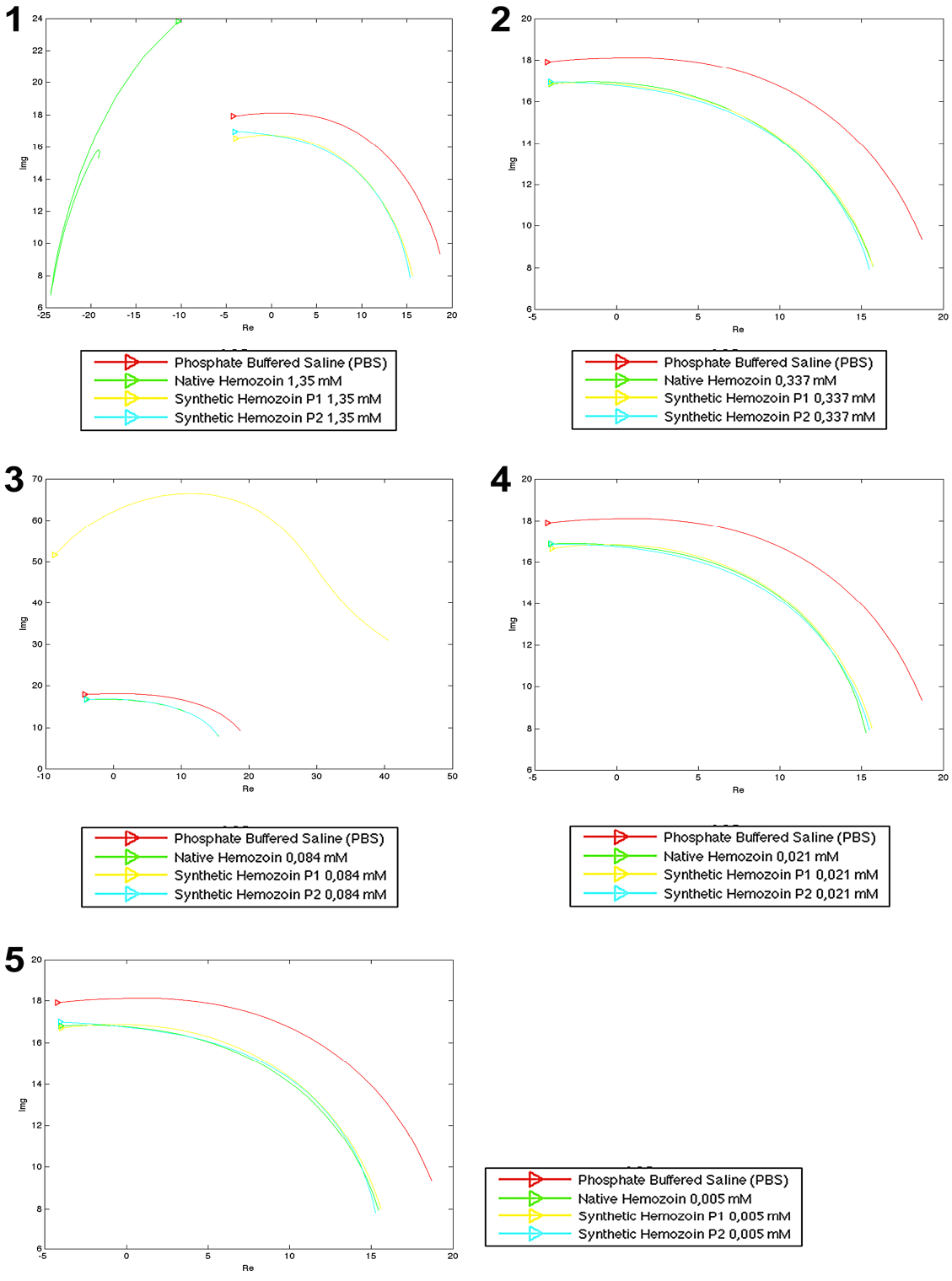

Figure 3.7 - Nyquist plots of impedance spectroscopy for native (*P. falciparum* strain Dd2) and synthetic (Protocol 1 and 2) hemozoin crystals assays with low frequencies device, $I_{freq} \in$ [10 kHz – 82.5 kHz], using electrodes in parallel configuration. The nyquist plots overlaid on the image shows the variation of impedance in function of a frequency response for hemozoin (nHz and sHz) suspensions concentrations in PBS (white). Concentrations 0.337 mM (2), 0.084 mM (3), 0.021 mM (4) and 0.005 mM (5) were obtained from successive dilutions 1:4 an initial concentration of 1.35 mM (1). The initial value of the impedance and of the lower frequency (10 kHz) is represented by the symbol **Δ** in each plot**.** The Nyquist plot has a Real part (x axis), equivalent to electrical resistance in Ohms, and an Imaginary part (y axis), given by reactance in Ohms, which together constitute the impedance.

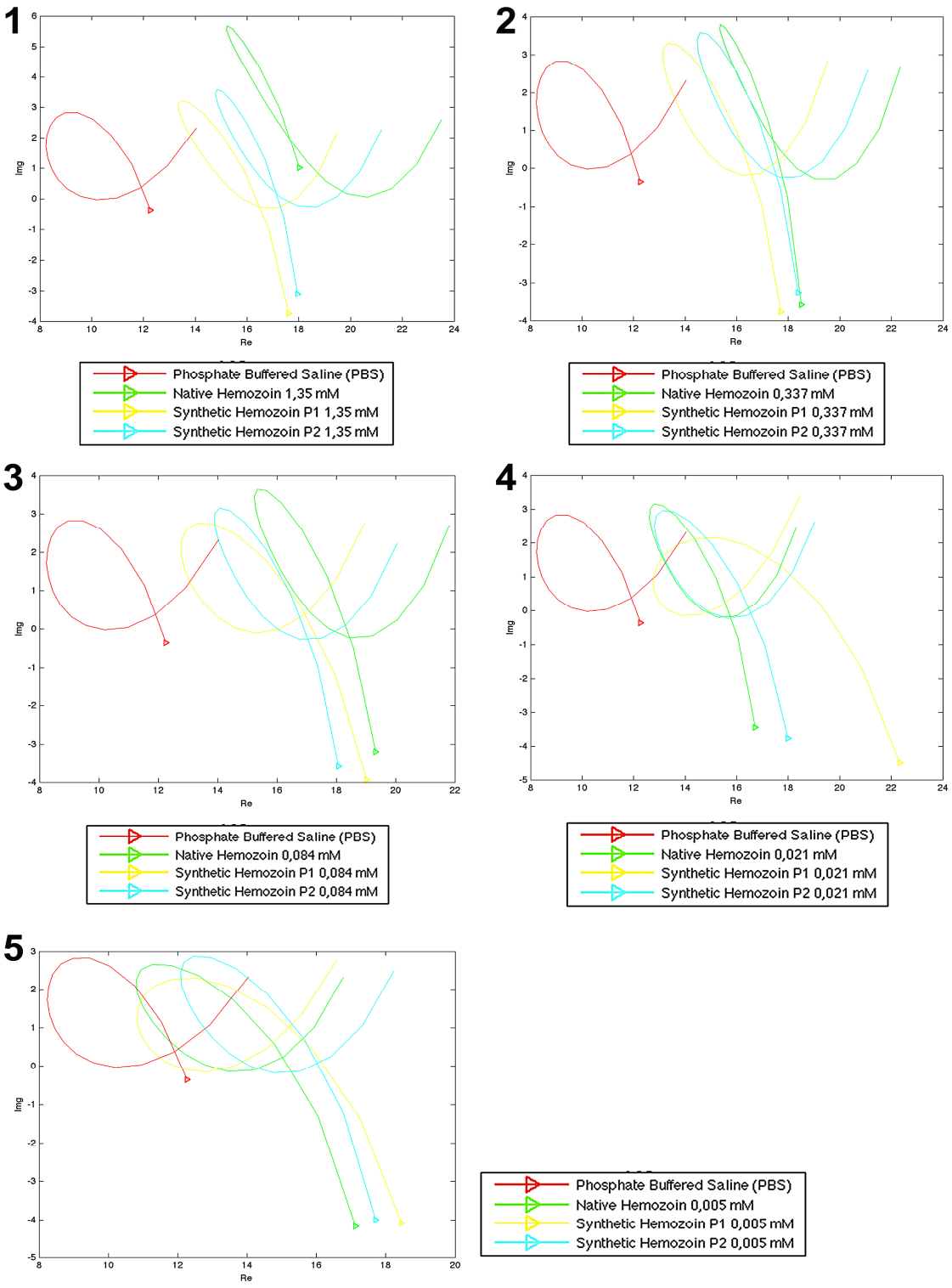

Figure 3.8 - Nyquist plots of impedance spectroscopy for native (*P. falciparum* strain Dd2) and synthetic (Protocol 1 and 2) hemozoin crystals assays with high frequencies device, $I_{freq} \in$ [250 kHz – 5 MHz], using electrodes in cross configuration. The nyquist plots overlaid on the image shows the variation of impedance in function of a frequency response for hemozoin (nHz and sHz) suspensions concentrations in PBS (white). Concentrations 0.337 mM (2), 0.084 mM (3), 0.021 mM (4) and 0.005 mM (5) were obtained from successive dilutions 1:4 an initial concentration of 1.35 mM (1). The initial value of the impedance and of the lower frequency (250 kHz) is represented by the symbol **Δ** in each plot**.** The Nyquist plot has a Real part (x axis), equivalent to electrical resistance in Ohms, and an Imaginary part (y axis), given by reactance in Ohms, which together constitute the impedance.

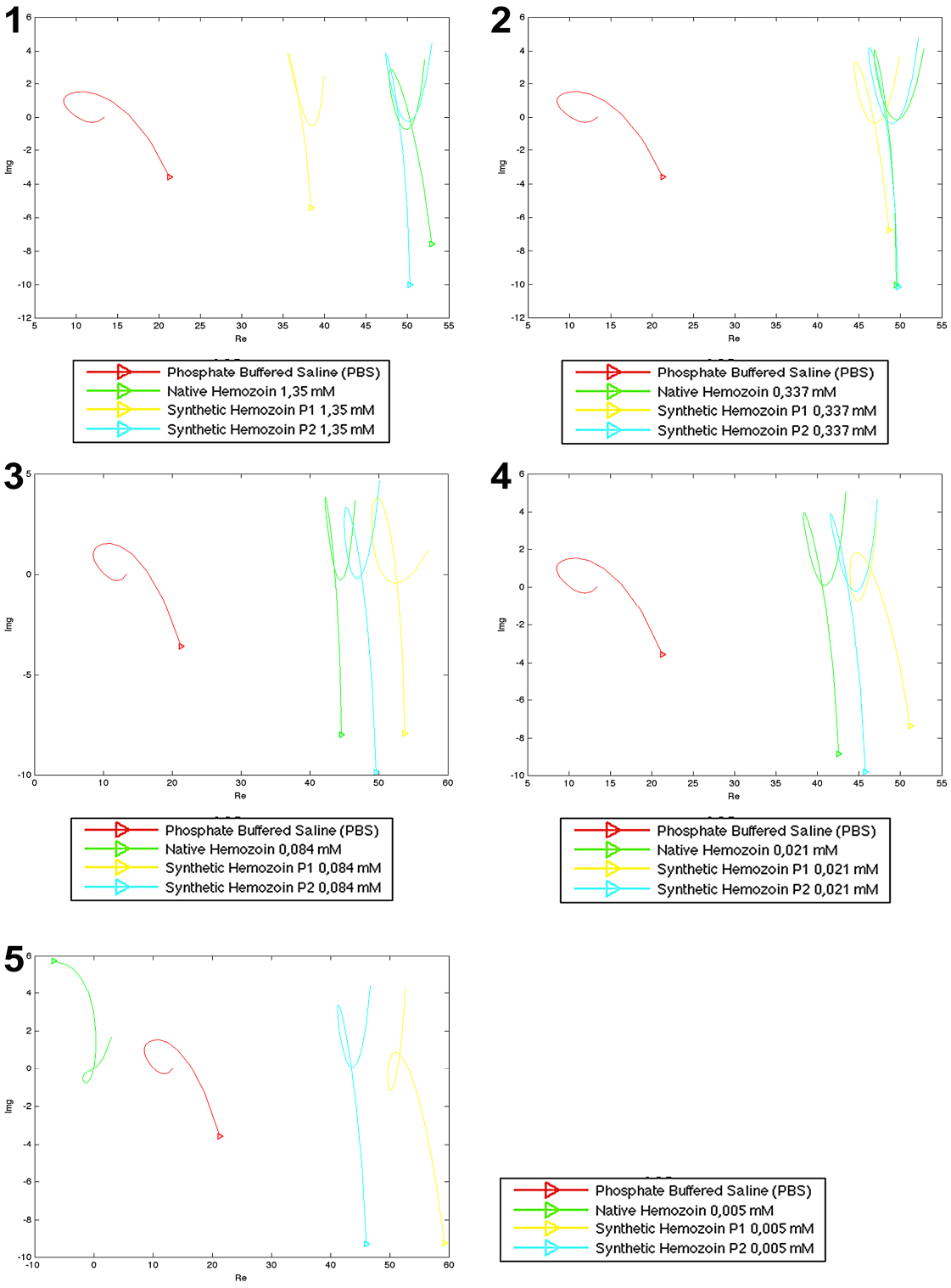

Figure 3.9 - Nyquist plots of impedance spectroscopy for native (*P. falciparum* strain Dd2) and synthetic (Protocol 1 and 2) hemozoin crystals assays with high frequencies device, $I_{freq} \in$ [250 kHz – 5 MHz], using electrodes in parallel configuration. The nyquist plots overlaid on the image shows the variation of impedance in function of a frequency response for hemozoin (nHz and sHz) suspensions concentrations in PBS (white). Concentrations 0.337 mM (2), 0.084 mM (3), 0.021 mM (4) and 0.005 mM (5) were obtained from successive dilutions 1:4 an initial concentration of 1.35 mM (1). The initial value of the impedance and of the lower frequency (250 kHz) is represented by the symbol **Δ** in each plot**.** The Nyquist plot has a Real part (x axis), equivalent to electrical resistance in Ohms, and an Imaginary part (y axis), given by reactance in Ohms, which together constitute the impedance.

3.2. Impedance spectroscopy as diagnostic method

3.2.1. Non-parasitized and parasitized red blood cells assays

The following figures show the overlapped Nyquist plots (Fig. 3.10 to 3.25), concerning the impedance measurements carried out in mixtures of parasitized (by *P. falciparum* strain 3D7) and non-parasitized RBCs. The prepared parasitized mixtures contain *P. falciparum* – infected RBCs (*Pf*-iRBCs) with all stages of the parasite (male and female gametocytes, ring, trophozoite and schizont) or only with a unique stage of the parasite (ring or schizont). Moreover, the mixtures have different percentages of parasitemia which were obtained from dilutions of 1:2 with culture medium (RPMI) or with Whole Blood (WB), from an initial mixture with a determinate percentage of parasitemia. The non-parasitized mixture contains uninfected RBCs (uRBCs) in RPMI or WB, acting as a control (protocol 2.7.3.3). The prepared mixtures for assays were analyzed using two identical devices but with different ranges for the frequency of the excitation signal - one with a high frequency range, the other with a low frequency range - and likely to operate in the traditional tetrapolar configuration for impedance measurement with variable arrangement of electrodes: crossed and parallel.

3.2.1.1. Culture Medium with all stages (unsynchronized culture)

In figures (Fig. 3.10 to 3.13), the graphs are numbered by ascending order 1 (RPMI), 2 (uRBCs), and from 3 (lower % of parasitemia in *Pf*-iRBCs) to 9 (greatest % of parasitemia in *Pf*-iRBCs), in order to analyze the variation of the impedance curves as a function of the increasing percentage of parasitemia in the culture medium, and to verify whether there are differences between its impedances and in relation to the impedance curve of uRBCs. It should be noted that the dilution and impedance measures for parasitemias ≤ 0.14% were only done 3 hours after the dilution and impedance measures of parasitemias ≥ 0.28%.

Qualitative analysis of the Nyquist graphs for **low frequencies** shows that:

In the **crossed configuration** (Fig. 3.10), erroneously, the evolution paths of the control impedance curve and of the *Pf*-iRBC's curves with different percentages of parasitemia differ from each other (1 to 9).

In the **parallel configuration** (Fig. 3.11), the impedance of the *Pf*-iRBC's curves with different percentages of parasitemia, do not exhibit a good distinction between its impedances and the impedance of the control curve (2 to 9).

Qualitative analysis of the Nyquist graphs for **high frequencies** shows that:

In the **crossed configuration** (Fig. 3.12), the impedance of the *Pf*-iRBC's curves with parasitemia of 0.0175%, 0.035% and 0.07%, increases with the increasing percentage of parasitemia over the graphs (2 to 9). However, the impedance of the *Pf*-iRCB's curve with a parasitemia of 0.14% is lower than the impedance of the curves with a parasitemia of 0.07% and 0.035%, and larger than the impedance of curve with a parasitemia of 0.0175% (6). Furthermore, the impedance of all the previous curves is larger than the impedance of the control curve and of the *Pf*-iRBC's curves with

parasitemias ranging from 0.28% to 1.12% (9). However, the impedance of the *Pf*-iRBC's curves with a percentage of parasitemias ranging from 0.14% to 1.12% incorrectly varies with the increasing percentage of parasitemia over the graphs (2 to 9). Moreover, the impedance of the *Pf*-iRBC´s curves with parasitemia of 0.28% to 1,12% is lower than the impedance of the control curve (7 and 9). In general, all the *Pf*-iRBC's curves with different percentages of show a distinction between its impedances and the impedance of the control curve.

In the **parallel configuration** (Fig. 3.13), the impedance of the *Pf*-iRBC's curves with parasitemia of 0.0175%, 0.035% and 0.14%, incorrectly varies with the increasing percentage of parasitemia over the graphs (2 to 9). The impedance of the *Pf*-iRBC's curve with a parasitemia of 0.07% is lower than the impedance of the curves with parasitemia of 0.0175%, 0.035% and 0.14% (6). Furthermore, the impedance of all the previous curves is larger than the impedance not only of the control curve but also of the *Pf*-iRBC's curves with a percentage of parasitemias ranging from 0.28% to 1.12% (9). However the impedance of the *Pf*-iRBC's curves with parasitemia of 0.28% and 1.12%, increases with the increasing percentage of parasitemia over the graphs (2 to 9). The impedance of the *Pf*-iRBC's curve with parasitemia 0.56% is lower than the impedance of the *Pf*-iRBC's curves with a percentage of parasitemias ranging from 0.28% to 1.12% (9). Besides, the impedance of the previous curves is larger than the impedance of the control curve (9). In general, all the *Pf*-iRBC's curves with different percentages of parasitemia exhibit a good distinction between its impedances and the impedance of the control curve.

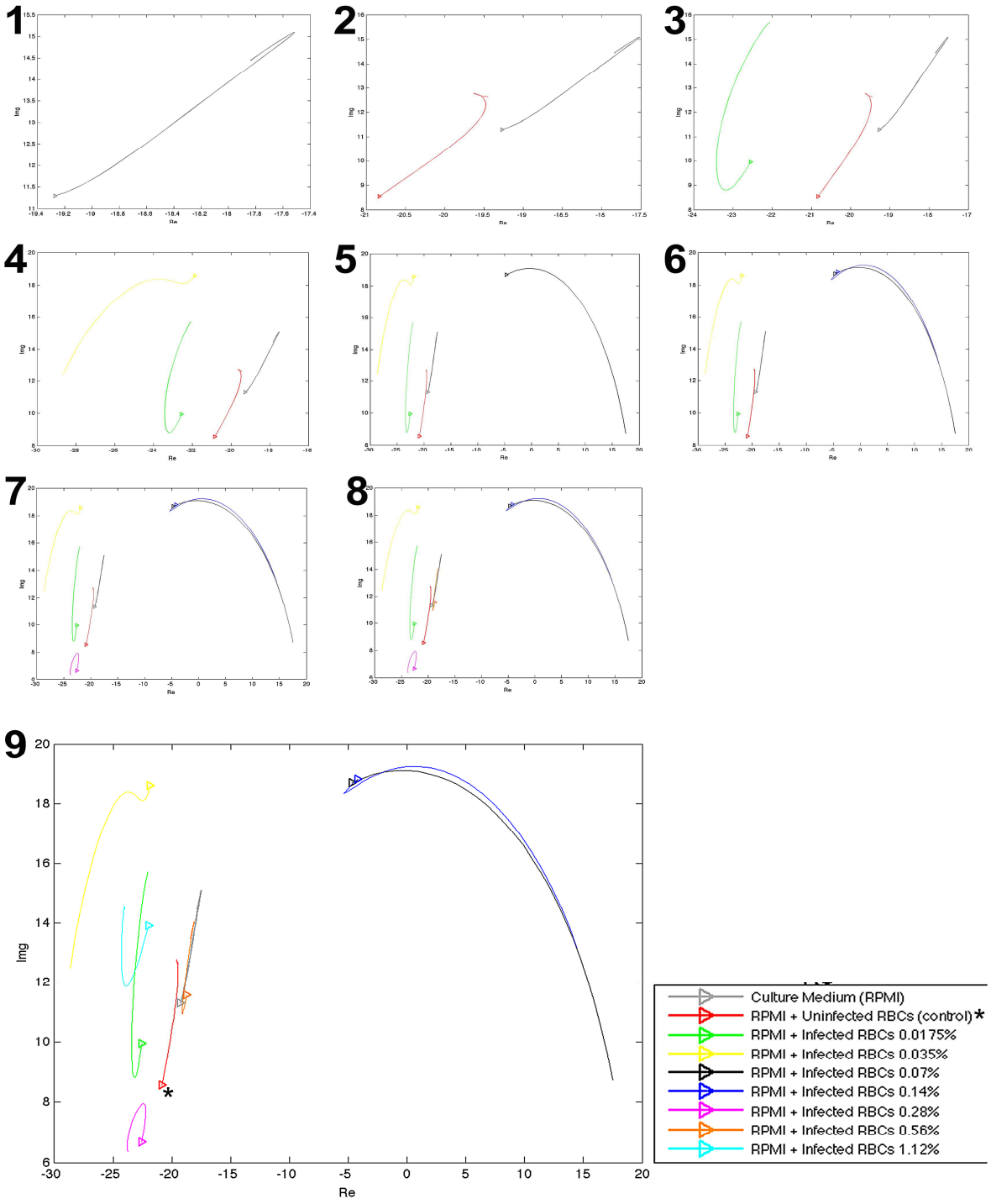

Figure 3.10 - Nyquist plots of impedance spectroscopy for non-parasitized and parasitized (by all stages of *P. falciparum* strain 3D7) RBC´s assays in culture medium (RPMI) with low frequencies device, $I_{freq} \in$ [10 kHz – 82.5 kHz], using electrodes in cross configuration. The Nyquist plots overlaid on the image show the variation of impedance as function of the frequency response for different percentages of infected RBCs (3 to 9, parasitemia) and for uninfected RBCs (2,control), both in RPMI. To the plots 3 to 9 is always added an impedance curve with a new percentage of parasitemia (by ascending order). The percentages of parasitemia from 0.0175% to 0.56% were obtained from successive dilutions (1:2) of a mixture containing infected RBCs with an initial percentage of parasitemia of 1.12%. The prepared mixtures of infected and uninfected RBCs have a hematocrit ≈ 5%. In the figure, an asterisk (*) identifies the control curve, and the symbol **Δ** represents the initial value of the impedance and of the lower frequency (10 kHz) in each plot. The Nyquist plot has a Real part (x axis), equivalent to electrical resistance in Ohms, and an Imaginary part (y axis), given by reactance in Ohms, which together constitute the impedance.

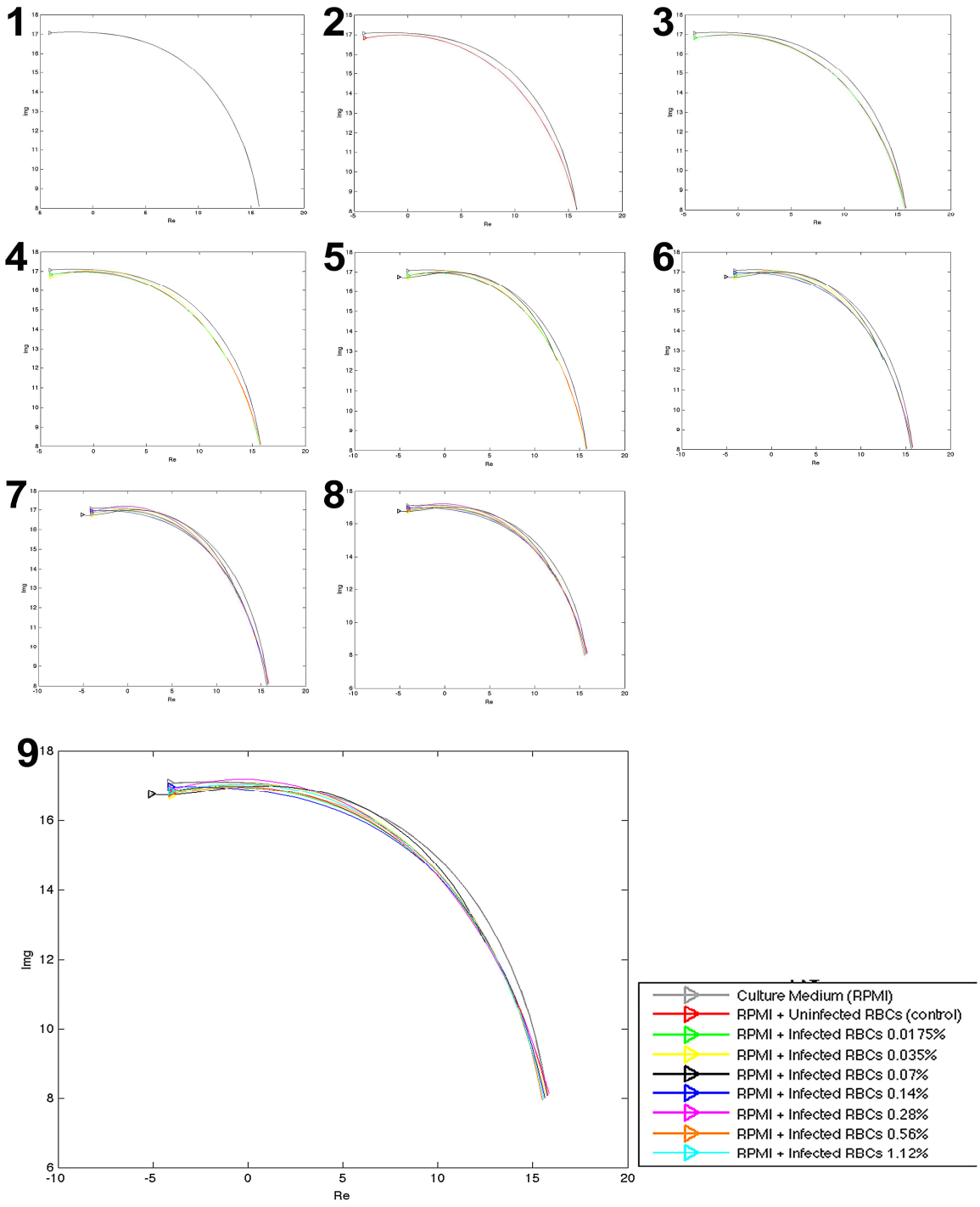

Figure 3.11 - Nyquist plots of impedance spectroscopy for non-parasitized and parasitized (by all stages of *P. falciparum* strain 3D7) RBC´s assays in culture medium (RPMI) with low frequencies device, $I_{freq} \in$ [10 kHz – 82.5 kHz], using electrodes in parallel configuration. The Nyquist plots overlaid on the image show the variation of impedance as function of the frequency response for different percentages of infected RBCs (3 to 9, parasitemia) and for uninfected RBCs (2,control), both in RPMI. To the plots 3 to 9 is always added an impedance curve with a new percentage of parasitemia (by ascending order). The percentages of parasitemia from 0.0175% to 0.56% were obtained from sucessive dilutions (1:2) of a mixture containing infected RBCs with an initial percentage of parasitemia of 1.12%. The prepared mixtures of infected and uninfected RBCs have a hematocrit ≈ 5%. In the figure, an asterisk (*) identifies the control curve, and the symbol **Δ** represents the initial value of the impedance and of the lower frequency (10 kHz) in each plot. The Nyquist plot has a Real part (x axis), equivalent to electrical resistance in Ohms, and an Imaginary part (y axis), given by reactance in Ohms, which together constitute the impedance.

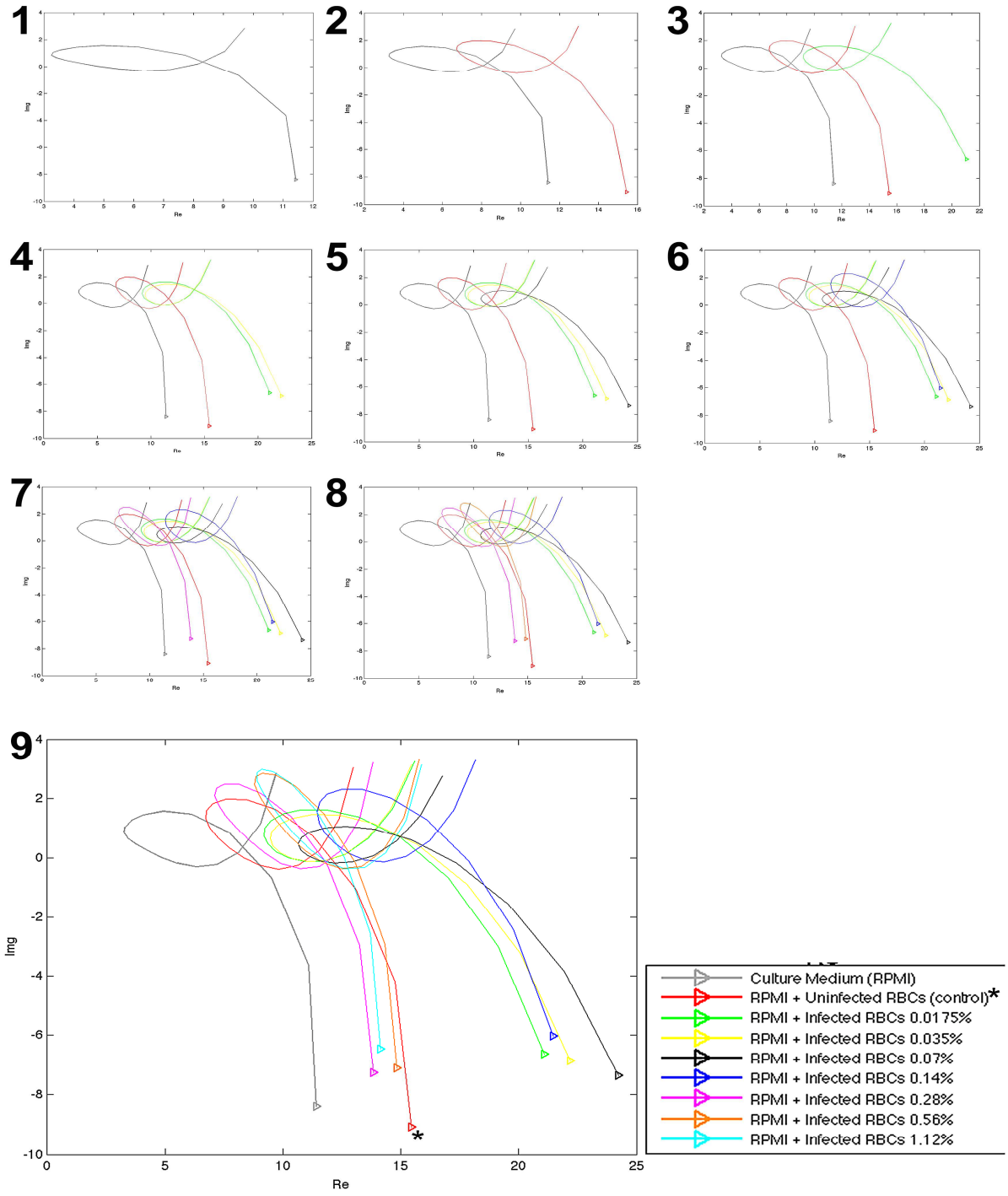

Figure 3.12 - Nyquist plots of impedance spectroscopy for non-parasitized and parasitized (by all stages of *P. falciparum* strain 3D7) RBC´s assays in culture medium (RPMI) with high frequencies device, $I_{freq} \in$ [250 kHz – 5 MHz], using electrodes in cross configuration. The Nyquist plots overlaid on the image show the variation of impedance as function of the frequency response for different percentages of infected RBCs (3 to 9, parasitemia) and for uninfected RBCs (2,control), both in RPMI. To the plots 3 to 9 is always added an impedance curve with a new percentage of parasitemia (by ascending order). The percentages of parasitemia from 0.0175% to 0.56% were obtained from successive dilutions (1:2) of a mixture containing infected RBCs with an initial percentage of parasitemia of 1.12%. The prepared mixtures of infected and uninfected RBCs have a hematocrit ≈ 5%. In the figure, an asterisk (*) identifies the control curve, and the symbol **Δ** represents the initial value of the impedance and of the lower frequency (250 kHz) in each plot. The Nyquist plot has a Real part (x axis), equivalent to electrical resistance in Ohms, and an Imaginary part (y axis), given by reactance in Ohms, which together constitute the impedance.

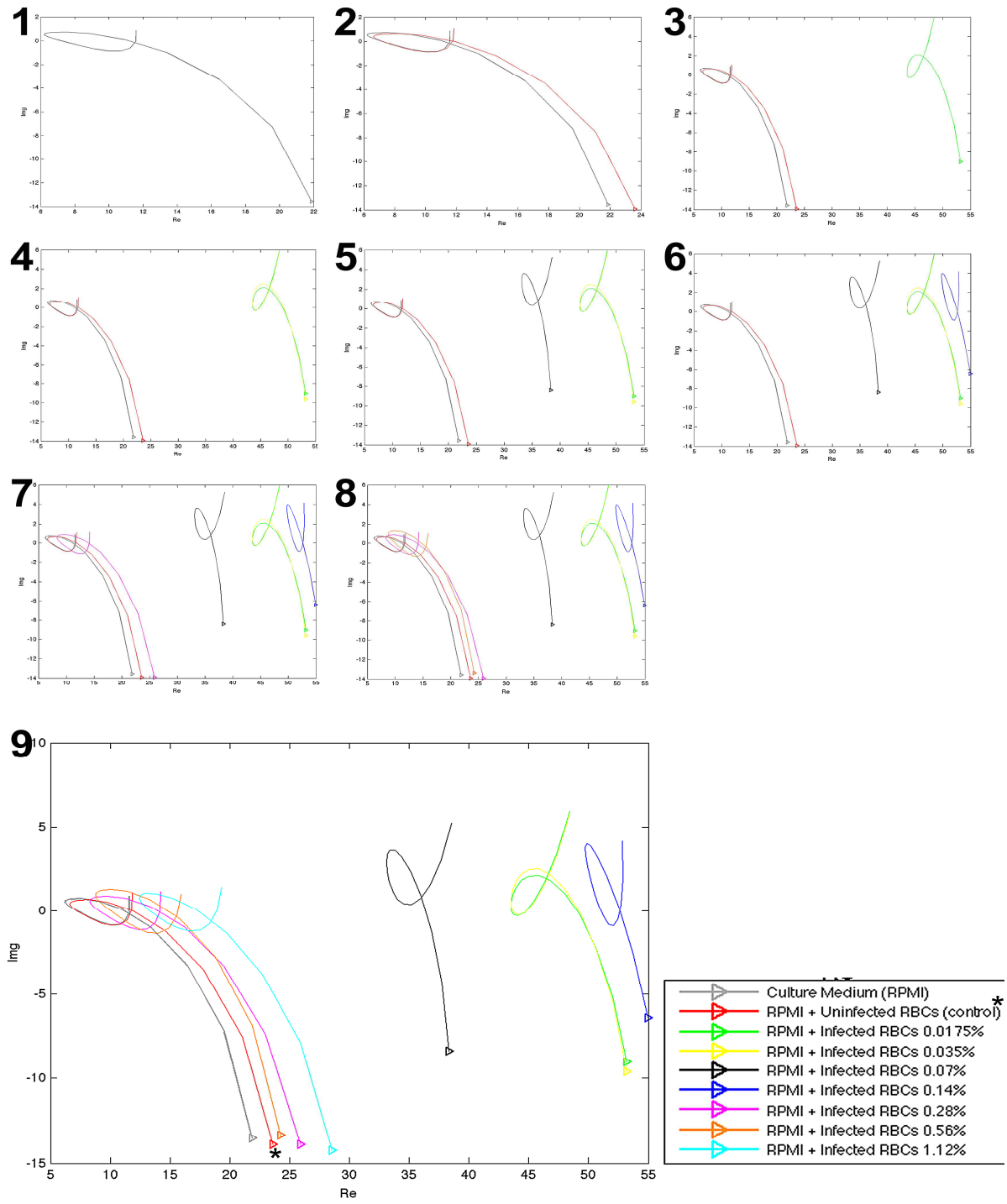

Figure 3.13 – Nyquist plots of impedance spectroscopy for non-parasitized and parasitized (by all stages of *P. falciparum* strain 3D7) RBC´s assays in culture medium (RPMI) with high frequencies device, $I_{freq} \in$ [250 kHz – 5 MHz], using electrodes in parallel configuration. The Nyquist plots overlaid on the image show the variation of impedance as function of the frequency response for different percentages of infected RBCs (3 to 9, parasitemia) and for uninfected RBCs (2,control), both in RPMI. To the plots 3 to 9 is always added an impedance curve with a new percentage of parasitemia (by ascending order). The percentages of parasitemia from 0.0175% to 0.56% were obtained from successive dilutions (1:2) of a mixture containing infected RBCs with an initial percentage of parasitemia of 1.12%. The prepared mixtures of infected and uninfected RBCs have a hematocrit ≈ 5%. In the figure, an asterisk (*) identifies the control curve, and the symbol **Δ** represents the initial value of the impedance and of the lower frequency (250 kHz) in each plot. The Nyquist plot has a Real part (x axis), equivalent to electrical resistance in Ohms, and an Imaginary part (y axis), given by reactance in Ohms, which together constitute the impedance.

3.2.1.2. Whole Blood with all stages (unsynchronized culture)

In figures (Fig. 3.14 to 3.17), the graphs are numbered in ascending order 1 (uRBCs), and from 2 (lower % of parasitemia in *Pf*-iRBCs) to 8 (larger % of parasitemia in *Pf*-iRBCs), with the purpose of analyzing the variation of the impedance curves due to the increase of the percentage of parasitemia in WB, and to verifying whether there are differences between its impedances and in relation to the impedance curve of uRBCs.

Qualitative analysis of the Nyquist graphs for **low frequencies** shows that:

In the **crossed configuration** (Fig. 3.14), the impedance of the *Pf*-iRBC's curves with different percentages of parasitemia wrongly varies with the increasing percentage of parasitemia over the graphs (2 to 8).

In the **parallel configuration** (Fig. 3.15), the impedance of the *Pf*-iRBC's curves with different percentages of parasitemia, do not exhibit a good distinction between its impedances and the impedance of the control curve (1 to 8).

Qualitative analysis of the Nyquist graphs for **high frequencies** shows that:

In the **crossed configuration** (Fig. 3.16) the impedance of the *Pf*-iRBC's curves with parasitemia of 0.0175%, 0.14% and 1.12% increases with the increasing percentage of parasitemia over the graphs (1 to 8). The impedance of the *Pf*-iRBC's curve with parasitemia of 0.035% is lower than the impedance of the *Pf*-iRBC's curves with parasitemia of 0.0175%, 0.14% and 1.12% (8). Furthermore, the impedance of all the previous curves is larger than the impedance not only of the control curve but also of the *Pf*-iRBC's curves with parasitemia of 0.07% and 0.28% (8). However, the impedance of the *Pf*-iRBC's curves with parasitemia of 0.035%, 0.07%, 0.28% and 0.56%, incorrectly varies with the increase of the percentage of parasitemia over the graphs (1 to 8). The impedance of the *Pf*-iRBC's curve with parasitemia 0.56% is larger than the impedance not only of the control curve but also of the curve with parasitemia 0.0175%, 0.035%, 0.07% and 0.28% (7), and is lower than the impedance of the curves with parasitemia of 0.14% and 1.12% (8). The impedance of the *Pf*-iRBC's curve with parasitemia 0.07% is larger than the impedance of the control curve (4). On the contrary, the impedance of the *Pf*-iRBC's curve with parasitemia 0.28% is lower than the impedance of the control curve (6). In general, all the *Pf*-iRBC's curves with different percentages of parasitemia show distinction between its impedances and the impedance of the control curve (8).

In the **parallel configuration** (Fig. 3.17), the impedance of the *Pf*-iRBC's curves with parasitemia of 0.035% and 0.14%, is larger than the impedance not only of the control curve but also of the *Pf*-iRBC's curves with parasitemia of 0.0175%, 0.07%, 0.28%, 0.56% and 1.12% (8). However, the impedance of the control curve is larger than the impedance of the *Pf*-iRBC's curves with parasitemia of 0.0175%, 0.07%, 0.28%, 0.56% and 1.12% (8). The impedance of the *Pf*-iRBC's curves with different percentages of parasitemia incorrectly varies with the increasing percentage of parasitemia over the graphs (1 to 8). In general, all the *Pf*-iRBC's curves with different percentages of

parasitemia exhibit a good distinction between its impedances and the impedance of the control curve (8).

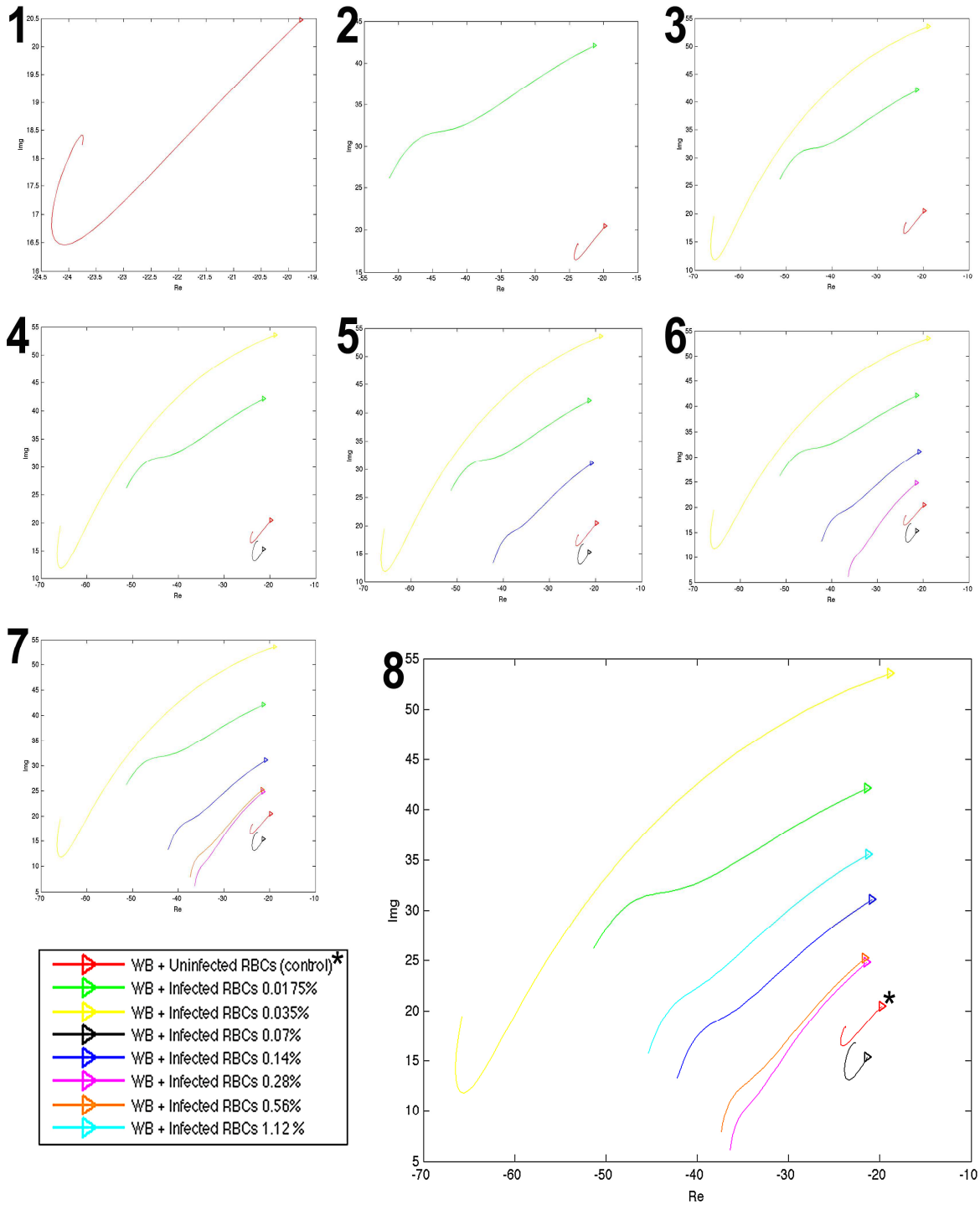

Figure 3.14 - Nyquist plots of impedance spectroscopy for non-parasitized and parasitized (by all stages of *P. falciparum* strain 3D7) RBC´s assays in Whole Blood (WB) with low frequencies device, $I_{freq} \in$ [10 kHz – 82.5 kHz], using electrodes in cross configuration. The Nyquist plots overlaid on the image show the variation of impedance as function of the frequency response for different percentages of infected RBCs (2 to 8, parasitemia) and for uninfected RBCs (1, control), both in WB (RBCs, WBCs and Plasma). To the plots 2 to 8 is always added an impedance curve with a new percentage of parasitemia (by ascending order). The percentages of parasitemia from 0.0175% to 0.56% were obtained from successive dilutions (1:2) of a mixture containing infected RBCs with an initial percentage of parasitemia of 1.12%. The prepared mixtures of infected and uninfected RBCs have a hematocrit ≈ 45%. In the figure, an asterisk (*) identifies the control curve, and the symbol **Δ** represents the initial value of the impedance and of the lower frequency (10 kHz) in each plot. The Nyquist plot has a Real part (x axis), equivalent to electrical resistance in Ohms, and an Imaginary part (y axis), given by reactance in Ohms, which together constitute the impedance.

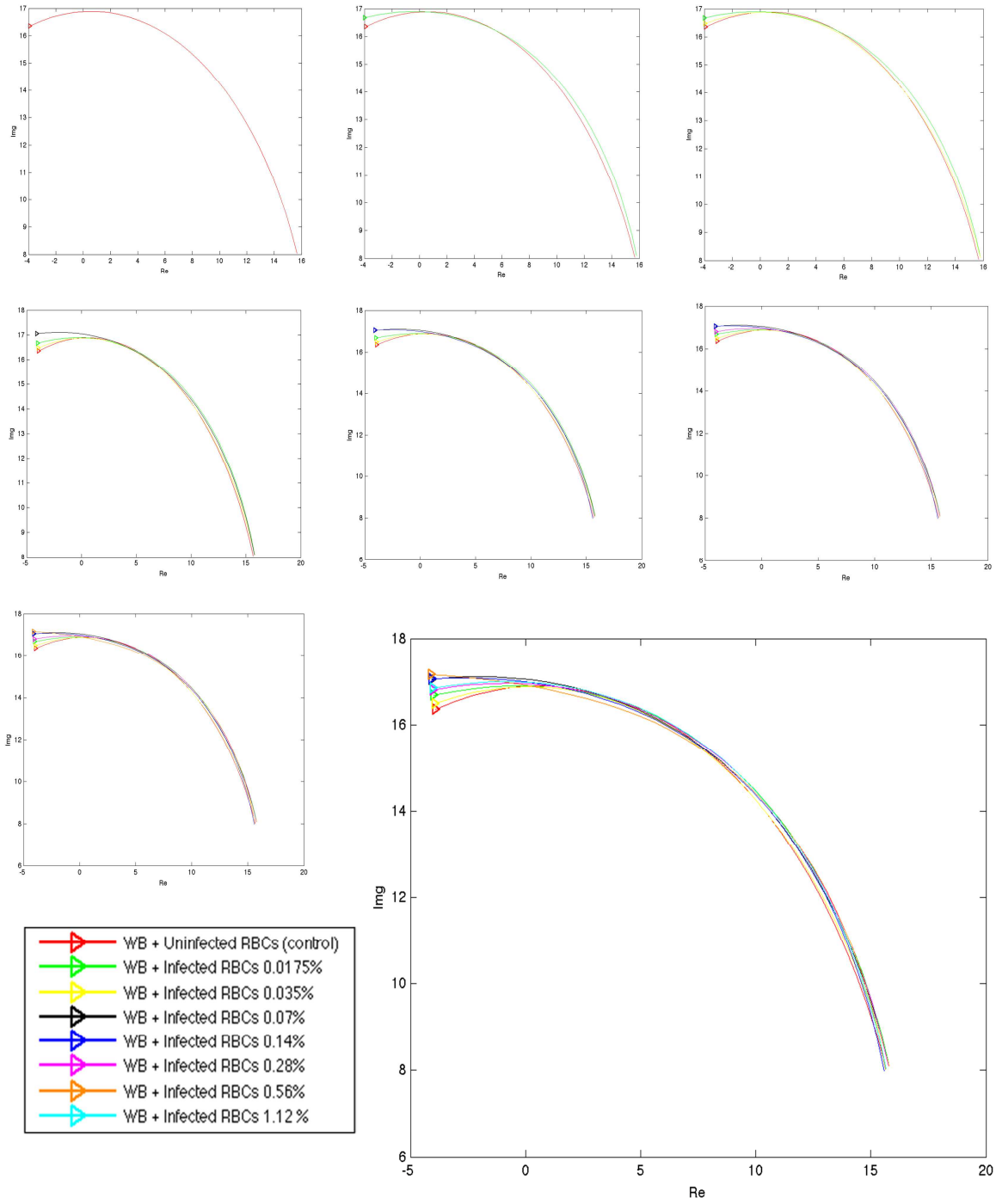

Figure 3.15 - Nyquist plots of impedance spectroscopy for non-parasitized and parasitized (by all stages of *P. falciparum* strain 3D7) RBC´s assays in Whole Blood (WB) with low frequencies device, $I_{freq} \in$ [10 kHz – 82.5 kHz], using electrodes in parallel configuration. The Nyquist plots overlaid on the image show the variation of impedance as function of the frequency response for different percentages of infected RBCs (2 to 8, parasitemia) and for uninfected RBCs (1, control), both in WB (RBCs, WBCs and Plasma). To the plots 2 to 8 is always added an impedance curve with a new percentage of parasitemia (by ascending order). The percentages of parasitemia from 0.0175% to 0.56% were obtained from successive dilutions (1:2) of a mixture containing infected RBCs with an initial percentage of parasitemia of 1.12%. The prepared mixtures of infected and uninfected RBCs have a hematocrit ≈ 45%. In the figure, an asterisk (*) identifies the control curve, and the symbol **Δ** represents the initial value of the impedance and of the lower frequency (10 kHz) in each plot. The Nyquist plot has a Real part (x axis), equivalent to electrical resistance in Ohms, and an Imaginary part (y axis), given by reactance in Ohms, which together constitute the impedance.

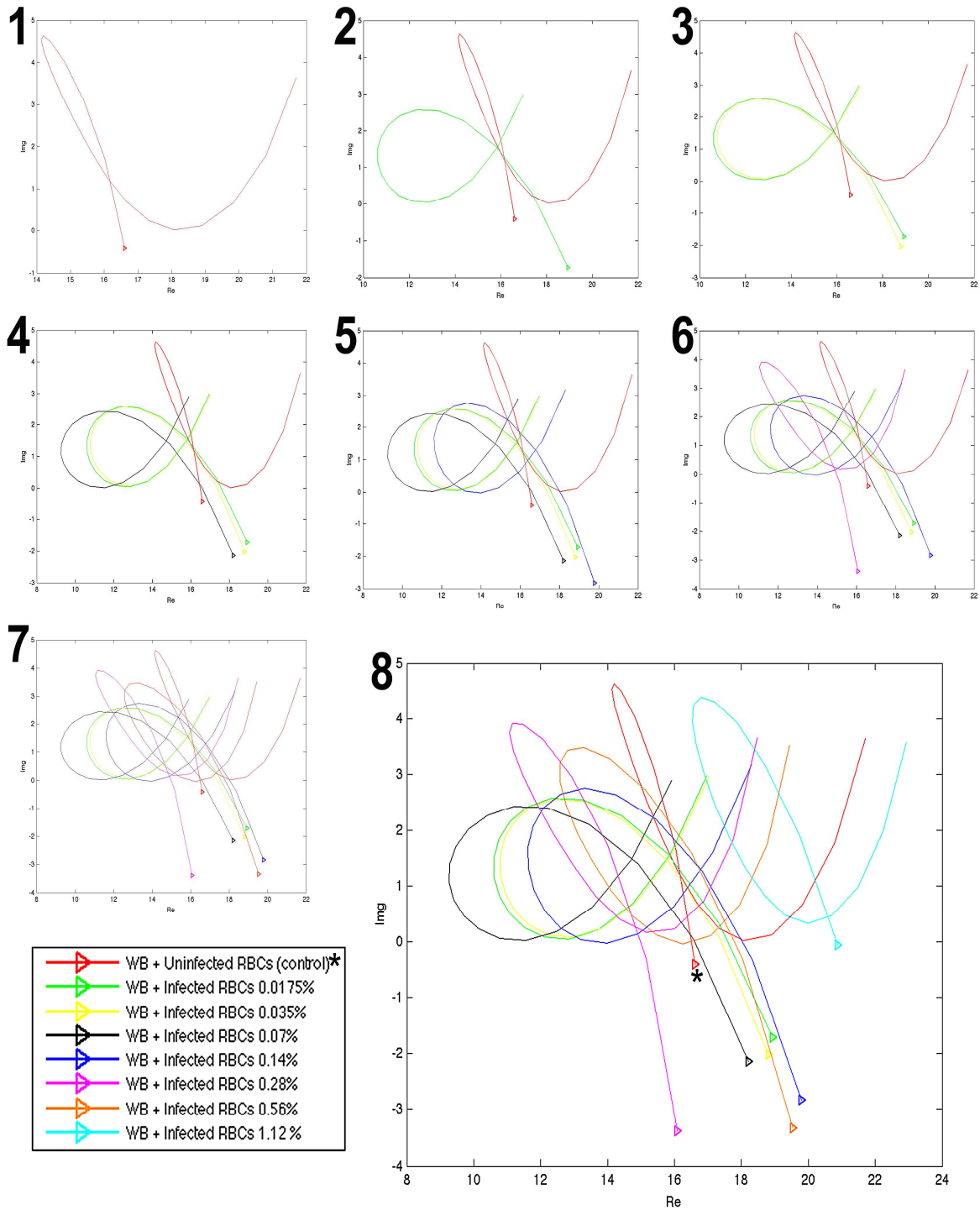

Figure 3.16 - Nyquist plots of impedance spectroscopy for non-parasitized and parasitized (by all stages of *P. falciparum* strain 3D7) RBC´s assays in Whole Blood (WB) with high frequencies device, $I_{freq} \in$ [250 kHz – 5 MHz], using electrodes in cross configuration. The Nyquist plots overlaid on the image show the variation of impedance as function of the frequency response for different percentages of infected RBCs (2 to 8, parasitemia) and for uninfected RBCs (1, control), both in WB (RBCs, WBCs and Plasma). To the plots 2 to 8 is always added an impedance curve with a new percentage of parasitemia (by ascending order). The percentages of parasitemia from 0.0175% to 0.56% were obtained from successive dilutions (1:2) of a mixture containing infected RBCs with an initial percentage of parasitemia of 1.12%. The prepared mixtures of infected and uninfected RBCs have a hematocrit ≈ 45%. In the figure, an asterisk (*) identifies the control curve, and the symbol **Δ** represents the initial value of the impedance and of the lower frequency (250 kHz) in each plot. The Nyquist plot has a Real part (x axis), equivalent to electrical resistance in Ohms, and an Imaginary part (y axis), given by reactance in Ohms, which together constitute the impedance.

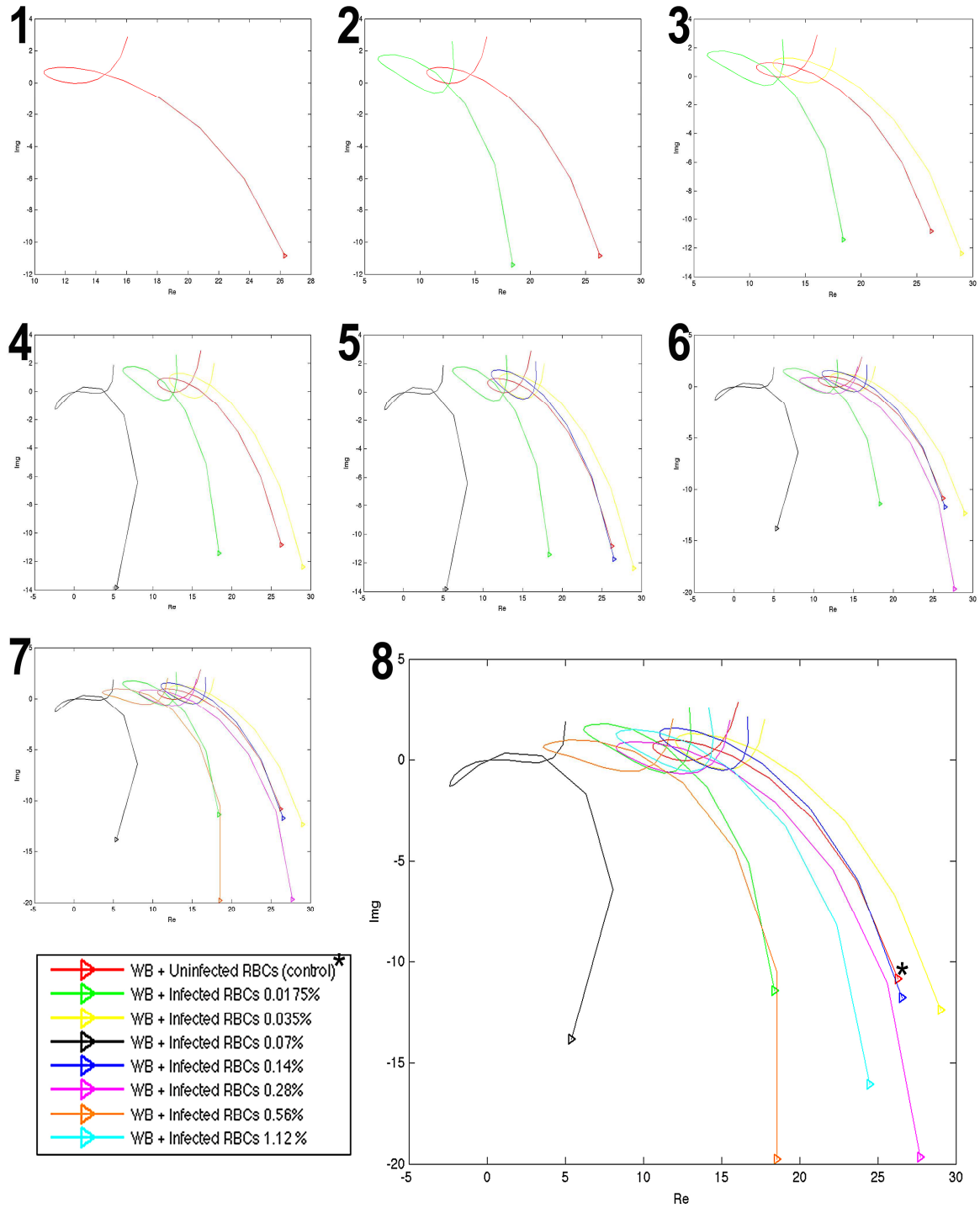

Figure 3.17 - Nyquist plots of impedance spectroscopy for non-parasitized and parasitized (by all stages of *P. falciparum* strain 3D7) RBC´s assays in Whole Blood (WB) with high frequencies device, $I_{freq} \in$ [250 kHz – 5 MHz], using electrodes in parallel configuration. The Nyquist plots overlaid on the image show the variation of impedance as function of the frequency response for different percentages of infected RBCs (2 to 8, parasitemia) and for uninfected RBCs (1, control), both in WB (RBCs, WBCs and Plasma). To the plots 2 to 8 is always added an impedance curve with a new percentage of parasitemia (by ascending order). The percentages of parasitemia from 0.0175% to 0.56% were obtained from successive dilutions (1:2) of a mixture containing infected RBCs with an initial percentage of parasitemia of 1.12%. The prepared mixtures of infected and uninfected RBCs have a hematocrit ≈ 45%. In the figure, an asterisk (*) identifies the control curve, and the symbol **Δ** represents the initial value of the impedance and of the lower frequency (250 kHz) in each plot. The Nyquist plot has a Real part (x axis), equivalent to electrical resistance in Ohms, and an Imaginary part (y axis), given by reactance in Ohms, which together constitute the impedance.

3.2.1.3. Whole Blood with ring stage (synchronized culture)

In figures (Fig. 3.18 to 3.21), the graphs are numbered by ascending order 1 (uRBCs), and from 2 (lower % of parasitemia in *Pf*-iRBCs) to 9 (greatest % of parasitemia in *Pf*-iRBCs), in order to analyze the variation of the impedance curves as a function of the increasing percentage of parasitemia in WB, and to verify whether there are differences between its impedances and in relation to the impedance curve of uRBCs.

Qualitative analysis of the Nyquist graphs for **low frequencies** shows that:

In the **crossed configuration** (Fig. 3.18), the impedance of the *Pf*-iRBC's curves with parasitemias ranging from 0.0156% to 2% is lower than the impedance of the control curve (1 to 9). Erroneously, the impedance of the *Pf*-iRBC's curves with different percentages of parasitemia wrongly varies with the increasing percentage of parasitemia over the graphs (1 to 9).

In the **parallel configuration** (Fig. 3.19), the impedance of the *Pf*-iRBC's curves with parasitemias ranging from 0.0156% to 2% is lower than the impedance of the control curve (1 to 9). Furthermore, the curves of the *Pf*-iRBC's do not exhibit a good distinction between their impedances (1 to 9). Erroneously, the evolution path of the control curve's impedance opposes that of the *Pf*-iRBC's impedance curves with different percentages of parasitemia (9).

Qualitative analysis of the Nyquist graphs for **high frequencies** shows that:

In the **crossed configuration** (Fig. 3.20) the impedance of the *Pf*-iRBC's curves with parasitemia of 0.031%, 0.062% and 2% increases with the increasing percentage of parasitemia over the graphs (1 to 9). Furthermore, the impedance of all the previous curves is larger than the impedance of the control curve (9). However, the impedance of the *Pf*-iRBC's curves with parasitemia of 0.0156%, 0.125%, 0.25%, 0.5% and 1%, wrongly varies with the increasing percentage of parasitemia over the graphs (1 to 9). The impedance of the *Pf*-iRBC's curve with parasitemia of 0.015%, 0.125% and 1% is lower than the impedance of the control curve (8). On the contrary, the impedance of the curves with parasitemia 0.25% and 0.5% is larger than the impedance of the control curve (7). In general, all the *Pf*-iRBC's curves with different percentages of parasitemia show distinction between its impedances and the impedance of the control curve (9).

In the **parallel configuration** (Fig. 3.21), the impedance of the *Pf*-iRBC's curves with parasitemia of 0.031%, 0.062% and 2% increases with the increasing percentage of parasitemia over the graphs (1 to 9). The impedance of the *Pf*-iRBC's curve with parasitemia 1% is lower than the impedance of the *Pf*-iRBC's curves with parasitemia of 0.062% and 2%, and larger than the impedance of the curve with parasitemia of 0.031% (9). Furthermore, the impedance of all the previous curves is larger than the impedance not only of the control curve but also of the *Pf*-iRBC's curves with parasitemias of 0.0156%, 0.125%, 0.25% and 0.5% (9). However, the impedance of the *Pf*-iRBC's curves with parasitemia of 0.0156%, 0.125%, 0.25%, 0.5% and 1%, wrongly varies with the increasing percentage of parasitemia over the graphs (1 to 9). Moreover, the impedance of the *Pf*-iRBC's curves with parasitemia of 0.015% and 0.125% (2 to 5) is lower than the impedance of the

control curve. It is also verified that the impedance of the curves with parasitemia of 0.25%, 0.5% and 1% is lower than the impedance of the control curve (6, 7 and 8). In general, all the *Pf*-iRBC's curves with different percentages of parasitemia exhibit a good distinction between its impedances and the impedance of the control curve (8).

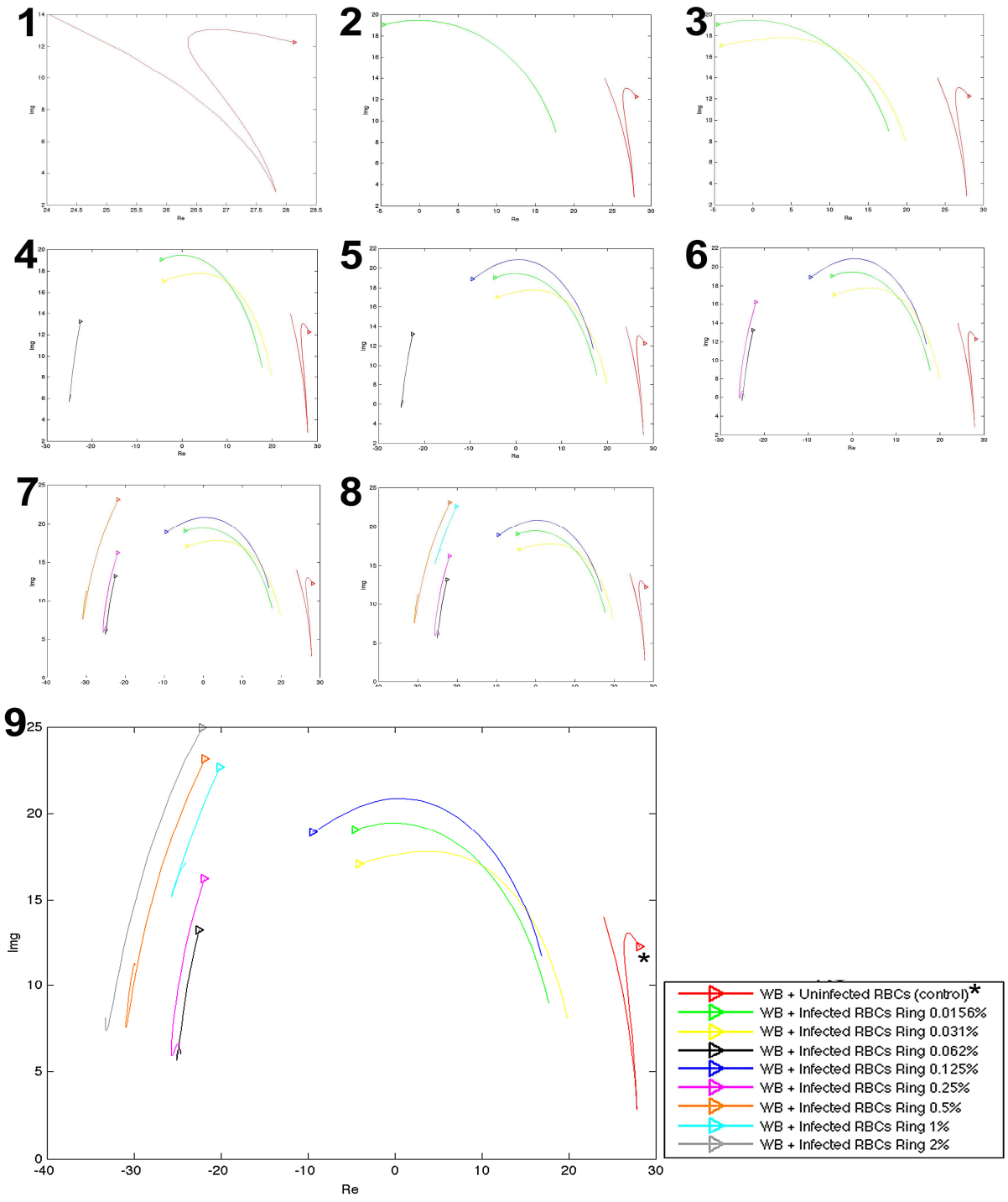

Figure 3.18 - Nyquist plots of impedance spectroscopy for non-parasitized and parasitized (by ring stage of *P. falciparum* strain 3D7) RBC´s assays in Whole Blood (WB) with low frequencies device, $I_{freq} \in$ [10 kHz – 82.5 kHz], using electrodes in cross configuration. The Nyquist plots overlaid on the image show the variation of impedance as function of the frequency response for different percentages of infected RBCs (2 to 9, parasitemia) and for uninfected RBCs (1, control), both in WB (RBCs, WBCs and Plasma). To the plots 2 to 9 is always added an impedance curve with a new percentage of parasitemia (by ascending order). The percentages of parasitemia from 0.0156% to 1% were obtained from successive dilutions (1:2) of a mixture containing infected RBCs with an initial percentage of parasitemia of 2%. The prepared mixtures of infected and uninfected RBCs have a hematocrit ≈ 45%. In the figure, an asterisk (*) identifies the control curve, and the symbol **Δ** represents the initial value of the impedance and of the lower frequency (10 kHz) in each plot. The Nyquist plot has a Real part (x axis), equivalent to electrical resistance in Ohms, and an Imaginary part (y axis), given by reactance in Ohms, which together constitute the impedance.

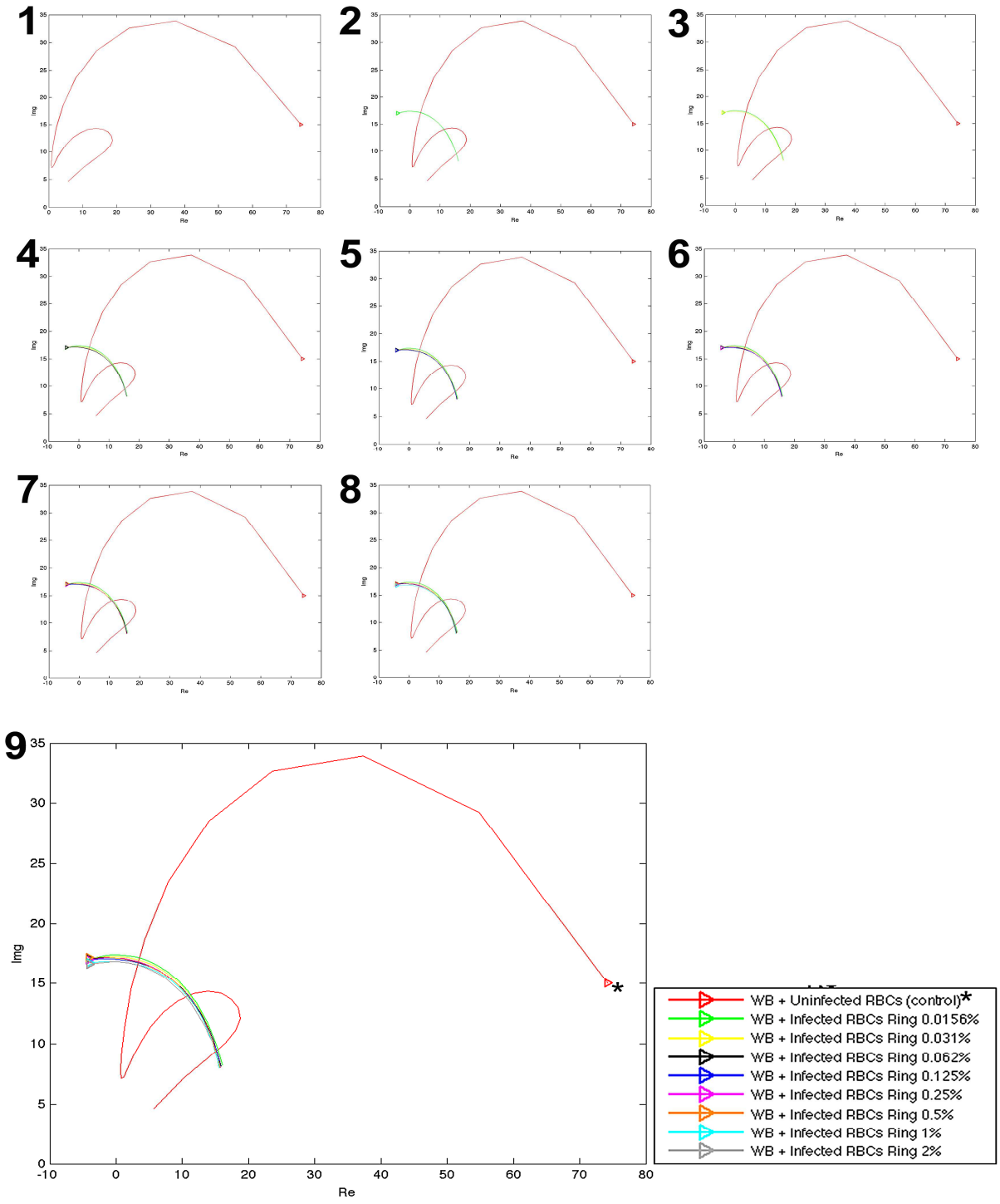

Figure 3.19 - Nyquist plots of impedance spectroscopy for non-parasitized and parasitized (by ring stage of *P. falciparum* strain 3D7) RBC´s assays in Whole Blood (WB) with low frequencies device, $I_{freq} \in$ [10 kHz – 82.5 kHz], using electrodes in parallel configuration. The Nyquist plots overlaid on the image show the variation of impedance as function of the frequency response for different percentages of infected RBCs (2 to 9, parasitemia) and for uninfected RBCs (1, control), both in WB (RBCs, WBCs and Plasma). To the plots 2 to 9 is always added an impedance curve with a new percentage of parasitemia (by ascending order). The percentages of parasitemia from 0.0156% to 1% were obtained from successive dilutions (1:2) of a mixture containing infected RBCs with an initial percentage of parasitemia of 2%. The prepared mixtures of infected and uninfected RBCs have a hematocrit ≈ 45%. In the figure, an asterisk (*) identifies the control curve, and the symbol **Δ** represents the initial value of the impedance and of the lower frequency (10 kHz) in each plot. The Nyquist plot has a Real part (x axis), equivalent to electrical resistance in Ohms, and an Imaginary part (y axis), given by reactance in Ohms, which together constitute the impedance.

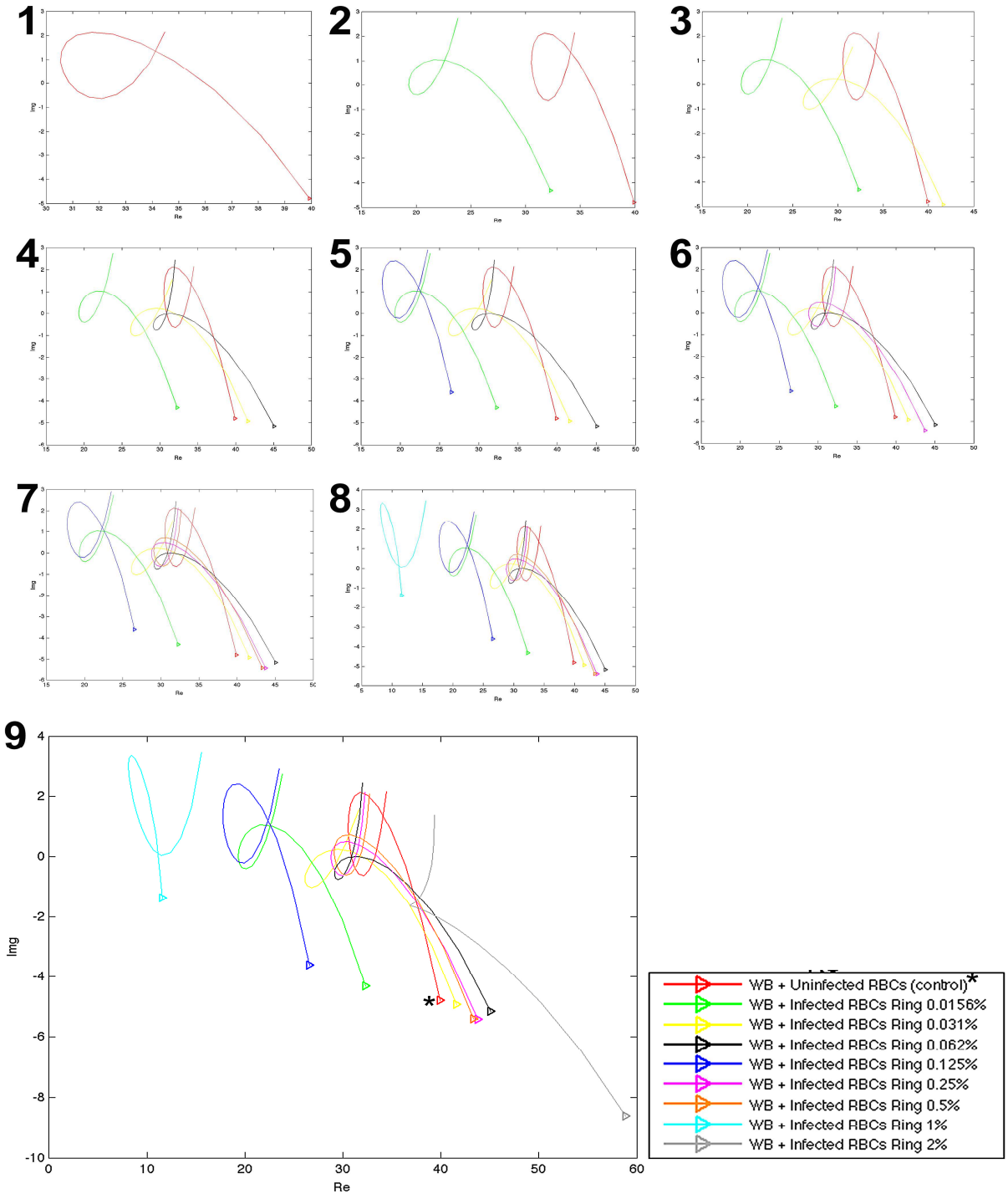

Figure 3.20 - Nyquist plots of impedance spectroscopy for non-parasitized and parasitized (by ring stage of *P. falciparum* strain 3D7) RBC´s assays in Whole Blood (WB) with high frequencies device, $I_{freq} \in$ [250 kHz – 5 MHz], using electrodes in cross configuration. The Nyquist plots overlaid on the image show the variation of impedance as function of the frequency response for different percentages of infected RBCs (2 to 9, parasitemia) and for uninfected RBCs (1, control), both in WB (RBCs, WBCs and Plasma). To the plots 2 to 9 is always added an impedance curve with a new percentage of parasitemia (by ascending order). The percentages of parasitemia from 0.0156% to 1% were obtained from successive dilutions (1:2) of a mixture containing infected RBCs with an initial percentage of parasitemia of 2%. The prepared mixtures of infected and uninfected RBCs have a hematocrit ≈ 45%. In the figure, an asterisk (*) identifies the control curve, and the symbol **Δ** represents the initial value of the impedance and of the lower frequency (250 kHz) in each plot. The Nyquist plot has a Real part (x axis), equivalent to electrical resistance in Ohms, and an Imaginary part (y axis), given by reactance in Ohms, which together constitute the impedance.

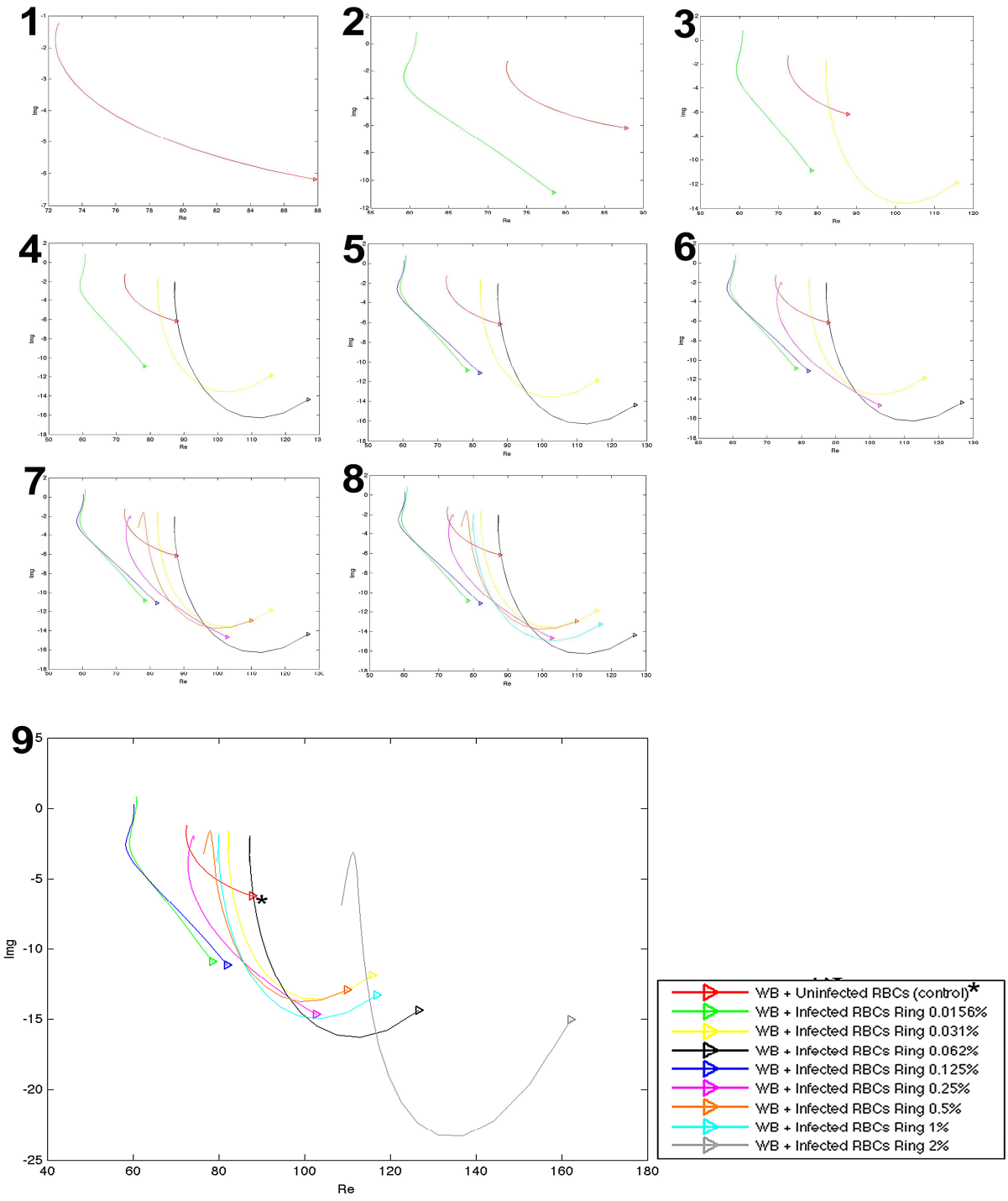

Figure 3.21 - Nyquist plots of impedance spectroscopy for non-parasitized and parasitized (by ring stage of *P. falciparum* strain 3D7) RBC´s assays in Whole Blood (WB) with high frequencies device, $I_{freq} \in$ [250 kHz – 5 MHz], using electrodes in parallel configuration. The Nyquist plots overlaid on the image show the variation of impedance as function of the frequency response for different percentages of infected RBCs (2 to 9, parasitemia) and for uninfected RBCs (1, control), both in WB (RBCs, WBCs and Plasma). To the plots 2 to 9 is always added an impedance curve with a new percentage of parasitemia (by ascending order). The percentages of parasitemia from 0.0156% to 1% were obtained from successive dilutions (1:2) of a mixture containing infected RBCs with an initial percentage of parasitemia of 2%. The prepared mixtures of infected and uninfected RBCs have a hematocrit ≈ 45%. In the figure, an asterisk (*) identifies the control curve, and the symbol **Δ** represents the initial value of the impedance and of the lower frequency (250 kHz) in each plot. The Nyquist plot has a Real part (x axis), equivalent to electrical resistance in Ohms, and an Imaginary part (y axis), given by reactance in Ohms, which together constitute the impedance.

3.2.1.4. Whole Blood with schizont stage (synchronized culture)

In figures (Fig. 3.22 to 3.25), the graphs are numbered by ascending order 1 (uRBCs), and from 2 (lower % of parasitemia in *Pf*-iRBCs) to 9 (greatest % of parasitemia in *Pf*-iRBCs), in order to analyze the variation of the impedance curves as a function of the increasing percentage of parasitemia in the WB, and to verify whether there are differences between its impedances and relative to the impedance curve of uRBCs.

Qualitative analysis of the Nyquist graphs for **low frequencies** shows that:

In the **crossed configuration** (Fig. 3.22) the impedance of the *Pf*-iRBC's curves with parasitemia of 0.0156%, 0.062%, 0.125% and 1%, increases with the increasing percentage of parasitemia over the graphs (1 to 9). The impedance of the *Pf*-iRBC's curve with parasitemia of 2% is larger than the impedance of the curve with parasitemias ranging from 0.0156% to 0.125% (9), and lower than the impedance of the curve with parasitemia of 1% (9). Furthermore, the impedance of all the previous curves is larger than the impedance not only of the control curve but also of the *Pf*-iRBC's curves with parasitemia of 0.031%, 0.25% and 0.5% (9). However, the impedance of the *Pf*-iRBC's curves with parasitemia of 0.031%, 0.25% and 0.5%, wrongly varies with the increasing percentage of parasitemia over the graphs (1 to 9). Moreover, the impedance of all the previous curves is lower than the impedance of the control curve (3, 6 and 7). The evolution path of the impedance of the *Pf*-iRBC's curve with parasitemia of 0.5% opposes to the impedance of the other curves (7), which is contrary to the expected behaviour. In general, all the *Pf*-iRBC's curves with different percentages of parasitemia show distinction between its impedances and the impedance of the control curve (9).

In the **parallel configuration** (Fig. 3.23), the impedance of the *Pf*-iRBC's curves with parasitemia of 0.0156%, 0.25% and 1%, increases with the increasing percentage of parasitemia over the graphs (1 to 9). The impedance of the *Pf*-iRBC's curve with parasitemia 2% is larger than the impedance of the curve with parasitemia ranging from 0.0156% to 0.25% (9), and lower than the impedance of the *Pf*-iRBC's curves with parasitemia of 1% (9). Furthermore, the impedance of all the previous curves is larger than the impedance not only of the control curve but also of the *Pf*-iRBC's curves with parasitemia of 0.031%, 0.062% and 0.125% (9). However, the impedance of the *Pf*-iRBC's curves with parasitemia of 0.031%, 0.125%, 0.25%, 0.5%, 1% and 2%, wrongly varies with the increasing percentage of parasitemia over the graphs (1 to 9). The impedance of the *Pf*-iRBC's curves with parasitemia of 0.031%, 0.062%, 0.125%, 0.5% (3, 4, 5 and 7), is lower than the impedance of the control curve. In general, all the *Pf*-iRBC's curves with different percentages of parasitemia exhibit a good distinction between its impedances and the impedance of the control curve (9).

Qualitative analysis of the Nyquist graphs for **high frequencies** shows that:

In the **crossed configuration** (Fig. 3.24) the impedance of the *Pf*-iRBC's curves with parasitemia of 0.062%, 0.125% and 1%, increases with the increasing percentage of parasitemia over the graphs (1 to 9). The impedance of the *Pf*-iRBC's curve with parasitemia of 2% is lower than the impedance of the *Pf*-iRBC's curve with parasitemia of 0.062%, 0.125% and 1% (9). The impedance of the *Pf*-iRBC's curve with parasitemia of 0.5% is lower than the impedance of the curve with

parasitemia of 0.062%, 0.125%, 1% and 2% (9). Furthermore, the impedance of all the previous curves is larger than the impedance not only of the control curve but also of the *Pf*-iRBC's curve with parasitemia of 0.0156%, 0.031% and 0.25% (9). However, the impedance of the *Pf*-iRBC's curves with parasitemia of 0.0156%, 0.031%, 0.25%, 0.5% and 2%, incorrectly varies with the increase of the percentage of parasitemia over the graphs (1 to 9). Moreover, the impedance of the *Pf*-iRBC's curves with parasitemia of 0.0156%, 0.031% and 0.25%, is lower than the impedance of the control curve (2, 3 and 6). In general, all the *Pf*-iRBC's curves with different percentages of parasitemia show distinction between its impedances and the impedance of the control curve (9).

In the **parallel configuration** (Fig. 3.25), the impedance of the *Pf*-iRBC's curves with parasitemia of 0.0156%, 0.062%, 0.125% and 1%, increases with the increasing percentage of parasitemia over the graphs (1 to 9). Furthermore, the impedance of all the previous curves is larger than the impedance not only of the control curve but also of the *Pf*-iRBC's curves with parasitemia of 0.031%, 0.25%, 0.5% and 2% (9). However, the impedance of the *Pf*-iRBC's curves with parasitemia of 0.031%, 0.25%, 0.5% and 2%, wrongly varies with the increasing percentage of parasitemia over the graphs (1 to 9). Moreover, the impedance of the *Pf*-iRBC's curves with parasitemia of 0.25%, 0.5% and 2%, is larger than the impedance not only of the control curve (6, 7 and 9) but also of the *Pf*-iRBC's curve with parasitemia of 0.031%. The impedance of the *Pf*-iRBC's curve with parasitemia 0.031% is lower than the impedance of the control curve (3). In general, all the *Pf*-iRBC's curves with different percentages of parasitemia exhibit a good distinction between its impedances and the impedance of the control curve (9).

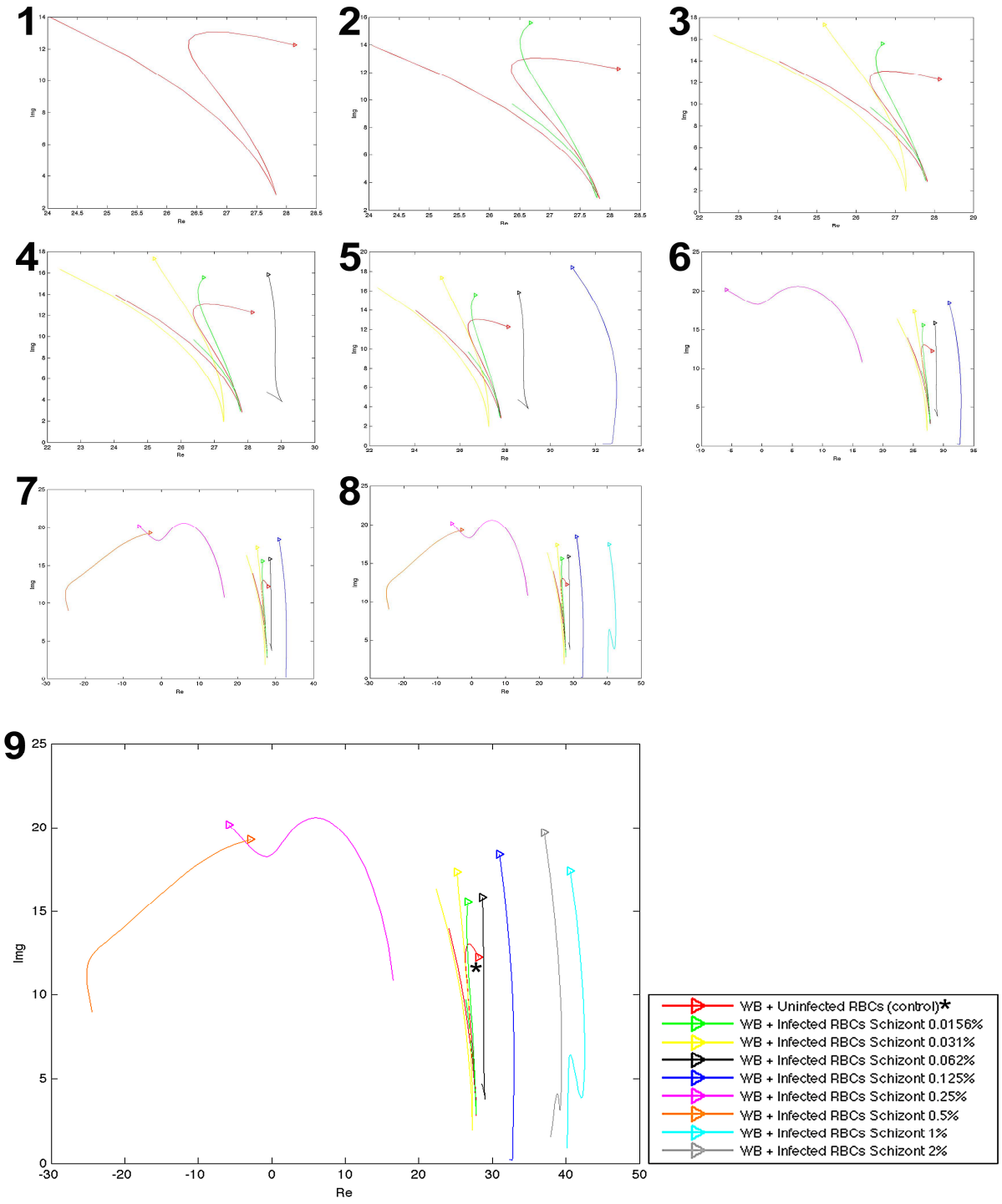

Figure 3.22 – Nyquist plots of impedance spectroscopy for non-parasitized and parasitized (by schizont stage of *P. falciparum* strain 3D7) RBC´s assays in Whole Blood (WB) with low frequencies device, $I_{freq} \in$ [10 kHz – 82.5 kHz], using electrodes in cross configuration. The Nyquist plots overlaid on the image show the variation of impedance as function of the frequency response for different percentages of infected RBCs (2 to 9, parasitemia) and for uninfected RBCs (1, control), both in WB (RBCs, WBCs and Plasma). To the plots 2 to 9 is always added an impedance curve with a new percentage of parasitemia (by ascending order). The percentages of parasitemia from 0.0156% to 1% were obtained from successive dilutions (1:2) of a mixture containing infected RBCs with an initial percentage of parasitemia of 2%. The prepared mixtures of infected and uninfected RBCs have a hematocrit ≈ 45%. In the figure, an asterisk (*) identifies the control curve, and the symbol **Δ** represents the initial value of the impedance and of the lower frequency (10 kHz) in each plot. The Nyquist plot has a Real part (x axis), equivalent to electrical resistance in Ohms, and an Imaginary part (y axis), given by reactance in Ohms, which together constitute the impedance.

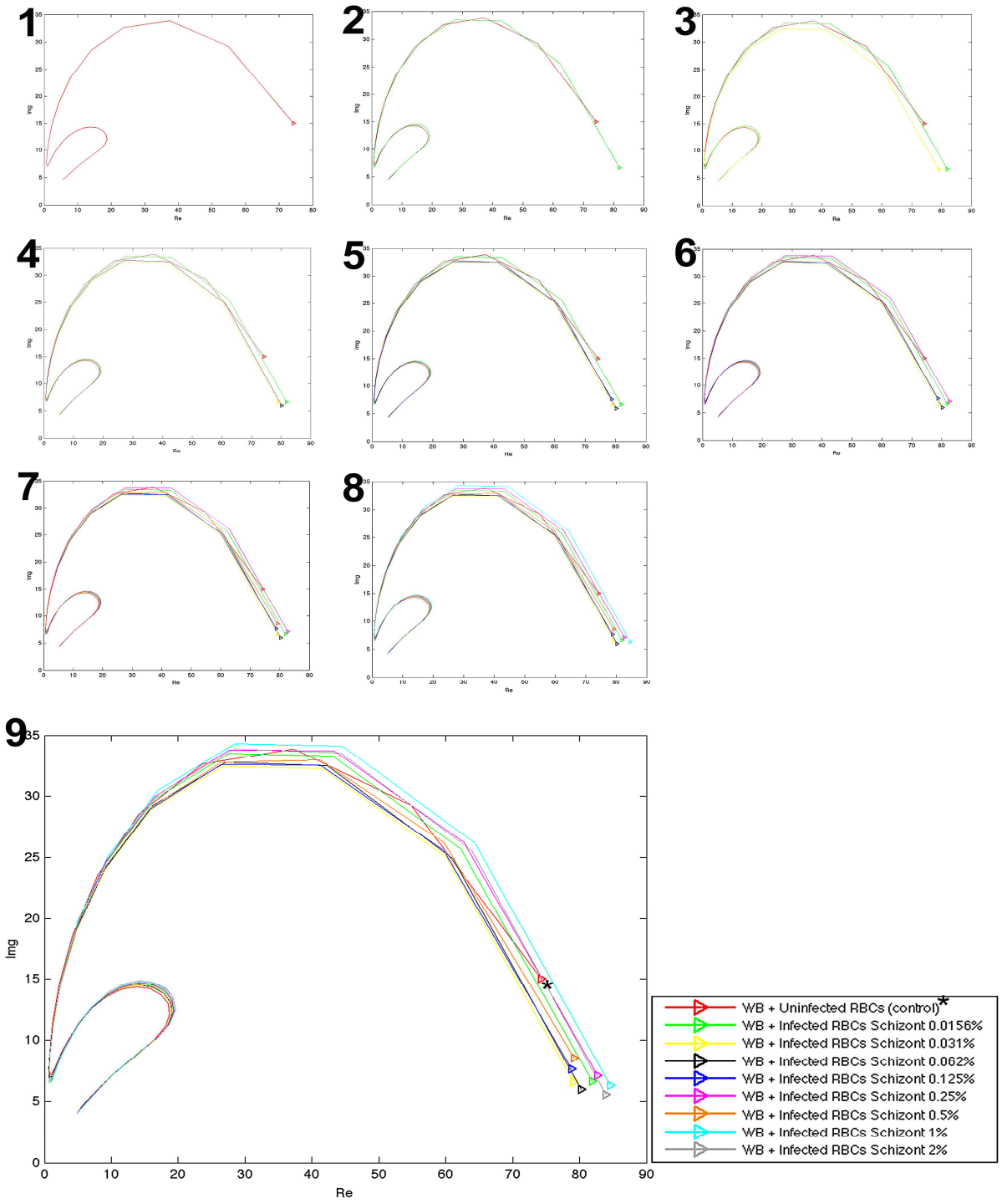

Figure 3.23 - Nyquist plots of impedance spectroscopy for non-parasitized and parasitized (by schizont stage of *P. falciparum* strain 3D7) RBC´s assays in Whole Blood (WB) with low frequencies device, $l_{freq} \in$ [10 kHz – 82.5 kHz], using electrodes in parallel configuration. The Nyquist plots overlaid on the image show the variation of impedance as function of the frequency response for different percentages of infected RBCs (2 to 9, parasitemia) and for uninfected RBCs (1, control), both in WB (RBCs, WBCs and Plasma). To the plots 2 to 9 is always added an impedance curve with a new percentage of parasitemia (by ascending order). The percentages of parasitemia from 0.0156% to 1% were obtained from successive dilutions (1:2) of a mixture containing infected RBCs with an initial percentage of parasitemia of 2%. The prepared mixtures of infected and uninfected RBCs have a hematocrit ≈ 45%. In the figure, an asterisk (*) identifies the control curve, and the symbol **Δ** represents the initial value of the impedance and of the lower frequency (10 kHz) in each plot. The Nyquist plot has a Real part (x axis), equivalent to electrical resistance in Ohms, and an Imaginary part (y axis), given by reactance in Ohms, which together constitute the impedance.

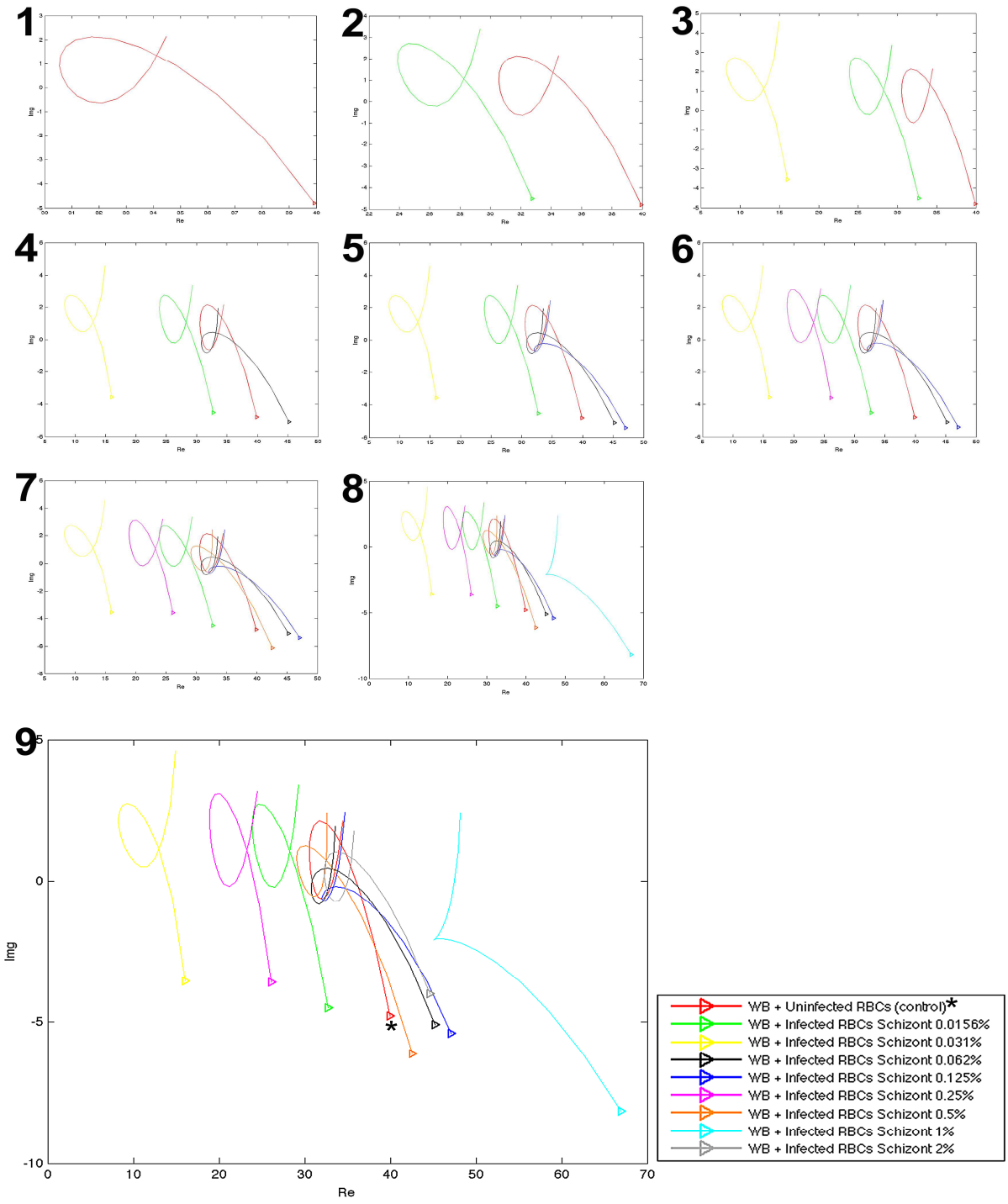

Figure 3.24 - Nyquist plots of impedance spectroscopy for non-parasitized and parasitized (by schizont stage of *P. falciparum* strain 3D7) RBC´s assays in Whole Blood (WB) with high frequencies device, $I_{freq} \in$ [250 kHz – 5 MHz], using electrodes in cross configuration. The Nyquist plots overlaid on the image show the variation of impedance as function of the frequency response for different percentages of infected RBCs (2 to 9, parasitemia) and for uninfected RBCs (1, control), both in WB (RBCs, WBCs and Plasma). To the plots 2 to 9 is always added an impedance curve with a new percentage of parasitemia (by ascending order). The percentages of parasitemia from 0.0156% to 1% were obtained from successive dilutions (1:2) of a mixture containing infected RBCs with an initial percentage of parasitemia of 2%. The prepared mixtures of infected and uninfected RBCs have a hematocrit ≈ 45%. In the figure, an asterisk (*) identifies the control curve, and the symbol **Δ** represents the initial value of the impedance and of the lower frequency (250 kHz) in each plot. The Nyquist plot has a Real part (x axis), equivalent to electrical resistance in Ohms, and an Imaginary part (y axis), given by reactance in Ohms, which together constitute the impedance.

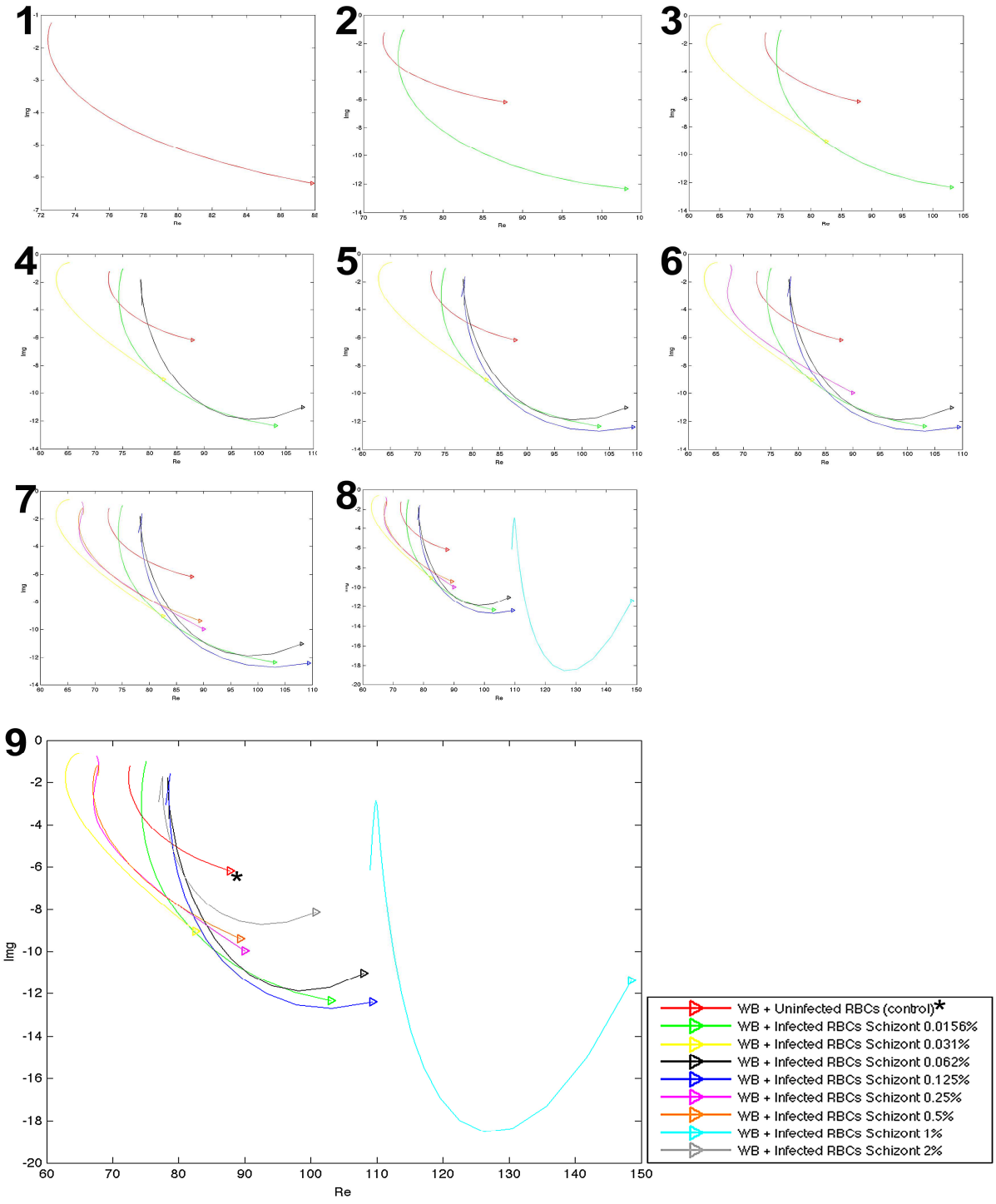

Figure 3.25 - Nyquist plots of impedance spectroscopy for non-parasitized and parasitized (by schizont stage of *P. falciparum* strain 3D7) RBC´s assays in Whole Blood (WB) with high frequencies device, $I_{freq} \in$ [250 kHz – 5 MHz], using electrodes in parallel configuration. The Nyquist plots overlaid on the image show the variation of impedance as function of the frequency response for different percentages of infected RBCs (2 to 9, parasitemia) and for uninfected RBCs (1, control), both in WB (RBCs, WBCs and Plasma). To the plots 2 to 9 is always added an impedance curve with a new percentage of parasitemia (by ascending order). The percentages of parasitemia from 0.0156% to 1% were obtained from successive dilutions (1:2) of a mixture containing infected RBCs with an initial percentage of parasitemia of 2%. The prepared mixtures of infected and uninfected RBCs have a hematocrit ≈ 45%. In the figure, an asterisk (*) identifies the control curve, and the symbol **Δ** represents the initial value of the impedance and of the lower frequency (250 kHz) in each plot. The Nyquist plot has a Real part (x axis), equivalent to electrical resistance in Ohms, and an Imaginary part (y axis), given by reactance in Ohms, which together constitute the impedance.

3.2.2. Repetition of non-parasitized and parasitized red blood cells assays

Following a general observation of the results of impedance spectroscopy obtained in section 3.2.1., proceeded a repetition of the assays in mixtures of parasitized red blood cells (by *P. falciparum* Dd2 strain) and non-parasitized in RPMI and WB. The mixtures made for the assay repetition process contain all stages (male and female gametocytes, ring, trophozoite and schizont) as well as a single stage (ring) of the parasite. For the new assay, it was decided to use only the device capable of measuring the high frequency range of the excitation signal. However, the crossed and parallel configurations were kept and applied for these measurements.

3.2.2.1. Culture Medium with all stages (unsynchronized culture) and ring stage (synchronized culture)

As in previous assays, the figures (Fig. 3.26 to 3.29) show the overlapped Nyquist plots numbered by ascending order 1 (uRBCs, control), and from 2 (lower % of parasitemia in *Pf*-iRBCs) to 7 (greatest % of parasitemia in *Pf*-iRBCs), in order to analyze the variation of the impedance curves as a function of the increasing percentage of parasitemia in the RPMI, and to verify whether there are differences between its impedances and in relation to the impedance curve of uRBCs.

In a general and qualitative analysis of the results obtained for the impedance of the mixtures containing all stages (Fig. 3.26 and 3.27) and the ring stage (Fig. 3.28 and 3.29), both in a RPMI medium using crossed and parallel configuration, it is possible to observe that the impedance of the *Pf*-iRBC's curves increases with the increasing percentage of parasitemia and in relation to the impedance of the control curve (1 to 7). It is also possible to verify that the discrimination between the values of impedance of the control curve and *Pf*-iRBC's curve is greater for parasitemia over 0.5% (7). Comparing the results obtained for both configurations, it is observable an increase in discrimination and stability as well when a parallel configuration is applied (Fig. 3.27 and 3.29).

However, the Nyquist plots resulting from the assay with a mixture containing the stage ring done in a crossed configuration (Fig.3.28), show that the impedance of the *Pf*-iRBC's curve doesn't increase with the increasing parasitemia (1 to 7), which is contrary to what was expected. Furthermore, the impedance of the *Pf*-iRBC's curve with parasitemia 0.25%, 0.5% and 1% is lower than the impedance of the control curve (7).

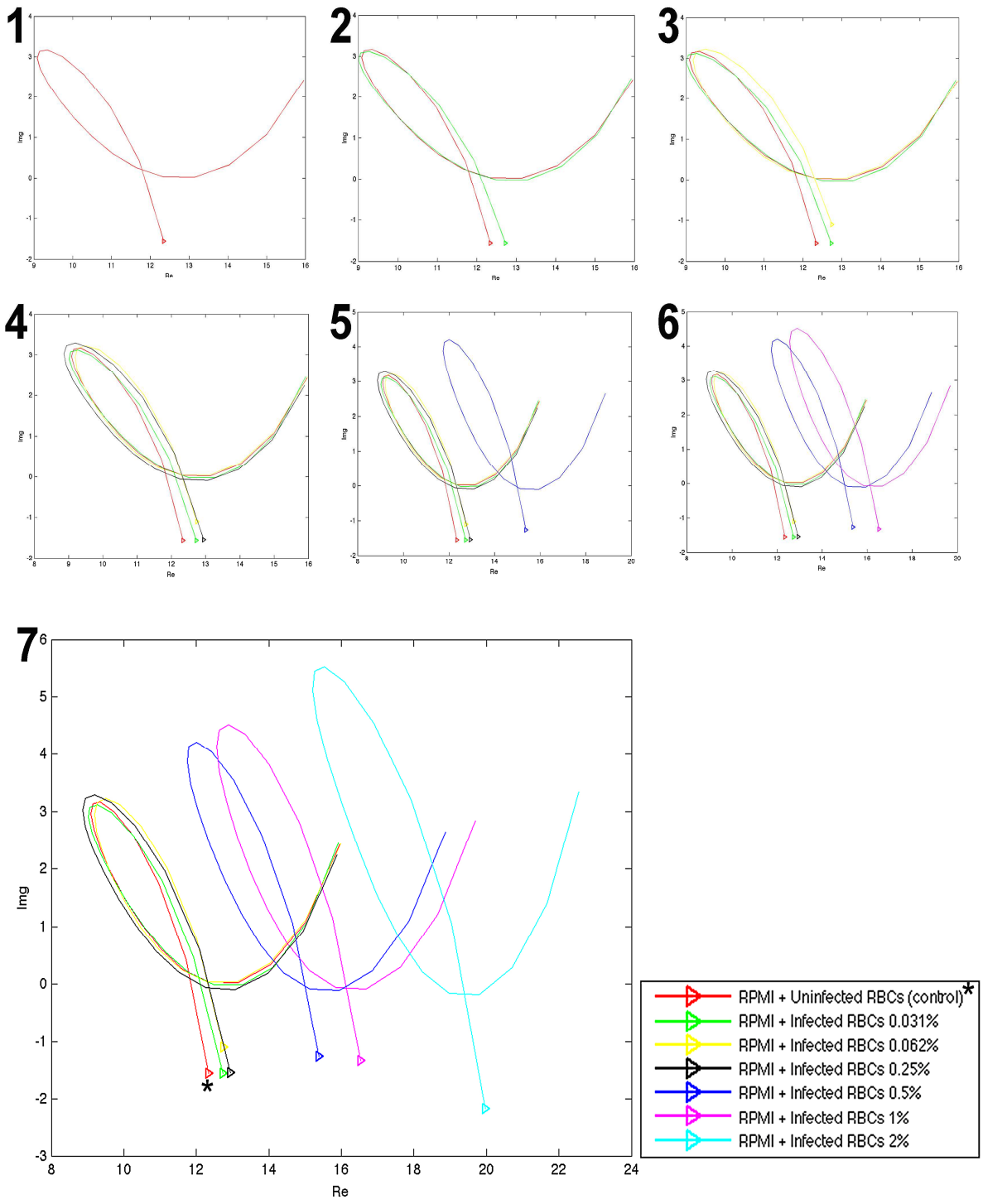

Figure 3.26 - Nyquist plots of impedance spectroscopy for non-parasitized and parasitized (by all stages of *P. falciparum* strain Dd2) RBC´s assays in culture medium (RPMI) with high frequencies device, $I_{freq} \in$ [250 kHz – 5 MHz], using electrodes in cross configuration. The Nyquist plot overlaid on the image show the variation of impedance as function of the frequency response for different percentages of infected RBCs (2 to 7, parasitemia) and for uninfected RBCs (2,control), both in RPMI. To the plots 2 to 7 is always added an impedance curve with a new percentage of parasitemia (by ascending order). The percentages of parasitemia from 0.031% to 1% were obtained from successive dilutions (1:2) of a mixture containing infected RBCs with an initial percentage of parasitemia of 2%. The prepared mixtures of infected and uninfected RBCs have a hematocrit ≈ 5%. In the figure, an asterisk (*) identifies the control curve, and the symbol **Δ** represents the initial value of the impedance and of the lower frequency (250 kHz) in each plot. The Nyquist plot has a Real part (x axis), equivalent to electrical resistance in Ohms, and an Imaginary part (y axis), given by reactance in Ohms, which together constitute the impedance.

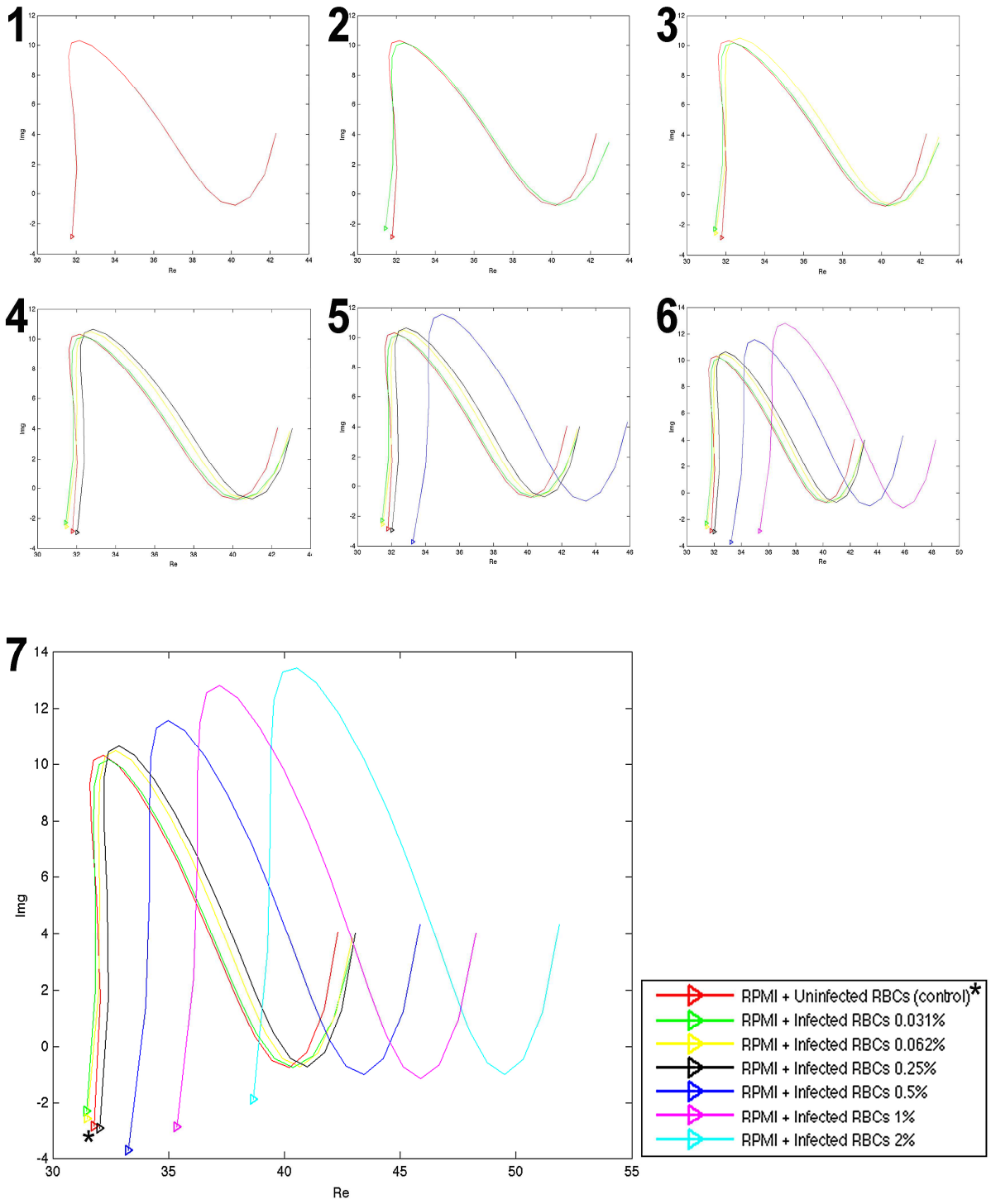

Figure 3.27 - Nyquist plots of impedance spectroscopy for non-parasitized and parasitized (by all stages of *P. falciparum* strain Dd2) RBC´s assays in culture medium (RPMI) with high frequencies device, $I_{freq} \in$ [250 kHz – 5 MHz], using electrodes in parallel configuration. The Nyquist plot overlaid on the image show the variation of impedance as function of the frequency response for different percentages of infected RBCs (2 to 7, parasitemia) and for uninfected RBCs (2,control), both in RPMI. To the plots 2 to 7 is always added an impedance curve with a new percentage of parasitemia (by ascending order). The percentages of parasitemia from 0.031% to 1% were obtained from successive dilutions (1:2) of a mixture containing infected RBCs with an initial percentage of parasitemia of 2%. The prepared mixtures of infected and uninfected RBCs have a hematocrit ≈ 5%. In the figure, an asterisk (*) identifies the control curve, and the symbol **Δ** represents the initial value of the impedance and of the lower frequency (250 kHz) in each plot. The Nyquist plot has a Real part (x axis), equivalent to electrical resistance in Ohms, and an Imaginary part (y axis), given by reactance in Ohms, which together constitute the impedance.

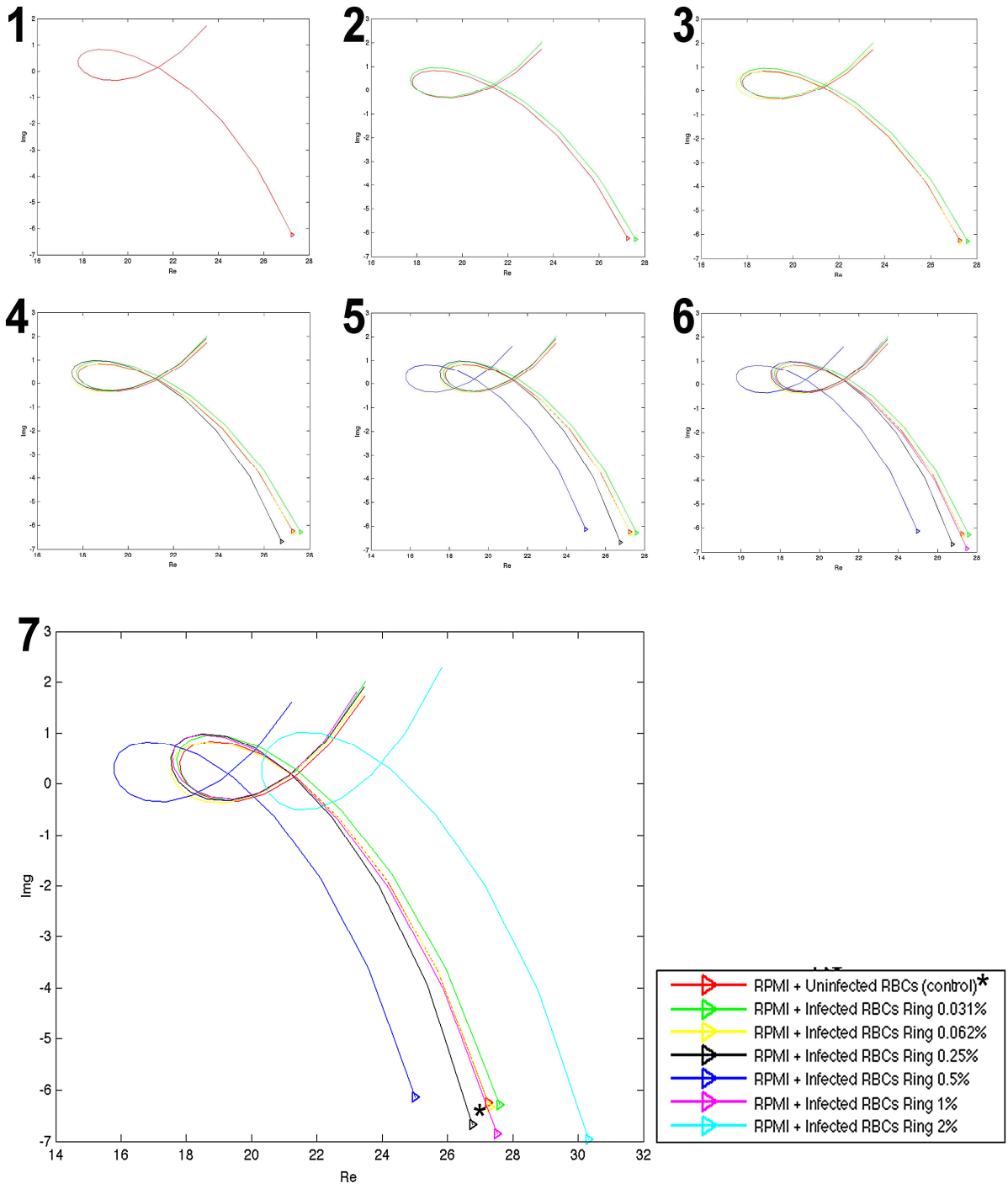

Figure 3.28 - Nyquist plots of impedance spectroscopy for non-parasitized and parasitized (by ring stage of *P. falciparum* strain Dd2) RBC´s assays in culture medium (RPMI) with high frequencies device, $I_{freq} \in$ [250 kHz – 5 MHz], using electrodes in cross configuration. The Nyquist plot overlaid on the image show the variation of impedance as function of the frequency response for different percentages of infected RBCs (2 to 7, parasitemia) and for uninfected RBCs (2,control), both in RPMI. To the plots 2 to 7 is always added an impedance curve with a new percentage of parasitemia (by ascending order). The percentages of parasitemia from 0.031% to 1% were obtained from successive dilutions (1:2) of a mixture containing infected RBCs with an initial percentage of parasitemia of 2%. The prepared mixtures of infected and uninfected RBCs have a hematocrit ≈ 5%. In the figure, an asterisk (*) identifies the control curve, and the symbol **Δ** represents the initial value of the impedance and of the lower frequency (250 kHz) in each plot. The Nyquist plot has a Real part (x axis), equivalent to electrical resistance in Ohms, and an Imaginary part (y axis), given by reactance in Ohms, which together constitute the impedance.

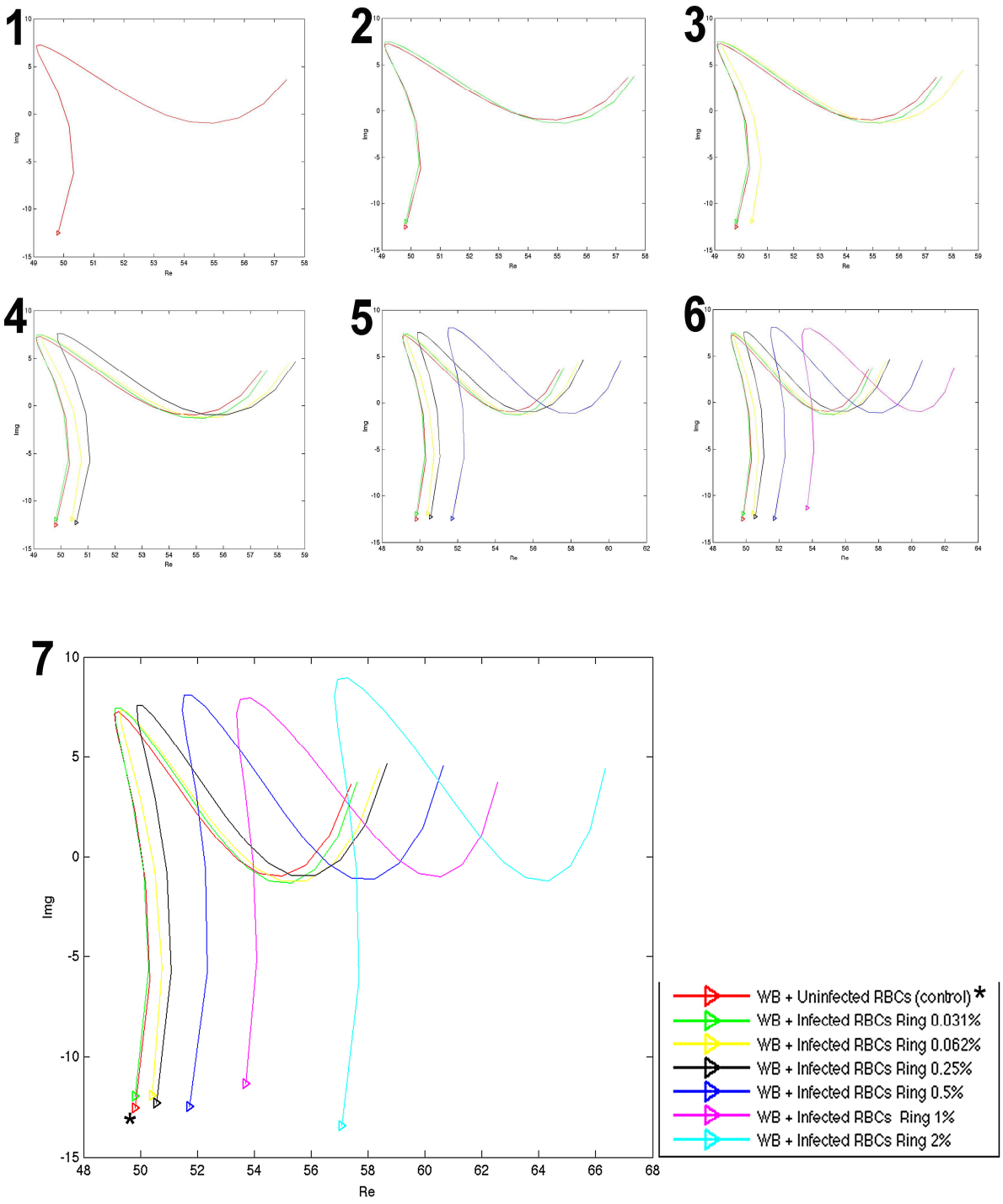

Figure 3.29 - Nyquist plots of impedance spectroscopy for non-parasitized and parasitized (by ring stage of *P. falciparum* strain Dd2) RBC´s assays in culture medium (RPMI) with high frequencies device, $I_{freq} \in$ [250 kHz – 5 MHz], using electrodes in parallel configuration. The Nyquist plot overlaid on the image show the variation of impedance as function of the frequency response for different percentages of infected RBCs (2 to 7, parasitemia) and for uninfected RBCs (2,control), both in RPMI. To the plots 2 to 7 is always added an impedance curve with a new percentage of parasitemia (by ascending order). The percentages of parasitemia from 0.031% to 1% were obtained from successive dilutions (1:2) of a mixture containing infected RBCs with an initial percentage of parasitemia of 2%. The prepared mixtures of infected and uninfected RBCs have a hematocrit ≈ 5%. In the figure, an asterisk (*) identifies the control curve, and the symbol **Δ** represents the initial value of the impedance and of the lower frequency (250 kHz) in each plot. The Nyquist plot has a Real part (x axis), equivalent to electrical resistance in Ohms, and an Imaginary part (y axis), given by reactance in Ohms, which together constitute the impedance.

3.2.2.2. Whole Blood with all stages (unsynchronized culture) and ring stage (synchronized culture)

In figures (Fig. 3.30 to 3.33), the overlapped Nyquist plots are numbered by ascending order 1 (uRBCs, control), and from 2 (lower % of parasitemia in *Pf*-iRBCs) to 7 (greatest % of parasitemia in *Pf*-iRBCs), in order to analyze the variation of the impedance curves as a function of the increasing percentage of parasitemia in the WB, and to verify whether there are differences between its impedances and in relation to the impedance curve of uRBCs.

A general and qualitative analysis of the results obtained for the impedance of the mixtures with all stages (Fig. 3.30 and 3.31) and with ring stage (Fig. 3.32 e 3.33), both in a WB medium for crossed and parallel configurations, shows that the impedance of the *Pf*-iRBC's curves increases with the increasing percentage of parasitemia and in relation to the impedance of the control curve (1 to 7). In addition, the impedance of the *Pf*-iRBC's curves present a good discrimination from the lowest percentage of parasitemia, 0.031% (7). In all assays, both the crossed and parallel configurations allowed for stable results, however the crossed configuration showed a better discrimination of the impedance values between the *Pf*-iRBC's curves and the control curve.

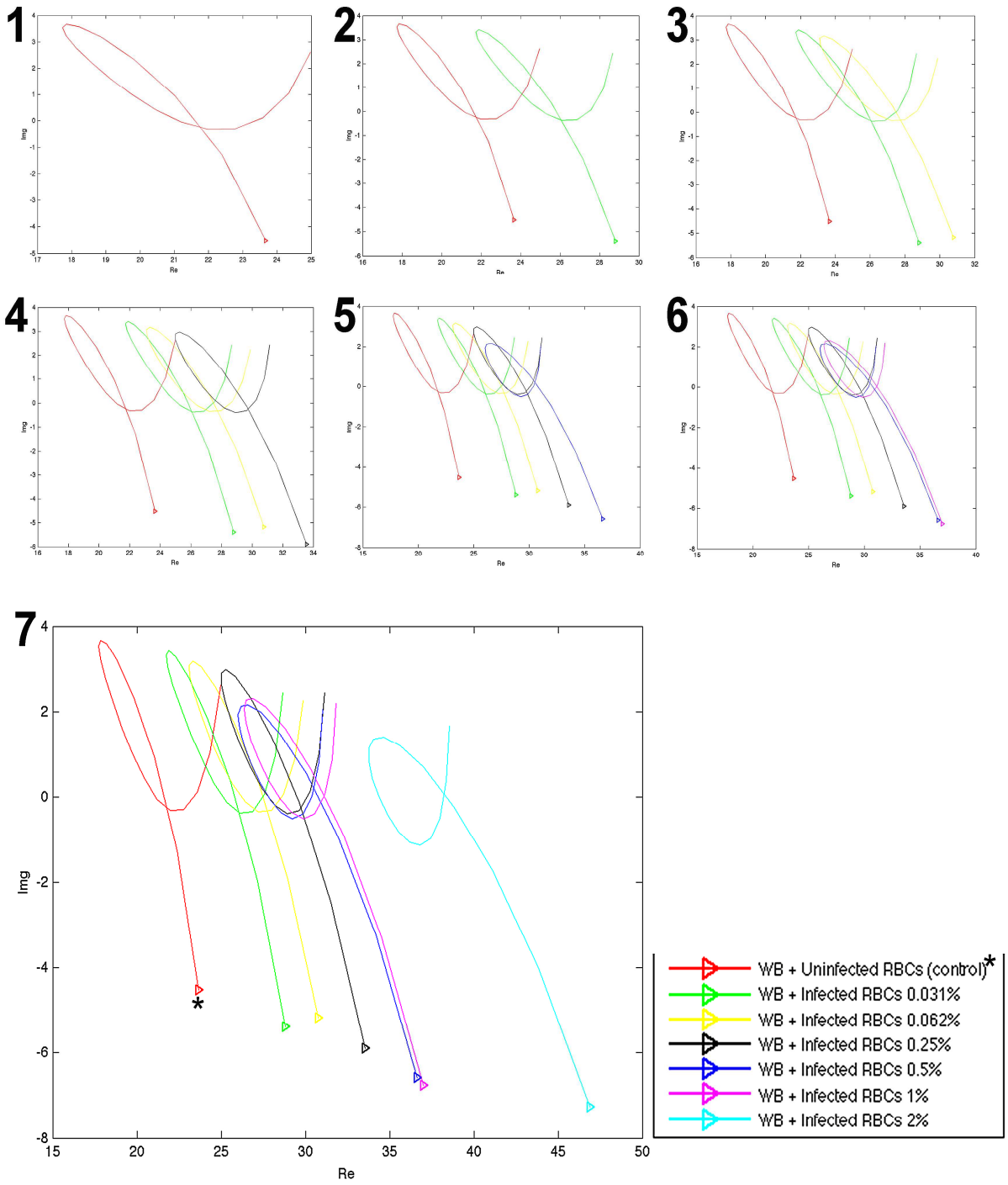

Figure 3.30 - Nyquist plots of impedance spectroscopy for non-parasitized and parasitized (by all stages of *P. falciparum* strain Dd2) RBC´s assays in Whole Blood (WB) with high frequencies device, $I_{freq} \in$ [250 kHz – 5 MHz], using electrodes in cross configuration. The Nyquist plots overlaid on the image show the variation of impedance as function of the frequency response for different percentages of infected RBCs (2 to 7, parasitemia) and for uninfected RBCs (1, control), both in WB (RBCs, WBCs and Plasma). To the plots 2 to 7 is always added an impedance curve with a new percentage of parasitemia (by ascending order). The percentages of parasitemia from 0.031% to 1% were obtained from successive dilutions (1:2) of a mixture containing infected RBCs with an initial percentage of parasitemia of 2%. The prepared mixtures of infected and uninfected RBCs have a hematocrit ≈ 45%. In the figure, an asterisk (*) identifies the control curve, and the symbol **Δ** represents the initial value of the impedance and of the lower frequency (250 kHz) in each plot. The Nyquist plot has a Real part (x axis), equivalent to electrical resistance in Ohms, and an Imaginary part (y axis), given by reactance in Ohms, which together constitute the impedance.

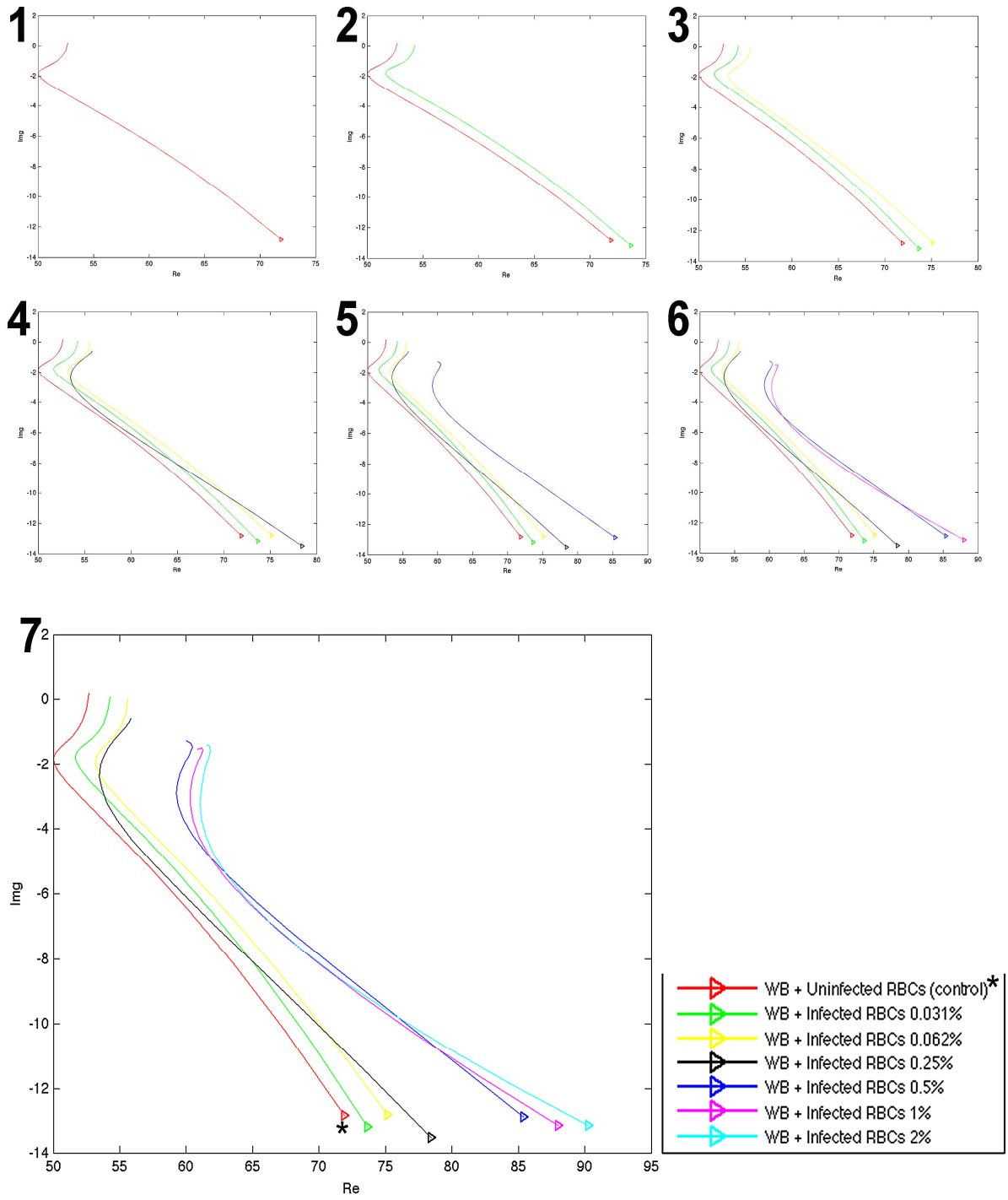

Figure 3.31 - Nyquist plots of impedance spectroscopy for non-parasitized and parasitized (by all stages of *P. falciparum* strain Dd2) RBC´s assays in Whole Blood (WB) with high frequencies device, $I_{freq} \in$ [250 kHz – 5 MHz], using electrodes in parallel configuration. The Nyquist plots overlaid on the image show the variation of impedance as function of the frequency response for different percentages of infected RBCs (2 to 7, parasitemia) and for uninfected RBCs (1, control), both in WB (RBCs, WBCs and Plasma). To the plots 2 to 7 is always added an impedance curve with a new percentage of parasitemia (by ascending order). The percentages of parasitemia from 0.031% to 1% were obtained from successive dilutions (1:2) of a mixture containing infected RBCs with an initial percentage of parasitemia of 2%. The prepared mixtures of infected and uninfected RBCs have a hematocrit ≈ 45%. In the figure, an asterisk (*) identifies the control curve, and the symbol **Δ** represents the initial value of the impedance and of the lower frequency (250 kHz) in each plot. The Nyquist plot has a Real part (x axis), equivalent to electrical resistance in Ohms, and an Imaginary part (y axis), given by reactance in Ohms, which together constitute the impedance.

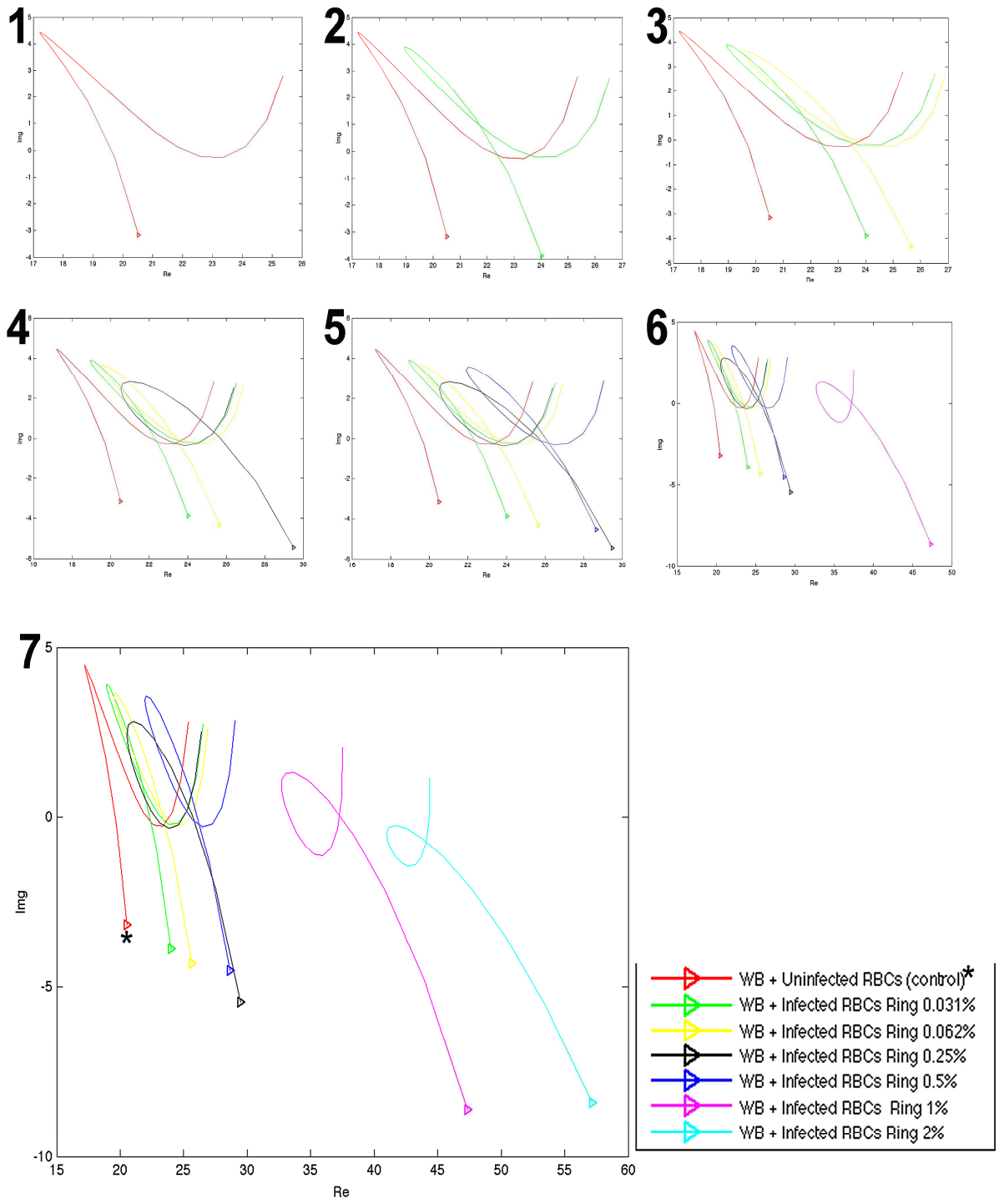

Figure 7.32 - Nyquist plots of impedance spectroscopy for non-parasitized and parasitized (by ring stage of *P. falciparum* strain Dd2) RBC´s assays in Whole Blood (WB) with high frequencies device, $I_{freq} \in$ [250 kHz – 5 MHz], using electrodes in cross configuration. The Nyquist plots overlaid on the image show the variation of impedance as function of the frequency response for different percentages of infected RBCs (2 to 7, parasitemia) and for uninfected RBCs (1, control), both in WB (RBCs, WBCs and Plasma). To the plots 2 to 7 is always added an impedance curve with a new percentage of parasitemia (by ascending order). The percentages of parasitemia from 0.031% to 1% were obtained from successive dilutions (1:2) of a mixture containing infected RBCs with an initial percentage of parasitemia of 2%. The prepared mixtures of infected and uninfected RBCs have a hematocrit ≈ 45%. In the figure, an asterisk (*) identifies the control curve, and the symbol **Δ** represents the initial value of the impedance and of the lower frequency (250 kHz) in each plot. The Nyquist plot has a Real part (x axis), equivalent to electrical resistance in Ohms, and an Imaginary part (y axis), given by reactance in Ohms, which together constitute the impedance.

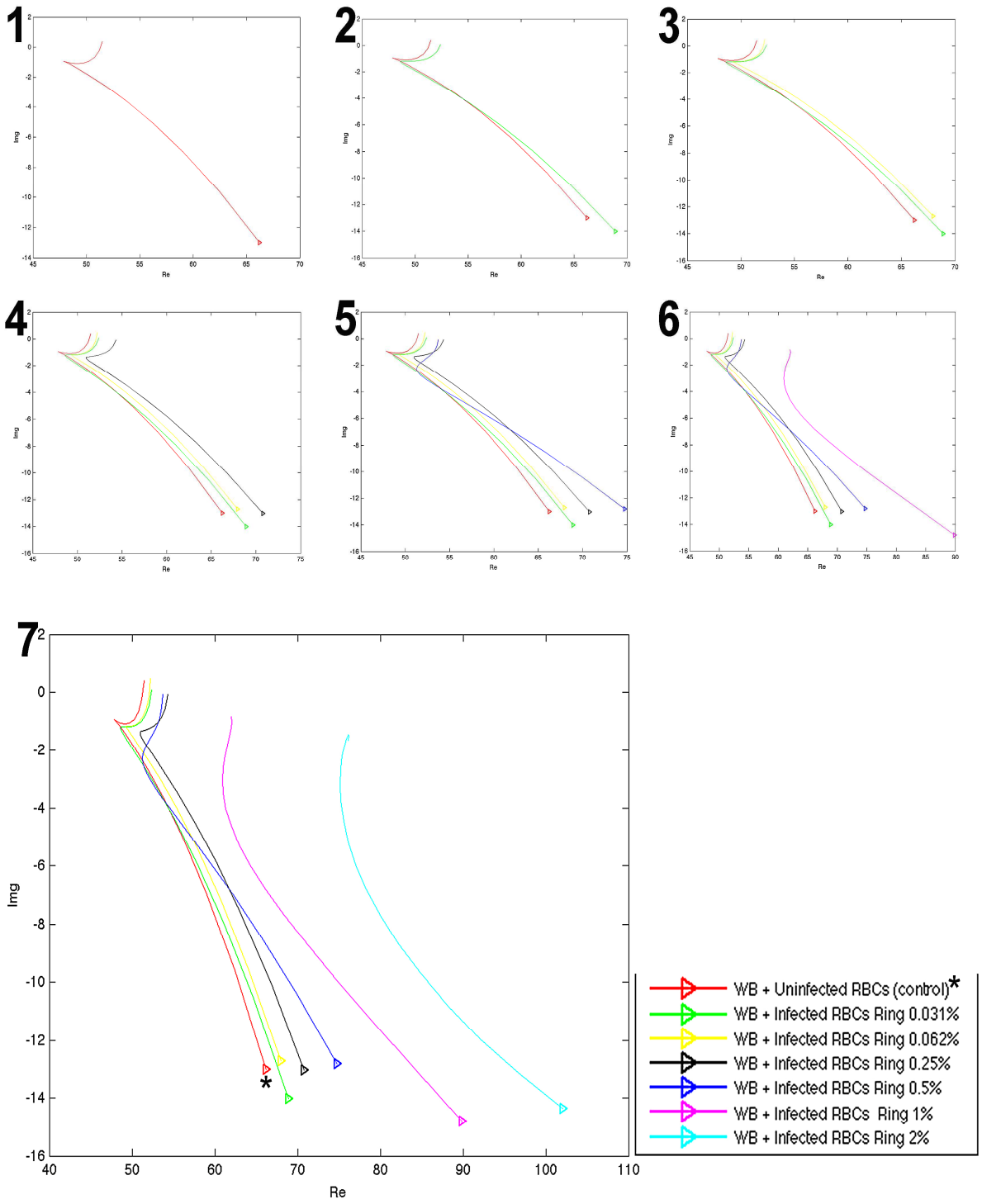

Figure 3.33 - Nyquist plots of impedance spectroscopy for non-parasitized and parasitized (by ring stage of *P. falciparum* strain Dd2) RBC´s assays in Whole Blood (WB) with high frequencies device, $I_{freq} \in$ [250 kHz – 5 MHz], using electrodes in parallel configuration. The Nyquist plots overlaid on the image show the variation of impedance as function of the frequency response for different percentages of infected RBCs (2 to 7, parasitemia) and for uninfected RBCs (1, control), both in WB (RBCs, WBCs and Plasma). To the plots 2 to 7 is always added an impedance curve with a new percentage of parasitemia (by ascending order). The percentages of parasitemia from 0.031% to 1% were obtained from successive dilutions (1:2) of a mixture containing infected RBCs with an initial percentage of parasitemia of 2%. The prepared mixtures of infected and uninfected RBCs have a hematocrit ≈ 45%. In the figure, an asterisk (*) identifies the control curve, and the symbol **Δ** represents the initial value of the impedance and of the lower frequency (250 kHz) in each plot. The Nyquist plot has a Real part (x axis), equivalent to electrical resistance in Ohms, and an Imaginary part (y axis), given by reactance in Ohms, which together constitute the impedance.

4. Discussion

4.1. Characterization of hemozoin crystals

4.1.1. Importance of characterizing synthetic and native hemozoin

Hemozoin crystals can be obtained in different ways: naturally, through the process of biocrystallization of hemozoin's heme by *P. falciparum* (*in vivo*); synthetically (β-hematin), from hemin chloride on acidic conditions (*in vitro*) [60]. The synthetic route is cheaper and faster, production wise, in comparison to the natural route, however it can have some drawbacks if the process of crystal formation is not identical to the natural. The different shapes and sizes of the hemozoin crystals appear to have an important role as a biological modulator in innate and inflammatory response *in vitro* and *in vivo* [30, 32, 60]. Furthermore, their studies have contributed to understanding the pathology of malaria [60]. However, hemozoin remains a good source for continuous search for new anti-malarial drugs (*in vitro* assays), which inhibit the formation process of crystals via synthetic route [15, 22, 29, 30, 49].

There are several protocols for production and purification of hemozoin that have been developed over the years aiming to create synthetic crystals with uniform characteristics, that is, shapes and sizes similar to the natural ones [60]. However, the experimental conditions of the protocols are difficult to control, which causes differences between the formation process of synthetic and natural crystals. In order to assess whether there are similarities or differences in the characteristics and properties of those crystals, the scientific community has used techniques such as scanning electron microscopy (SEM), transmission electron microscopy (TEM), light and depolarizing microscopy, X-ray diffraction and infrared spectroscopy [20]. β-hematin (sHz) has been demonstrated to be synthetic analog to hemozoin chemically, spectroscopically and crystallographically [20, 29]. However, it is not yet proven that hemozoin crystals synthetically obtained are really equal to the naturally obtained ones.

4.1.2. Morphology, microstructure and size of hemozoin

By examining the results obtained for different micrographs in scanning electron microscopy (SEM) and transmission electron microscopy (TEM), it is possible to verify that, depending on the formation process of the hemozoin crystals – natural source (*P. falciparum* strain 3D7 e Dd2) or synthetic source (protocol 1 and 2) – these present differences or similarities in their shapes and sizes. In all micrographs of SEM and TEM, the crystals showed habits in their shape (Fig. 3.1 to 3.5), as already reported in previous studies [20, 64].

Correlating the results of SEM and TEM micrographs for crystals nHz of strain 3D7 (sensitive) and Dd2 (resistant) of the parasite *P. falciparum*, it is possible to observe that these show shapes with the same habits, mostly parallelepiped, with well-defined faces and with similar size with nm and μm dimensions, which indicates that regardless of the strain, the biocrystallization process of the heme in hemozoin by the parasite *P. falciparum* is identical. However it is possible to verify that for the resistant strain Dd2 there are some crystals with brick-like shapes aggregated to each other in an

organized fashion. This result is in agreement with results from previous studies on the characterization of nHz obtained from *P. falciparum* [56, 59].

Taking into consideration the result of SEM and TEM micrographs of hemozoin crystals synthetically obtained by modifying protocol 1 in accordance to Slater *et al.* [53] and by protocol 2 already pre-established, it is possible to observe that the crystals have two types of forms. The first one is a needle-like shape, with long length and thin width; the second is a parallelepiped shape, with smaller length but with width similar to the needle-like shape. Nevertheless the needle-like shape is more visible in the crystals obtained with protocol 1 than with protocol 2. Noticeably, the crystals obtained with protocol 2 appear to be more evenly spread than the ones obtained with protocol 1, which shows a greater heterogeneity. These results indicate that the experimental process for production of sHz for protocol 2 leads to crystals with a more controlled and homogeneous morphology and size.

By comparing SEM and TEM micrographs of nHz 3D7 (sensitive) and Dd2 (resistant) strains with the micrographs of crystals of sHz obtained with protocols 1 and 2, it is verifiable that the shapes and sizes of the crystals produced with protocol 2 shows similarities with the nHz crystals produced by *P. falciparum*. Moreover, the shapes and sizes of the crystals obtained with protocol 1 show a greater distinction from the nHz crystals. This result proves once again that it is possible to control experimental conditions during the formation process of sHz (*in vitro*), in order to create synthetic crystals that share similar properties and characteristics with the nHz crystals. In the previous assertion, it is concluded that similar or identical synthetic and nHz crystals were obtained, which indicates that their formation process is occur under similar conditions. The previous observations and findings have great relevance, as mentioned above, in studies where assays are performed in order to inhibit the formation of sHz with antimalarial drugs, such as quinolones and artemisinins [15, 22]. These drugs, when applied to malaria treatment, target the detoxification process of the heme by *P. falciparum* (nHz formation), causing its inhibition and the changing of the crystals' morphology [15, 16, 25].

Considering all previous observations, if the formation process of sHz (*in vitro*) is identical to the formation of nHz (*in vivo*) obtained by *P. falciparum*, it is possible to obtain more reliable results in assays of inhibition of the heme's transformation into hemozoin *in vitro*, while testing antimalarial drugs.

By examining TEM micrographs, obtained for higher resolutions, of the results of the nHz´s crystals microstructure of strains 3D7 and Dd2, as well as synthetic hemozoin of protocol 1 and 2, it is shown that there are differences in their structures. The nHz crystals for both strains present layered structures on the faces of their tips, which show a uniform organization with parallelepiped shape (Fig. 3.4 E4 and F4). On the contrary, in protocol 1 most synthetic crystal have no layers in their tips and have the tendency to create a more tapered needle-like shape (Fig. 3.5 G). On the other hand, the crystals obtained by protocol 2 do not show the differences outlined above in relation to native crystals, however they also present long crystals with a needle-like shape, as can be observed in micrograph H1 (Fig. 3.5 H1). Notably, at higher resolutions, the crystals of protocol 2 demonstrate

again parallelepiped shapes as in nHz crystals, although with some disruption in their structure and without any layers at the tips of the crystal's faces. In general, these observations support the need to develop new protocols with controlled conditions which allow for the production of synthetic crystals with properties and characteristics similar to those of the native crystals.

4.1.3. Impedance Spectroscopy

According to the results obtained for the suspensions of nHz (strain Dd2) and sHz (Protocol 1 and Protocol 2), by impedance spectroscopy, it is possible to observe that the impedance curves for the low frequencies unit in crossed and parallel configuration (Fig. 3.6 and 3.7) cannot distinguish between the electrical properties of the crystals. The fact that the device measures in the low frequencies range, $I_{freq} \in$ [10 kHz – 82.5 kHz], can reduce the level of discrimination possible with the frequency response of the material analyzed, here the crystals. Moreover, in SEM micrographs (Fig. 3.1 and 3.2), some native and synthetic crystals have irregularities in their shape or aggregated materials in their structure (unpolymerized heme, membranes and proteins), and those factors might influence the actual measurements of the passive electrical properties of the crystals, causing a large discrepancy in the impedance curves obtained.

Examining the impedance results obtained using the high frequencies device, $I_{freq} \in$ [250 kHz – 5 MHz], for the various crossed and parallel configurations, it is verified that there are differences in the passive electrical properties among the crystals studied and these are presented more coherently. The results suggest that the fact that the measures are taken in the high frequencies range cause an increase in the level of discrimination and thereby obtain a good frequency response of the crystals analyzed using impedance spectroscopy.

By analyzing the passive electrical properties as well as their evolution over the Nyquist graphs (Fig. 3.8 and 3.9), in ascending order (1, 2, 3, 4 and 5), it can be said that the nHz and sHz P2 crystals, for a crossed and parallel configuration, show a greater reactance than in the case of sHz P1 crystals. This means that the material forming the nHz and sHz P2 crystals has a lower ability to disperse electric charge from the applied alternating current than the material of the sHz P1 crystals. However, for this evolution the sHz P1 crystals show greater resistive electrical properties, that is, the crystal structures have a higher charge transfer resistance with decreasing concentration in material resistivity, than for nHz and sHz P2 crystals. This result, correlated with the results of SEM and TEM micrographs, may suggest that sHz P1 crystals (Fig 3.2 C and 3.5 G) have larger sizes with elongated shapes, than nHz and sHz P2 crystals. This can cause saturation of the solution and deposition of crystals at high concentrations, in this case 1.35 mM and 0.337 mM, thus leading to reading errors of the device while analyzing the solutions. All these observations suggest that lower concentrations of sHz P2 crystals are necessary in order to reduce reading errors and measure the actual passive electrical properties.

On one hand, the fact that there are similarities in the passive electrical properties of nHz and sHz P2 crystals, for different electrode configurations, suggests that their formation processes are almost identical. On the other hand, the passive electrical properties of the sHz P1 crystals point out some inequalities in their formation process in relation to the formation process of nHz and sHz P2

crystals. Moreover, these similarities and inequalities among crystals for the different electrodes configurations indicate that the parallel configuration is more likely to achieve a data set more reproducible and stable than the crossed configuration, in other words, a better distinction and characterization of the impedance spectroscopy crystals.

4.2. Impedance spectroscopy as diagnostic method

4.2.1. Challenges of technique for detection of Malaria

The idea behind the search for new diagnosis methods which allow to detect the malaria parasite faster, simpler, more sensitive and specific manner, has been implemented in some recent studies related with the impedance spectroscopy technique [67]. These studies are focused on the *P. falciparum*, which is the species that causes the severest forms of the disease; only a single stage of the parasite circulates in the peripheral blood, the ring stage. The challenge of applying this technique of impedance spectroscopy focuses on the differentiation of *Pf*-iRBCs with the ring stage from uRBCs [4, 72, 73]. However the same technique is also important for the detection of malaria caused by others species of the parasite, in which its various stages circulate in the peripheral blood [4, 67]. Another relevant factor and one that adds to these challenges is the detection of very lower parasitemias. One of the problems associated to the areas with low malaria transmission is related with infections by submicroscopic parasitemia, which are hardly ever identified by conventional microscopes. Molecular techniques, such as Polymerase Chain Reaction (PCR), are effective in the detection of submicroscopic infections, however they are disadvantageous regarding the time needed to obtain results. Impedance spectroscopy can be an alternative to the PCR technique for the detection of submicroscopic infections, with the same efficacy but with an improvements regarding to the acquisition time of the results, thus functioning as a rapid diagnostic test (RDT) [84, 85].

4.2.2. Impedance of parasitized and non-parasitized red blood cells assays

Before proceeding to the discussion of the results, it is important to understand that, according to the results of studies performed with the technique of impedance spectroscopy, the impedance of *Pf*-iRBCs increases with increasing parasitemia [72, 73].

Examining the results of the impedance obtained from testing mixtures of non-parasitized and parasitized with all the stages (ring, trophozoite and schizont) of the *P. falciparum* in RPMI (Fig. 3.10 and 3.11) and in WB (Fig. 3.14 and 3.15), it is possible to verify that in the low frequency range, $I_{freq} \in$ [10 kHz – 82.5 kHz], for a crossed configuration the impedance curve present very incoherent evolution paths. On the contrary, for the parallel configuration, the impedance curves exhibit more coherence and a more logical path of evolution, without presenting a good distinction between them. Since the discrimination is very low, it is difficult to distinguish the curve of uRBCs from the curve of iRBCs. The inconsistencies as well as the low discrimination could be justified by the fact that the impedance measures are conducted at a low frequency range, which can lead to a bad signal response to the impedance of the cells, and consequently, to incoherent results. Comparing the results of the different

mixtures, RPMI and WB, for a parallel configuration it can be observed that only for the mixture in WB is possible to consistently differentiate the impedance of the curve of uRBCs from the curve of *Pf*-iRBCs with parasitemia of 0.0175%. The observations related to the parallel configuration demonstrate that it contributes to an optimization of the signal response of the impedance of *Pf*-iRBCs and uRBCs.

According to the values of impedance obtained in the high frequency range, $I_{freq} \in$ [250 kHz – 5 MHz], for the different mixtures, RPMI (Fig. 3.12 and 3.13) and WB (Fig. 3.16 and 3.17), it is possible to verify that in both configurations there is some coherence and an increase in the discrimination between the impedance of the curves. It is noted that the discrimination is larger for the parallel configuration. The results obtained for the mixtures in RPMI show that in both configurations the impedance of the *Pf*-iRBC´s curves with parasitemia ≤ 0.14% is incoherent since it is higher than the impedance of the *Pf*-iRBC´s curves with parasitemia ≥ 0.28%. The previous result can be justified by an experimental error, which may have been caused during the dilutions of parasitemia and the measures of impedance. Although, it is possible to observe that in the crossed configuration the impedance of the *Pf*-iRBC´s curves with parasitemia ≤ 0.07 %, converge to the impedance of the uRBC´s curve with the decrease of parasitemia percentage. On the contrary, in the parallel configuration the impedance of the *Pf*-iRBC´s curve with parasitemia of 1.12% and 0.28%, are the only that demonstrate convergence. By comparing the results of the two configurations it is possible to verify that the impedance values of the *Pf*-iRBC´s curve with parasitemia ≥ 0.28 % are more coherent in the parallel configuration. These are higher than the impedance values of the uRBC´s curves, as opposed to what is verified in the crossed configuration. These results demonstrate once more that the parallel configuration has advantages such as consistency and discrimination.

From the results obtained for mixtures in WB, interestingly it is observed that for a crossed configuration the impedance of the *Pf*-iRBC´s curves with parasitemia ≤ 0.14% and ≥ 0.56% present more coherent results since these are higher than the values of impedance for the uRBC's curve, as opposed to what is verified in the parallel configuration. However the distinction between the impedances of the various curves is still higher for the parallel configuration. In the crossed configuration it is possible to verify that the impedances of the *Pf*-iRBC´s with parasitemia of 1.12%, 0.14% and 0.0175%, all converge to the impedance of the uRBC's curve, with the decrease of the parasitemia percentage. On the contrary, in the parallel configuration there is no convergence but a consistency between the impedance of the uRBC's curve with the *Pf*-iRBC´s curve, with parasitemia of 0.035%. These results suggest that, in this case, the signal response of the cells' impedance is optimized for a crossed configuration when making measurements in the high frequency range, for a mixture in WB with various stages of the parasite.

Examining the results of the impedance obtained from testing mixtures of non-parasitized and parasitized with the ring (Fig. 3.18 and 3.19) and the schizont (Fig. 3.22 and 3.23) stage of *P. falciparum* in WB, it is possible to observe that in the low frequency range, $I_{freq} \in$ [10 kHz – 82.5 kHz], for a crossed and parallel configuration the impedance of the curves obtained for the ring stage show many inconsistencies. As opposed to the impedance of the curves obtained for the schizont stage, which present coherence and distinction. In this stage it is possible to observe the convergence of the

impedance of the *Pf*-iRBC´s curves towards the impedance of the uRBC's curves, with the decrease of parasitemia to such percentages as 1%, 0.062%, 0.125% and 0.0156% in the crossed configuration, and 1%, 0.25% and 0.0156% in the parallel configuration. By comparing the previous observations for the two stages, it is possible to verify that *Pf*-iRBCs with the ring stage prevent obtaining a good signal response of the impedance for low frequencies range, as opposed to what is verified for *Pf*-iRBCs with the schizont stage. The *Pf*-iRBCs with ring stage are non-mature cells of the malaria parasite and that still initially possess dielectric properties similar to those of the uRBC's membrane, such as capacitance. The membrane capacitance of the uRBCs shields the cell interior from the external electric field at low frequencies [72], which originates a non-existing or incoherent signal response of the impedance of *Pf*-iRBCs with the ring stage. On the contrary, the *Pf*-iRBCs with schizont stage are mature cells resulting from the process of maturation of the malaria parasite, which causes striking structural and morphological changes in the *Pf*-iRBCs [68, 72, 73]. The changed in the cell will lead to changes in the dielectric properties of the membrane thus changing its capacitance. This change lowers the membrane's resistance and consequently the surrounding layer becomes less insulating [73]. The external electric field at low frequencies will be able to penetrate *Pf*-iRBCs with schizont stage thus originating a coherent response from its impedance.

The results obtained for impedance in the high frequency range, $I_{freq} \in$ [250 kHz – 5 MHz], for the ring (Fig. 3.20 and 3.21) and schizont (Fig. 3.24 and 3.25) stage, demonstrate that for the two configurations in both stages there is consistency and an increase in the discrimination level between the impedance of the curves. These results are not observed for the ring stage in the low frequencies range. At higher frequencies, owing to the short circuiting effect of membrane capacitance, the electric field penetrates to the cellular interior and reaches the parasite [72], thus optimizing the signal response of the impedance of *Pf*-iRBCs and uRBCs, obtaining at the same time better results. In the ring stages it is possible to observe a convergence in the impedance of the *Pf*-iRBC's curves towards the impedance of the uRBC's curves with the decrease of parasitemia to such percentages as 2%, 0.062% and 0.031% in the crossed configuration, and 2%, 0.062% and 0.031% in the parallel configuration. In the schizont stage it is possible to observe a convergence in the impedance of the *Pf*-iRBC's curves towards the impedance of the uRBC's curves with the decrease of parasitemia to such pecentages as 1%, 0.125% and 0.062% in the crossed configuration, and 1%, 0.125% and 0.062% in the parallel configuration. However, comparing the results of the two configurations for both stages it is possible to observe that for the crossed configuration there are greater number of *Pf*-iRBC's curves showing incoherent results, showing a impedance lower than the impedance of the uRBC's curve. This observation proves that the parallel configuration also contributes to the optimization of the signal response of the cells' impedance.

The analysis of all results for high frequencies indicate that the frequency increase contributes to an improvement of the impedance response of the cells, as well as the level of discrimination of the impedance measures.

Examining the results obtained from the second of assay for impedance measurements in the high frequency range, $I_{freq} \in$ [250 kHz – 5 MHz] (3.2.2), it was observed an improvement in their stability

and repeatability. Such results were not observed in previous assays (3.2.1) and were obtained from the mixtures containing all stages and well as a single stage (ring) of *P. falciparum* strain Dd2, in RPMI and WB medium. This stability and repeatability is indicated, in figures 3.26, and from 3.28 to 3.33, by the existence of a logical and coherent convergence of the impedance of the *Pf*-iRBC's curves towards the impedance of the uRBC's curve, with decreasing parasitemia. However, it is observed in figure 3.27, which represents the assay with the ring stage in the crossed configuration, an incoherent convergence of the impedance of the *Pf*-iRBC's curve towards the uRBC's curve, showing an incorrect variation on the value of the impedance with the increase of parasitemia. This result suggests that there are still errors associated with the experimental conditions or during the impedance measures. Furthermore, it indicates that the crossed configuration can contribute for measurement errors. Regarding the configurations for the different mediums, it is possible to observe that the parallel configuration allows for a better signal response of the impedance of cells in a RPMI medium, thus obtaining an optimized discrimination between the impedance of the various curves. On the contrary, with the crossed configuration it is obtained a better response and discrimination in a WB medium. Nevertheless, the results obtained show that both the crossed and parallel configuration enables a distinction between the *Pf*-iRBC's curve (with all the stages or with just the ring stage) and the uRBC's curve. Another relevant factor, present in all the results, regards the differentiation of the impedance of the uRBC's curve from the impedance of the *Pf*-iRBC's curve for the lowest parasitemia, 0.031%. Such differentiation is greater in WB medium.

By observing the impedance results for the different tests it is verified the existence of incorrect variations on the impedance values for some *Pf*-iRBC's curves, in both the crossed and parallel configuration. The *Pf*-iRBCs and uRBCs present different dielectric properties, and thus different values of impedance. When performing impedance measurements in the mixture, the cells are not immobilized, which means there is a flow of *Pf*-iRBCs and uRBCs, which can be aggravated or changed by exchanging tubes while doing a new measure, or by inserting the electrodes in the mixture. The before mentioned factors can cause instability in the signal response of the cells during measurements consequently resulting in wrong impedance values.

It is also observed that the fact the uRBCs and *Pf*-iRBCs are in a RPMI medium may contribute for more stable measures and results. One possible justification for the observed stability is the RPMI medium not containing any component such as WBCs, platelets and plasma, which are components of Whole Blood. Some of these components also have dielectric properties which influence the alternating current (AC) applied to the mixture medium, which may create some instability in the system and simultaneously incorrect impedance variations of uRBCs and *Pf*-IRBCs.

The convergence of the impedance of *Pf*-iRBC's curves towards the impedance of uRBC's curves, obtained for the various tests conducted, indicate the possibility of applying the impedance spectroscopy for the detection of the various stages of the *P. falciparum* parasite in peripheral blood, which means distinguishing the non-infected blood from blood infected with the malaria parasite for parasitemias between 0.0156-2 %, approximately 780-100 000 parasites per µl. More importantly, it demonstrates that it is possible to detect *Pf*-iRBCs in ring stage in peripheral blood.

In comparison with the PCR technique, IS technique allows obtaining results more efficiently and in less time. However, the detection limit for PCR is approximately 0.05-10 parasites per µl corresponding to parasitemias between 0.000001-0.0002 %, distinct values of the values detected by IS technique. To detect submicroscopic infections, where exists very low parasite density (for example, 1-10 parasites per µl), is necessary proceed to new assays of IS for parasitemias similar to molecular technique ones [86, 87].

5. Conclusions

SEM, TEM and IS techniques demonstrate that nHz crystals coming from the sensitive strain 3D7 and from the resistant strain Dd2 of *P. falciparum* present a size, morphology and passive electrical properties that are more similar to the sHz crystals obtained using Protocol 2 than to those obtained using Protocol 1. This observation allows us to conclude that through the optimization of the experimental conditions of sHz crystals formation it is possible to obtain synthetic crystals that resemble the native ones. The optimization of crystal formation processes will contribute to the optimization of trials using antimalarial drugs that enable the formation of such crystals thus contributing to the production of drugs that diminish the parasite resistance to an antimalarial treatment.

The Impedance Spectroscopy (IS) devices proposed (low and high frequencies) demonstrate that it is possible to detect several or a single stage of *P. falciparum* in the peripheral blood. The detection allows to differentiate uninfected blood from Malaria-infected blood thus concluding that the IS technique could work as a diagnostic method. The impedance data obtained present high discrimination when the parallel and cross configurations are combined with a high frequency range. The low and high frequencies can be conjugated in order to find an ideal range for the measurement of the impedance data. Overall, the parallel configuration can be better to reproduce and obtain a dataset of impedance data more accurate than the cross configuration. However, in the last impedance results it is shown that both configurations can be applied for detection of malaria in human host.

6. Future Work

In order to improve the current work, several suggestions are listed below:

- Create a new experimental procedure for the production of synthetic hemozoin by changing the experimental conditions with the purpose of obtaining a more controlled process.

- Analyze and compare the newly obtained synthetic crystals with native hemozoin crystals produced by different strains of *P. falciparum*.

- New impedance spectroscopy assays in order to analyze:

1. Parasitized blood (*P. falciparum)* with different strains;
2. Parasitized blood (*P. falciparum)* and non-parasitized blood classified in different blood groups;
3. Parasitized blood (*P. falciparum)* and infected with different types of disease;
4. Parasitized blood (*P. falciparum)* having parasitemia values within the detection range of RDT (100 – 200 parasites per µl), thick film microscopy (4 – 10 parasites per µl) and PCR (0.05-10 parasites per µl);
5. Blood from a human host infected with *P. falciparum* (real case) and verify if the obtained results are comparable to the ones from cultures of parasitized blood.

- To increase the distinguish rate and reduce false positives in malaria diagnosis by impedance spectroscopy through the development of capillary spectroscopy technique. Such technique would, in theory, allow for an isolation of individual red blood cells in a capillary and then measuring the electrical potential directly on the isolated red blood cell and not on a blood solution where a great biological variability.

7. References

1. Poinar G, Jr.: **Plasmodium dominicana n. sp. (Plasmodiidae: Haemospororida) from Tertiary Dominican amber**. *Systematic parasitology* 2005, **61**(1):47-52.
2. Schlagenhauf P: **Malaria: from prehistory to present**. *Infectious disease clinics of North America* 2004, **18**(2):189-205, table of contents.
3. Carter R, Mendis KN: **Evolutionary and historical aspects of the burden of malaria**. *Clinical microbiology reviews* 2002, **15**(4):564-594.
4. Garcia LS: **Malaria**. *Clinics in laboratory medicine* 2010, **30**(1):93-129.
5. Greenwood BM, Bojang K, Whitty CJ, Targett GA: **Malaria**. *Lancet* 2005, **365**(9469):1487-1498.
6. Miller LH, Baruch DI, Marsh K, Doumbo OK: **The pathogenic basis of malaria**. *Nature* 2002, **415**(6872):673-679.
7. http://www.cdc.gov/malaria/about/distribution.html
8. Organization WH: **World Malaria Report 2013**. 2013.
9. Cai H, Zhou Z, Gu J, Wang Y: **Comparative Genomics and Systems Biology of Malaria Parasites**. *Current bioinformatics* 2012, **7**(4).
10. Greenwood BM, Fidock DA, Kyle DE, Kappe SH, Alonso PL, Collins FH, Duffy PE: **Malaria: progress, perils, and prospects for eradication**. *The Journal of clinical investigation* 2008, **118**(4):1266-1276.
11. Michalakis Y, Renaud F: **Malaria: Evolution in vector control**. *Nature* 2009, **462**(7271):298-300.
12. Cox FE: **History of human parasitology**. *Clinical microbiology reviews* 2002, **15**(4):595-612.
13. Cox FEG: **History of the discovery of the malaria parasites and their vectors**. *Parasite Vector* 2010, **3**.
14. Tilley L, Dixon MW, Kirk K: **The *Plasmodium falciparum*-infected red blood cell**. *The international journal of biochemistry & cell biology* 2011, **43**(6):839-842.
15. Egan TJ, Ncokazi KK: **Quinoline antimalarials decrease the rate of beta-hematin formation**. *Journal of inorganic biochemistry* 2005, **99**(7):1532-1539.
16. Solomonov I, Osipova M, Feldman Y, Baehtz C, Kjaer K, Robinson IK, Webster GT, McNaughton D, Wood BR, Weissbuch I *et al*: **Crystal nucleation, growth, and morphology of the synthetic malaria pigment beta-hematin and the effect thereon by quinoline additives: the malaria pigment as a target of various antimalarial drugs**. *Journal of the American Chemical Society* 2007, **129**(9):2615-2627.
17. Silvie O, Mota MM, Matuschewski K, Prudencio M: **Interactions of the malaria parasite and its mammalian host**. *Current opinion in microbiology* 2008, **11**(4):352-359.
18. Kirk K: **Membrane transport in the malaria-infected erythrocyte**. *Physiological reviews* 2001, **81**(2):495-537.
19. Bannister LH, Hopkins JM, Fowler RE, Krishna S, Mitchell GH: **A brief illustrated guide to the ultrastructure of *Plasmodium falciparum* asexual blood stages**. *Parasitol Today* 2000, **16**(10):427-433.
20. Egan TJ: **Biomimetic Approaches to Understanding the Mechanism of Haemozoin Formation**; 2011.
21. Frosch T, Koncarevic S, Zedler L, Schmitt M, Schenzel K, Becker K, Popp J: **In situ localization and structural analysis of the malaria pigment hemozoin**. *The journal of physical chemistry B* 2007, **111**(37):11047-11056.
22. Gildenhuys J, le Roex T, Egan TJ, de Villiers KA: **The single crystal X-ray structure of beta-hematin DMSO solvate grown in the presence of chloroquine, a beta-hematin growth-rate inhibitor**. *Journal of the American Chemical Society* 2013, **135**(3):1037-1047.
23. Egan TJ: **Haemozoin formation**. *Molecular and biochemical parasitology* 2008, **157**(2):127-136.
24. Lew VL, Tiffert T, Ginsburg H: **Excess hemoglobin digestion and the osmotic stability of *Plasmodium falciparum*-infected red blood cells**. *Blood* 2003, **101**(10):4189-4194.

25. Rathore D, Jani D, Nagarkatti R, Kumar S: **Heme detoxification and antimalarial drugs – Known mechanisms and future prospects**. *Drug Discovery Today: Therapeutic Strategies* 2006, **3**(2):153-158.
26. Bohle DS, Kosar AD, Stephens PW: **Phase homogeneity and crystal morphology of the malaria pigment beta-hematin**. *Acta crystallographica Section D, Biological crystallography* 2002, **58**(Pt 10 Pt 1):1752-1756.
27. Hempelmann E: **Hemozoin biocrystallization in *Plasmodium falciparum* and the antimalarial activity of crystallization inhibitors**. *Parasitology research* 2007, **100**(4):671-676.
28. Kumar S, Guha M, Choubey V, Maity P, Bandyopadhyay U: **Antimalarial drugs inhibiting hemozoin (beta-hematin) formation: a mechanistic update**. *Life sciences* 2007, **80**(9):813-828.
29. Fong KY, Wright DW: **Hemozoin and antimalarial drug discovery**. *Future medicinal chemistry* 2013, **5**(12):1437-1450.
30. Hanscheid T, Egan TJ, Grobusch MP: **Haemozoin: from melatonin pigment to drug target, diagnostic tool, and immune modulator**. *Lancet Infect Dis* 2007, **7**(10):675-685.
31. Sandlin RD, Carrell HM, Wright DW: **Hemozoin: Crystal Engineering Survivability**. In: *Encyclopedia of Inorganic and Bioinorganic Chemistry.* John Wiley & Sons, Ltd; 2011.
32. Egan TJ, Chen JY, de Villiers KA, Mabotha TE, Naidoo KJ, Ncokazi KK, Langford SJ, McNaughton D, Pandiancherri S, Wood BR: **Haemozoin (beta-haematin) biomineralization occurs by self-assembly near the lipid/water interface**. *FEBS letters* 2006, **580**(21):5105-5110.
33. Egan TJ: **Recent advances in understanding the mechanism of hemozoin (malaria pigment) formation**. *Journal of inorganic biochemistry* 2008, **102**(5-6):1288-1299.
34. Achan J, Talisuna AO, Erhart A, Yeka A, Tibenderana JK, Baliraine FN, Rosenthal PJ, D'Alessandro U: **Quinine, an old anti-malarial drug in a modern world: role in the treatment of malaria**. *Malaria journal* 2011, **10**:144.
35. Meshnick SR, Dobson MJ: **The history of antimalarial drugs**. In: *Antimalarial chemotherapy.* Springer; 2001: 15-25.
36. Schlitzer M: **Malaria Chemotherapeutics Part I: History of Antimalarial Drug Development, Currently Used Therapeutics, and Drugs in Clinical Development**. *ChemMedChem* 2007, **2**(7):944-986.
37. Bloland PB, Organization WH: **Drug resistance in malaria**: World Health Organization Geneva; 2001.
38. Watkins ER, Meshnick SR: **Drugs for malaria**. In: *Seminars in Pediatric Infectious Diseases: 2000*. Elsevier: 202-212.
39. White NJ: **Cardiotoxicity of antimalarial drugs**. *The Lancet infectious diseases* 2007, **7**(8):549-558.
40. Aditya NP, Vathsala PG, Vieira V, Murthy RS, Souto EB: **Advances in nanomedicines for malaria treatment**. *Advances in colloid and interface science* 2013, **201-202**:1-17.
41. Klein EY: **Antimalarial drug resistance: a review of the biology and strategies to delay emergence and spread**. *International journal of antimicrobial agents* 2013, **41**(4):311-317.
42. Lee SJ, Seo E, Cho Y: **Proposal for a new therapy for drug-resistant malaria using Plasmodium synthetic lethality inference**. *International Journal for Parasitology: Drugs and Drug Resistance* 2013, **3**(0):119-128.
43. Plowe CV: **The evolution of drug-resistant malaria**. *Transactions of the Royal Society of Tropical Medicine and Hygiene* 2009, **103 Suppl 1**:S11-14.
44. Schrader FC, Barho M, Steiner I, Ortmann R, Schlitzer M: **The antimalarial pipeline--an update**. *International journal of medical microbiology : IJMM* 2012, **302**(4-5):165-171.
45. Calderon F, Wilson DM, Gamo FJ: **Antimalarial drug discovery: recent progress and future directions**. *Progress in medicinal chemistry* 2013, **52**:97-151.
46. AlKadi HO: **Antimalarial drug toxicity: a review**. *Chemotherapy* 2007, **53**(6):385-391.
47. Biamonte MA, Wanner J, Le Roch KG: **Recent advances in malaria drug discovery**. *Bioorganic & medicinal chemistry letters* 2013, **23**(10):2829-2843.

48. Delves M, Plouffe D, Scheurer C, Meister S, Wittlin S, Winzeler EA, Sinden RE, Leroy D: **The activities of current antimalarial drugs on the life cycle stages of Plasmodium: a comparative study with human and rodent parasites**. *PLoS medicine* 2012, **9**(2):e1001169.
49. Egan TJ: **Haemozoin (malaria pigment): a unique crystalline drug target**. *TARGETS* 2003, **2**(3):115-124.
50. Egan TJ: **Physico-chemical aspects of hemozoin (malaria pigment) structure and formation**. *Journal of inorganic biochemistry* 2002, **91**(1):19-26.
51. Pandey AV, Babbarwal VK, Okoyeh JN, Joshi RM, Puri SK, Singh RL, Chauhan VS: **Hemozoin formation in malaria: a two-step process involving histidine-rich proteins and lipids**. *Biochemical and biophysical research communications* 2003, **308**(4):736-743.
52. Fitch CD, Kanjananggulpan P: **The state of ferriprotoporphyrin IX in malaria pigment**. *The Journal of biological chemistry* 1987, **262**(32):15552-15555.
53. Slater AF, Swiggard WJ, Orton BR, Flitter WD, Goldberg DE, Cerami A, Henderson GB: **An iron-carboxylate bond links the heme units of malaria pigment**. *Proceedings of the National Academy of Sciences of the United States of America* 1991, **88**(2):325-329.
54. Walczak MS, Lawniczak-Jablonska K, Sienkiewicz A, Klepka MT, Suarez L, Kosar AJ, Bellemare MJ, Bohle DS: **XAFS studies of the synthetic substitutes of hemozoin**. *Journal of Non-Crystalline Solids* 2010, **356**(37–40):1908-1913.
55. Bohle DS, Dinnebier RE, Madsen SK, Stephens PW: **Characterization of the products of the heme detoxification pathway in malarial late trophozoites by X-ray diffraction**. *The Journal of biological chemistry* 1997, **272**(2):713-716.
56. Pagola S, Stephens PW, Bohle DS, Kosar AD, Madsen SK: **The structure of malaria pigment beta-haematin**. *Nature* 2000, **404**(6775):307-310.
57. Oliveira MF, Kycia SW, Gomez A, Kosar AJ, Bohle DS, Hempelmann E, Menezes D, Vannier-Santos MA, Oliveira PL, Ferreira ST: **Structural and morphological characterization of hemozoin produced by Schistosoma mansoni and Rhodnius prolixus**. *FEBS letters* 2005, **579**(27):6010-6016.
58. Klonis N, Dilanian R, Hanssen E, Darmanin C, Streltsov V, Deed S, Quiney H, Tilley L: **Hematin-hematin self-association states involved in the formation and reactivity of the malaria parasite pigment, hemozoin**. *Biochemistry* 2010, **49**(31):6804-6811.
59. Noland GS, Briones N, Sullivan DJ, Jr.: **The shape and size of hemozoin crystals distinguishes diverse Plasmodium species**. *Molecular and biochemical parasitology* 2003, **130**(2):91-99.
60. Shio MT, Kassa FA, Bellemare MJ, Olivier M: **Innate inflammatory response to the malarial pigment hemozoin**. *Microbes and infection / Institut Pasteur* 2010, **12**(12-13):889-899.
61. Goldstein J, Newbury DE, Joy DC, Lyman CE, Echlin P, Lifshin E, Sawyer L, Michael JR: **Scanning electron microscopy and X-ray microanalysis**: Springer; 2003.
62. Fultz B, Howe JM: **Transmission electron microscopy and diffractometry of materials**, 4th edn. Heidelberg ; New York: Springer; 2013.
63. Williams DB, Carter CB: **The Transmission Electron Microscope**: Springer; 1996.
64. Buller R, Peterson ML, Almarsson Ö, Leiserowitz L: **Quinoline binding site on malaria pigment crystal: a rational pathway for antimalaria drug design**. *Crystal growth & design* 2002, **2**(6):553-562.
65. Tangpukdee N, Duangdee C, Wilairatana P, Krudsood S: **Malaria diagnosis: a brief review**. *The Korean journal of parasitology* 2009, **47**(2):93-102.
66. Rebelo M, Shapiro HM, Amaral T, Melo-Cristino J, Hanscheid T: **Haemozoin detection in infected erythrocytes for *Plasmodium falciparum* malaria diagnosis-prospects and limitations**. *Acta tropica* 2012, **123**(1):58-61.
67. Han E-T, Watanabe R, Sattabongkot J, Khuntirat B, Sirichaisinthop J, Iriko H, Jin L, Takeo S, Tsuboi T: **Detection of four Plasmodium species by genus-and species-specific loop-mediated isothermal amplification for clinical diagnosis**. *Journal of clinical microbiology* 2007, **45**(8):2521-2528.

68. Cooke BM, Mohandas N, Coppel RL: **Malaria and the red blood cell membrane**. *Seminars in hematology* 2004, **41**(2):173-188.
69. Hafalla JC, Silvie O, Matuschewski K: **Cell biology and immunology of malaria**. *Immunological reviews* 2011, **240**(1):297-316.
70. http://www.cdc.gov/dpdx/resources/pdf/benchAids/malaria/Pfalciparum_benchaidV2.pdf
71. Barsoukov E, Macdonald JR: **Impedance spectroscopy: theory, experiment, and applications**: John Wiley & Sons; 2005.
72. Du E, Ha S, Diez-Silva M, Dao M, Suresh S, Chandrakasan AP: **Electric impedance microflow cytometry for characterization of cell disease states**. *Lab on a chip* 2013, **13**(19):3903-3909.
73. Ribaut C, Reybier K, Reynes O, Launay J, Valentin A, Fabre PL, Nepveu F: **Electrochemical impedance spectroscopy to study physiological changes affecting the red blood cell after invasion by malaria parasites**. *Biosensors & bioelectronics* 2009, **24**(8):2721-2725.
74. Trager W, Jensen JB: **Human malaria parasites in continuous culture**. *Science* 1976, **193**(4254):673-675.
75. Thaithong S, Seugorn A, Beale GH: **Culturing *Plasmodium falciparum* from finger-prick samples of infected blood**. *Transactions of the Royal Society of Tropical Medicine and Hygiene* 1994, **88**(4):490.
76. Cranmer SL, Magowan C, Liang J, Coppel RL, Cooke BM: **An alternative to serum for cultivation of *Plasmodium falciparum* in vitro**. *Transactions of the Royal Society of Tropical Medicine and Hygiene* 1997, **91**(3):363-365.
77. Nolasco PA: **Structural and mechanical characterization of sialoliths**. Lisboa: Insituto Superior Técnico; 2011.
78. Brophy JJ: **Basic electronics for scientists**, 3d edn. New York: McGraw-Hill; 1977.
79. Lasia A: **Electrochemical Impedance Spectroscopy and its Applications**. In: *Modern Aspects of Electrochemistry.* Edited by Conway BE, Bockris JOM, White R, vol. 32: Springer US; 2002: 143-248.
80. Macdonald JR: **Impedance spectroscopy**. *Annals of biomedical engineering* 1992, **20**(3):289-305.
81. Fogel BJ, Shields CE, Von Doenhoff AE, Jr.: **The osmotic fragility of erythrocytes in experimental malaria**. *The American journal of tropical medicine and hygiene* 1966, **15**(3):269-275.
82. Shen SC, Fleming EM, Castle WB: **Osmotic and mechanical fragilities of erythrocytes of monkeys infected with P. knowlesi malaria**. *Proc Soc Exp Biol Med* 1946, **63**(2):419-422.
83. Lambros C, Vanderberg JP: **Synchronization of *Plasmodium falciparum* erythrocytic stages in culture**. *The Journal of parasitology* 1979, **65**(3):418-420.
84. Ochola LB, Vounatsou P, Smith T, Mabaso ML, Newton CR: **The reliability of diagnostic techniques in the diagnosis and management of malaria in the absence of a gold standard**. *Lancet Infect Dis* 2006, **6**(9):582-588.
85. Okell LC, Ghani AC, Lyons E, Drakeley CJ: **Submicroscopic infection in *Plasmodium falciparum*-endemic populations: a systematic review and meta-analysis**. *The Journal of infectious diseases* 2009, **200**(10):1509-1517.
86. Garcia L: **Malaria Could You Recognize the World's Number Two Killer?**
87. Okell LC, Bousema T, Griffin JT, Ouedraogo AL, Ghani AC, Drakeley CJ: **Factors determining the occurrence of submicroscopic malaria infections and their relevance for control**. *Nature communications* 2012, **3**:1237.

Appendixs

Appendix A – Hemozoin crystals quantitation (heme equivalents)

Appendix A – Hemozoin crystals quantitation (heme equivalents)

A.1. Table of standard concentrations of hemin solution

Wells	Standard [M]	1 (ABS)	2 (ABS)	3 (ABS)	Mean ABS (nm)
A	0.002	2.459	2.4568	2.5824	2.4994
B	0.001	1.3629	1.4058	1.3911	1.3866
C	0.0005	0.703	0.6932	0.7227	0.7063
D	0.000333333	0.3659	0.3666	0.3802	0.3709
E	0.00025	0.1891	0.1899	0.2036	0.1942
F	0.0002	0.1131	0.111	0.1098	0.1113
G	0.000166667	0.0765	0.0854	0.0844	0.0821
H	0.000142857	0.0519	0.0624	0.0658	0.060033333
Rep A	0.000125	0.042	0.0424	0.0433	0.042566667
Rep B	0.000111111	0.0351	0.0344	0.0355	0.035
Rep C	0.0001	0.0316	0.0316	0.036	0.033066667
Rep D	9.09091E-05	0.0427	0.0297	0.0304	0.034266667
Rep E	8.33333E-05	0.0312	0.031	0.0292	0.030466667
Rep F	7.69231E-05	0.0304	0.0311	0.0325	0.031333333

A.2. Calibration curve of standard concentrations of hemin as *x* and the respective absorbances as *y*.